THESIS ON MECHANICAL ENGINEERING E107

Technology and Properties of Fine-grained Nd-Fe-B Magnets

ZORJANA MURAL

TUT
PRESS

TALLINN UNIVERSITY OF TECHNOLOGY
School of Engineering
Department of Mechanical and Industrial Engineering

Dissertation was accepted for the defence of the degree of Doctor of Philosophy in Engineering on June 29th, 2016

Supervisors: Professor Renno Veinthal, Department of Mechanical and Industrial Engineering, School of Engineering, Tallinn University of Technology, Estonia

Dr. Lauri Kollo, Senior Research Scientist, Department of Mechanical and Industrial Engineering, School of Engineering, Tallinn University of Technology, Estonia

Opponents: Dr. Minna Haavisto, Executive Manager, The Greens of Finland, Finland

Dr. Raivo Stern, Lead Research Scientist, National Institute of Chemical Physics and Biophysics, Estonia

Defence of the thesis: February 17th, 2017 at 13:00, Tallinn University of Technology, room U05-216.

Declaration:
Hereby I declare that this doctoral thesis, my original investigation and achievement, submitted for the doctoral degree at Tallinn University of Technology, has not been submitted for any academic degree.

/Zorjana Mural/

ISSN 1406-4758
ISBN 978-9949-83-073-2 (publication)
ISBN 978-9949-83-074-9 (PDF)

MEHHANOTEHNIKA E107

Nd-Fe-B peenteramagnetite tehnoloogia ja omadused

ZORJANA MURAL

TTÜ KIRJASTUS

Contents

LIST OF PUBLICATIONS

The present doctoral dissertation is based on the following peer reviewed publications, referred to in the text by **Paper I, II, IV** and the patent, referred by **Paper III**:

Paper I **Mural, Z**., Kolnes, M., Afshari, H., Kollo, L., Link, J. and Veinthal, R. Fabrication and microstructural analysis of didymium-iron-boron magnet alloys with cerium additions. *Proceedings of the Estonian Academy of Sciences*, 65 (2), 2016, 166 – 171.

Paper II **Mural, Z**., Kollo, L., Traksmaa, R., Kallip, K., Link, J. and Veinthal, R. Structure and Magnetic Properties of NdFeB Powder Prepared by Hydrogen Decrepitation and High-energy Ball Milling. *Key Engineering Materials*, 604, 2014, 262 – 266.

Paper III Kollo, L., Kallip. K., **Mural, Z**., Vallner, H., Veinthal, R., Kolnes, M., Tarraste, M. and Jõeleht, M. (2016). Method and device for manufacturing sintered material products. Patent number: EE 05786 B1. Publication date: 27.01.2017.

Paper IV **Mural, Z**., Kollo, L., Xia, M., Bahl, C., Abrahamsen, A.B., Neves Bez, H., Link. J. and Veinthal, R. The Effect of Nano-TiC Addition on Sintered Nd-Fe-B Permanent Magnets. *Journal of Magnetism and Magnetic Materials,* 429, 2017, 23-28 (in press).

Copies of the articles and the patent are included in the Appendices.

Author's contribution

The author of this thesis planned, prepared and conducted the experiments, interpreted the results and was responsible for writing and publishing of the articles. All the papers were revised and commented by co-authors.

FOREWORD

This thesis originated from the project "Permanent magnets for sustainable energy application (MagMat)", 2012-2015. During the project, Tallinn University of Technology, Department of Materials Engineering (TUT DME), Department of Fundamentals of Electrical Engineering and Electrical Machines (DFEEEM), National Institute of Chemical Physics and Biophysics (NICBP), functioning as research institutions, co-operated with several business organizations such as Molycorp Silmet AS, Neorem Magnets OY, Prizztech OY, and ABB AS to achieve the goals of the project.

As the challenges of the project and the PhD research are in good compliance, they are unveiled in detail in the body part of the thesis (Section 1.5 Aims of the study). Generally, the MagMat project was focused on the development of expertise and knowledge in the magnetic materials that contain Rare-Earth metals. The topic is of importantance on the national, EU- and global scale.

Each institution and organization involved had its own core competences. TUT DME team researched and developed magnetic materials technologies. TUT DFEEEM, NICBP and ABB AS were responsible for the characterization and modeling of machines utilizing the materials developed. Molycorp Silmet AS and Neorem Magnets OY provided most of the master alloys used in the preparation of Nd-Fe-B magnetic alloys and conducted industrial tests. Prizztech OY was the consolidating joint, uniting all MagMat project participants with guidance and recommendations.

Currently, the Rare-Earth (RE) permanent magnets (PMs) have nearly reached their theoretical limits in terms of maximum energy product $(BH)_{max}$ [1]. On the other hand, none of PMs provide all the properties required for demanding applications [2, 3]. Standard industrial processing procedures for PMs are often costly and difficult to implement on an industrial scale [4]. Therefore, it is highly desirable to develop PMs that have high magnetization, coercivity and thermal stability, achieved at low processing cost.

Microstructure and properties of the magnets are strongly connected to the preparation route. The most important parameters influencing the quality of the PM are chemical composition, particle size and size distribution of the magnetic powders, sintering regimes and contamination rate, especially with oxygen [1].

Current research is concentrated on the development and preparation of magnetic alloys with controlled composition and microstructure, optimization of milling techniques to obtain powders with fine grains and narrow size distribution. Design of magnets with improved magnetic performance, especially at higher temperatures is a key aspect along with magnet production route establishment on the laboratory scale.

The present work covers all the main steps for the magnet manufacturing process. Splat quenching is used to prepare small amounts of Ce-containing alloys with fine and homogeneous microstructure free of α-iron. Classic production route of sintered RE magnets has been adopted as the main fabrication technology. Alternatively, high-energy milling in a wet agent or in hydrogen and vacuum is implemented. Spark Plasma Sintering (SPS) is used as a consolidation alternative method for vacuum sintering. Nano-TiC powder addition to Nd-Fe-B powders is suggested to enhance the magnetic properties, Curie temperature and thermal stability. This could be considered as one of the main novelties and scientific achievements of the work.

Splat quenching method for processing of small quantities of Ce-containing magnetic alloys is demonstrated. Cooling rate up to 10^5 K/s was achieved, an alloy with fine microstructure and free of α-iron was obtained. Quenching technique also resulted in a more homogeneous magnetic alloy with a lower Nd-rich phase content present in the microstructure. The optimized parameters implementing HD and JM of Nd-Fe-B powders yielded the lowest average particle size of 2 μm. As compared to JM, high-energy milling in an attritor with hydrogen gas and vacuum resulted in a 0.3 μm average particle size and lower level of oxidation.

Addition of nano-TiC to the RE magnets by mixing into hydrogen decrepitated strip cast powder was assessed. This processing step can be performed prior to jet milling by simple mixing, which offers new possibilities to tailor neodymium magnet properties in the sintering plant. Nano-TiC additions proved to result in improved magnetic properties, increased high temperature stability and higher Curie temperature. TiC particles are concentrated mainly intergranularly in the RE-rich phase and are almost unsolvable in the matrix. At as small concentrations as 0.1 wt.% of TiC, nanopowder leads already to a finer microstructure and decreased volume fraction of the nonmagnetic phase.

The thesis includes the introduction and the literature review where the aims of the studies, basics of magnetism, processing of rare earth magnets, their characterization and recent trends in the field of RE magnets are presented (Chapter 1). Chapter 2 contains the experimental part that describes materials and technological parameters. The main part (Chapter 3) covers major results, followed by the discussion part. Chapter 4 provides the main conclusions and novelty of the PhD research. Approbation, acknowledgements and the abstract are presented after the references. The copies of the articles and the patent are attached to the appendices.

LIST OF ABBREVIATIONS, TERMS AND SYMBOLS

Abbreviations

ABM	High-energy attritor milling in hydrogen and vacuum
BRP	Ball to powder ratio
CIP	Cold Isostatic Pressing
EBSD	Electron Backscattered Diffraction
EDS/EDX	Energy Dispersive X-ray spectrometry
fcc	face-centered cubic
HD	Hydrogen Decrepitation
HDDR	Hydrogenation, Disproportionation, Desorption and Recombination
HEM	High-energy milling
ICP-OES	Inductively Coupled Plasma Optical Emission Spectroscopy
JM	Jet Mill
MFM	Magnetic Force Microscopy
PLP	Pressless processing
PM	Permanent Magnet
PPMS	Physical Property Measurement System
RE	Rare-Earth
REE	Rare-Earth element
REM	Rare-Earth metal
SC	Strip Cast
SEM	Scanning Electron Microscopy
SPS	Spark Plasma Sintering
VSM	Vibrating Sample Magnetometry
wt%	Weight percentage

Terms

BH curve – shows the relation between magnetic flux density and magnetic field strength for the material

Curie temperature – temperature at which a ferromagnetic material becomes paramagnetic due to the loss of its magnetic properties

Demagnetization – reduction of the magnetization in a permanent magnet

Initial curve – initial magnetization curve reveals the coercivity mechanism

Kerr spectroscopy – magneto-optical spectroscopy for the detection of the domains

Magnetocrystalline anisotropy – directional dependence of the magnetic properties of the material

Maximum operating temperature – maximum recommended temperature of operation for magnetic material

MH (JH) curve – shows the relation between magnetization (magnetic polarization) and magnetic field strength for the material

$Nd_2Fe_{14}B$ – hard magnetic phase of the Nd-Fe-B magnetic material (frequently signed as 2-14-1)
Nd-Fe-B material – Neodymium Iron Boron magnet material
Sm-Co material – Samarium cobalt magnet material
Splat quenching – extremely rapid quenching of the molten alloy usually by pouring the melt onto a massive cooled copper plate

α-iron – soft magnetic phase of iron, bcc structure

Symbols

$BH_{(max)}$	Maximum energy product, kJ/m^3
B_r	Remanence of permanent magnet, T
H_{ci}	Intrinsic coercivity of a permanent magnet, A/m (usually kA/m)
J_r	Magnetic polarization, T
T_c	Curie temperature, °C
T_m	Maximum operating point, °C
α	Temperature coefficient for the remanence, 1/°C
β	Temperature coefficient for the coercivity, 1/°C

1. LITERATURE OVERVIEW

This chapter provides a concise theoretical background of magnetic materials and processing of Nd-Fe-B magnets. Microstructure, phases, chemical composition and domain structure, methods of manufacture, applications and cost will be covered. A brief history of Nd-Fe-B compound development and recent trends in neodymium magnets will be presented.

1.1. Introduction

In 600 BC, Greek philosopher Aristophanes discovered that amber mineral rubbed with a fur starts to attract small pieces of light materials. For centuries, this strange effect remained a mystery until Dr William Gilbert's discovery of magnetism and static electricity. He concluded that the Earth is magnetic and contains a centre of iron. He also detected that PM has always two poles and that the division of a PM results in smaller magnets. Later, Oersted proved that a magnetic field is generated also by an electric current passing through a conductor [4, 5].
In PM materials, the magnetic field arises from electrons circulating around the nucleus of an atom or the electron spins [6].

1.2. Magnetic hysteresis

Before discussing the magnetic materials it is essential to understand some of the core aspects in the interpretation of magnetic materials' properties. These fundamentals are covered in brief in this chapter.

1.2.1. Initial magnetization curve

In coercivity mechanisms, nucleation or pinning can be determined from the shape of the initial magnetization curve (Fig. 1.1) [4]. In a nucleation mechanism, magnetization increases rapidly already at low fields. This shows the easy movement of domain walls as they are not pinned significantly (Fig. 1.1a, b). In the pinning type magnet (Fig. 1.1c), magnetization increases drastically only when the strength of applied field is close to coercivity. It corresponds to the trapped domain walls; therefore, the increase in magnetization with the increase of the field is slow [7]. Pinning centres could be defects, inhomogeneities or inclusions in the material [4]. Generally, in a magnetic material with $Nd_2Fe_{14}B$ structure, the nucleation mechanism is dominating. Samarium cobalt PMs mainly show a pinning type coercivity mechanism [8].

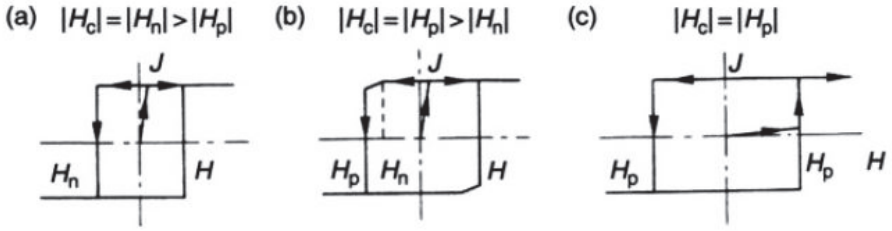

Figure 1.1. Initial magnetization curves (a) nucteation type PM; (b) nucleation and pinning of walls at grain boundaries type PM; (c) pinning type PM [8].

Durst and Kronmuller [9] suggest that nucleation is dominating for Nd-Fe-B PMs at low temperatures, while pinning of domain walls at the grain boundaries starts to play an important role at higher temperatures. The changes in the magnetic field affect the domain structure. As illustrated in Fig. 1.2, domains turn along the direction of the applied field as the magnetic material approaches the saturation magnetization [10].

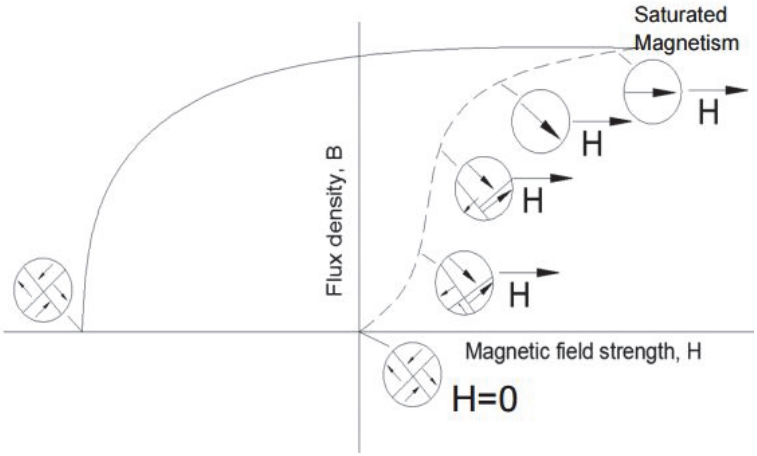

Figure 1.2. Stages of magnetization/demagnetization of the ferromagnetic material [10].

1.2.2. Hysteresis loop

The hysteresis loop common for hard magnetic materials is presented in Fig. 1.3. The vertical axis corresponds to the magnetization of the PM, while the horizontal axis represents the applied external field. Before applying the magnetic field, material is not magnetized (H=0). Magnetization starts to increase immediately with the external field ($\mu_0 H$ in Fig. 1.3) and rises until achieving saturation ($\mu_0 M$ in Fig. 1.3). Decreasing the field after reaching the saturation magnetization will remain almost constant close to the saturation level (MH curve in Fig. 1.3). The magnetization at the zero field after the material were saturated is called remanence ($\mu_0 M_r$ in Fig. 1.3) of the PM.

Increasing the reverse field at the some point will initiate the demagnetization of the material. The value of magnetization of the PM becomes zero once the coercivity ($_MH_c$ in Fig. 1.3) is reached. Reverse magnetization will start to increase once the coercive field is exceeded. At the saturation field the magnetization reaches its maximum.

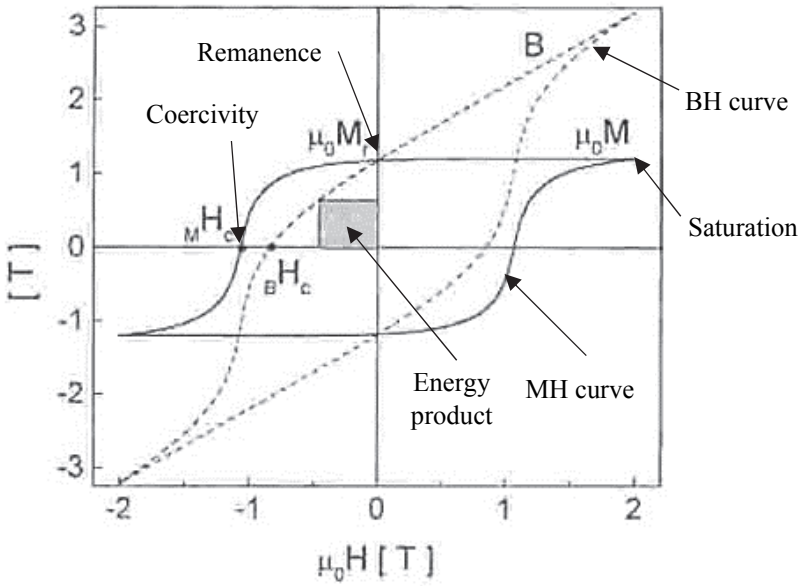

Figure 1.3. BH and MH loops [11].

Three fundamental features that describe PM performance are remanence B_r, intrinsic coercivity H_{ci} and maximum energy product $(BH)_{max}$. Remanence determines the magnetic field generated by the magnetic material. Intrinsic coercivity characterizes the material's resistivity to demagnetization. The grey rectangular marked in Fig. 1.3 represents the maximum energy product equivalent to the largest area that could be inscribed inside the BH curve. Fig. 1.4 shows evolution of the energy product of PM materials in the 20th century.
The shape of the hysteresis loop is directly connected to experimental conditions, geometry of the sample and preparation aspects (processing steps). For that reason it is difficult to associate magnetization loop with a specific material. Despite the apparent impracticability of the magnetization loop connection to the material and interpretation without additional information concerning the experimental history and shape of the magnet, the loops are widely used to compare scalar values of the magnetization components and also describe the behavior of the material easily and conviniently [11].

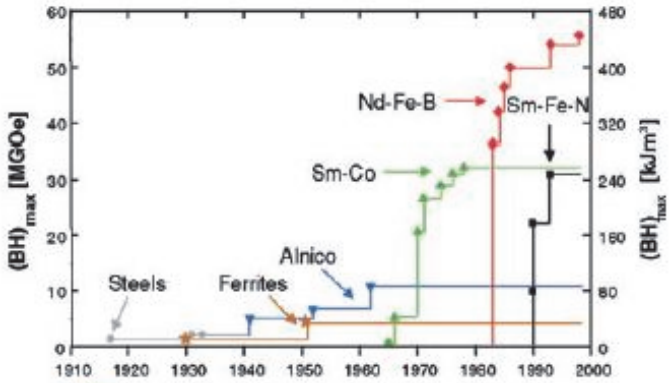

Figure 1.4. Energy product evolution of different kinds of PMs [12].

1.3. Nd-Fe-B permanent magnets

In the 1970s, the instability of Co supply and prices accelerated the search of new magnetic materials other than Sm-Co. In 1979, a Ukrainian researcher Kuzma reported the existence of the Nd-Fe-B compound [4]. Only four years later, Sagawa in Japan prepared a magnet with the chemical composition of $Nd_{15}Fe_{77}B_8$. Powder metallurgy processing similar to Sm-Co magnets was adopted to produce a magnet with $(BH)_{max}$ 290 kJ/m^3 [13]. At the same time, USA researchers Croat and Herbst developed melt-spun RE-Fe-B magnets with nanocrystalline structure; the same phase composition [14, 15] as reported by Sagawa. The tetragonal magnetic phase $Nd_2Fe_{14}B$ was identified [16].
Since that time, continuous efforts have been made to enhance both the magnetic properties and the thermal stability and corrosion resistance of RE-based magnets. These characters can be reached by optimizing the microstructure and chemical composition of the magnets.
Today China is the largest producer of Nd-Fe-B PMs in the world. Production amounts of both sintered and bonded magnets reach 95% of the total RE magnets production. The sales amounts of Nd-Fe-B magnets have a tendency to expand and other types of magnets decrease due to replacement by RE PMs [17, 18].

1.3.1. Methods of manufacture

PMs based on Nd-Fe-B are widely used in many areas as these provide a strong magnetic field. Two mass production methods have been developed. The first is powder metallurgy to achieve anisotropic high-performance and fully dense PMs; the other is used to produce bonded magnets mainly from rapidly quenched materials and HDDR (hydrogenation, disproportionation, desorption and recombination) powders. Bonded magnets are mainly used in sensors and actuators for electrical equipment. Sintered Nd-Fe-B magnets are effectively implemented in demanding applications, such as power generators and motors for electric automobiles and other vehicles [19].

1.3.2. Powder metallurgy technique

Sintered Nd-Fe-B magnets are mass produced through a powder metallurgical process, as shown in Fig. 1.5. The production technique is well established and optimized by many industrial manufacturers.
Generally, the production of a PM starts from melting of the elements like Nd, Pr, Dy, Fe or Fe-B in the induction furnace and ingot casting via book molding or strip casting (SC). Ingots are coarse crushed by the procedure called Hydrogen Decrepitation (HD). The following jet milling in the nitrogen flow disintegrates the powder to approximately 3…5 μm. It guarantees that the powder consists of single grain particles. Fine powders are compacted in the presence of an external field to align and lock the grains. Green bodies are consolidated during sintering in vacuum or protective gas atmosphere at temperatures above 1000 °C. To improve the performance of the magnet post sintering heat treatment at temperature up to 900 °C is essential. Finally, the machining and surface treatment is performed. The last step in magnet production is magnetization.
Each production step, except grinding, slicing and coating, has an impact on the final microstructure and properties of the magnet. The most influential manufacturing stages are casting, fine milling and sintering.
Rapid cooling is advantageous to avoid the formation of α-iron dendrites during ingot casting [20]. Firstly, α-iron increases the toughness of the ingots and it is therefore more difficult to refine [4]. Secondly, the presence of the soft α-iron phase deteriorates the magnetic properties of the final product, as the chemical composition of the phases changes [21]. Presence of α-iron leads to formation of extra Nd-rich regions and other secondary phases hindering the maximization of hard phase forming. Strip casting (SC), which allows higher cooling rates and results in a finer structure with homogeneous distribution of RE-rich phase, and addition of dopants, can effectively suppress the formation of an undesired soft iron phase [22, 23].
A major challenge for processing Nd-Fe-B powders is reactivity and easy oxidation of REEs. Milling the powders reduces the particle size, which makes these even more prone to oxidation. The final magnetic properties, especially coercivity, are influenced by the particle size and the total oxygen content in the magnet [24]. As a result, the Nd-Fe-B magnetic powders should be produced and handled carefully in a controlled environment. This increases the cost of the Nd-Fe-B magnets.
Oxidation is an issue also very important during sintering. It is beneficial to avoid any contamination as it is hardly possible to obtain fully dense magnets in an environment not sufficiently clean. Sintering temperature and post sintering heat treatment regime play an important role in the formation of microstructure and final magnetic properties. The sintering temperature should be high enough to liquefy the grain boundary, but not too high to prevent the grain growth [25]. Sintering regimes have been optimized for different chemical compositions of the magnetic materials. Usually, the sintering temperature is around 1080 °C while the RE phase starts to melt at about 650 °C. Heat treatment temperatures vary

between 500 °C and 950 °C. The heat treatment cycle is essential to optimize the microstructure, especially the morphology and content of intergranular RE-rich layers [26].

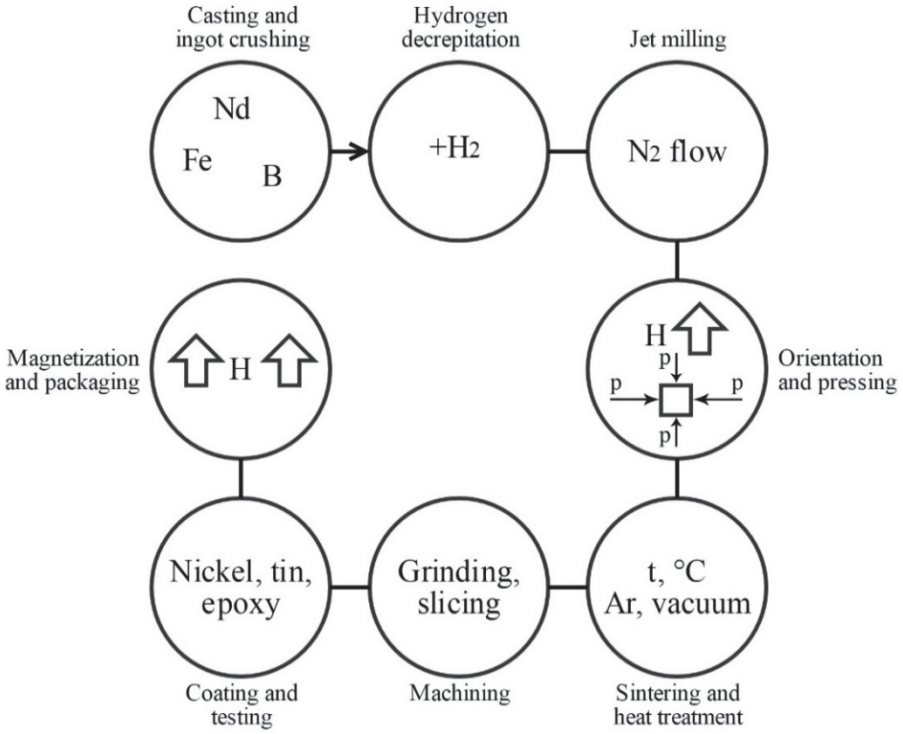

Figure 1.5. Production process of sintered Nd-Fe-B PMs.

The importance of HD and compaction of green bodies should not be underestimated. HD allows us to exclude jaw and raw crushing steps and obtain fine powders that are very friable and easily refined in the jet mill [4].
Oriented green compacts can be produced in a magnetic field either by parallel alignment and pressing, perpendicular alignment and pressing, isostatic or rubber isostatic pressing. Isostatic pressing normally results in a higher powder orientation. Pressing load should be sufficient to produce a green body strong enough to be handeled easily but not too high to avoid misorientation of the grains [4].

1.3.3. Bonded Neo magnets

Conventionally, the rapid solidification process (strip casting) is adopted to prepare alloys in the form of strips or flakes for bonded Nd-Fe-B PMs. Thin structured flakes are ground to fine powders and heat treated to develop an appropriate microstructure and magnetic properties [14]. The other mode is

HDDR processing, which requires several heat treatments in hydrogen and vacuum to refine the structure and enhance the properties of PMs [27, 28].
In bonded magnets magnetic particles are molded in a polymer matrix. Compression, injection [29] and extrusion [30] are used to fabricate bonded Nd-Fe-B PMs.
Both coercivity and remanence of the bonded magnets in comparison to sintered Nd-Fe-B PMs are lower (see Fig. 1.6). However, wider variety of shapes and lower cost makes the bonded magnets attractive for many applications [31].

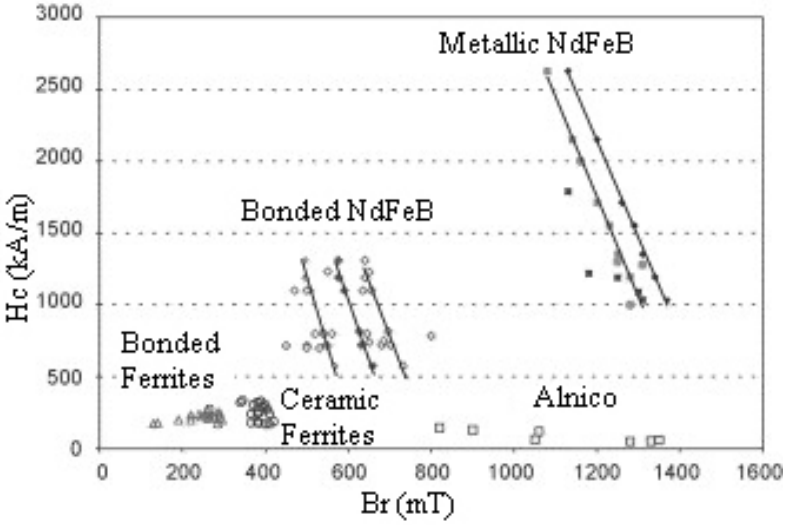

Figure 1.6. Comparison of commercial PMs [29].

1.3.4. Microstructure

Typical microstructures of sintered Nd-Fe-B PMs are shown in Fig. 1.7. The grains of the hard magnetic phase $RE_2Fe_{14}B$ (grey) are surrounded with thin RE-rich layers (white) at grain boundaries. RE oxides agglomerate in triple junctions [32]. Usually, a small amount of the B-rich phase is also present [33].
The RE-rich phase is amorphous and non-magnetic. The hard magnetic phase grains are commonly 5-8 μm in size, and the intergranular RE-rich layer is about 1 nm in thickness [32]. The hard magnetic phase defines the magnetic behavior of the PM. The RE-rich regions determine mostly the coercivity of the magnetic materials.

1.3.5. Soft and hard magnetic phases

As stated in the previous chapter, remanent magnetization originates from the magnetization of the hard magnetic phase. The remanence of the PM could be increased with a higher content of the hard phase. Higher alignment ratio of the crystals also contributes to the remanence [2, 34]. Rapid solidification of the

magnetic alloy is required to obtain the hard phase, otherwise the possibility of formation of α-iron is high, especially in the materials with lower RE content. The iron phase is unbeneficial as it tends to deteriorate magnetic properties due to inefficient grains alignment and more drastic oxidation of the RE regions [35]. The results of the microstructure analysis of the Nd-Fe-B PMs indicate a relation between coercivity and morphology of the intergranular RE-rich layers [36]. The RE-rich grain boundary isolates the grains, thus enhancing the nucleation of the reversal domains and inhibiting the propagation of the magnetic reversal in the grains.

Vial et. al. found positive influence from post sintering heat treatment on the coercivity of PMs [26]. The observation of the morphology of the RE-rich regions has shown the importance of the isolation between the grains for resistivity to demagnetization of the material [26]. In other words, the RE-rich layers should be continuous and thin to provide an enhanced coercive force (See Fig. 1.7a, b and c). The heat treatment (annealing) mainly dissolves the irregularities of the grain boundaries and defects disappear [26, 37].

The combination of EBSD and EDX allowed Woodcock [38] to define the Nd-rich phases in Dy-free magnet. Three different types of Nd-rich phases were identified: Nd_2O_3, NdO and fcc Nd-rich phase lean in oxygen. The investigations showed that the type of the Nd-rich phase depends on the total oxygen amount. The higher the oxygen content, the more Nd_2O_3 is present in PM. As it was stated earlier, the magnetic properties of the material decrease with the increased oxygen content. This issue is even of greater importance as the grain size decreases. The degradation of coercivity takes place when the critical grain size is achieved and the metallic Nd phase oxidizes actively to Nd oxides. The lack of Nd phase hinders the formation of continuous intergranular layers [39, 40]. Addition of Cu and Al improves the wettability of the grain boundaries and results in the formation of continuous RE-rich layers [41, 42].

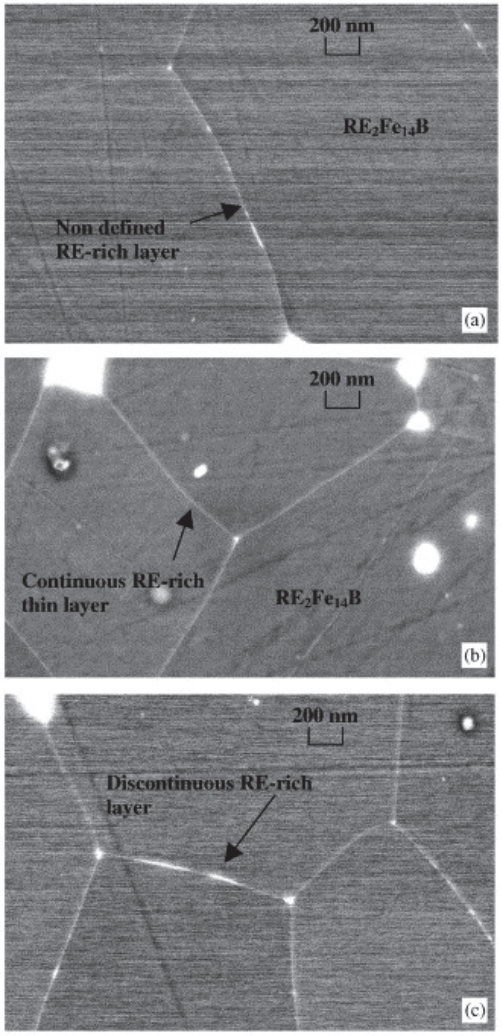

Figure 1.7. SEM image of as sintered Nd-Fe-B PM (a); PM after optimized annealing (b) and non-optimized annealing (c) [26].

1.3.6. Chemical composition

Additives and a dopants are usually intoduced to the Nd-Fe-B PMs to influence the properties of the materials. Commonly, these are added in order to increase the magnetization, coercivity, Curie temperature or magnetocrystalline anisotropy of the RE PMs. The influence of different additives investigated extensively, is summarized by Davies [25]. Most common additive elements and their effects on the microstructure and magnetic properties are displayed in Table 1.1.

Table 1.1. Common additions and their influence on the microstructure and magnetic properties [25]

Additive element	Location in microstructure	Effect on	
		Microstructure	Magnetic properties
Cu	Grain boundaries	Modifies grain boundary phases, wetting improved	iHc improved by small additions Br unaffected by small additions
Co	Matrix and grain boundaries	Nd_3Co phases formed at grain boundaries, Co substituted for Fe in matrix	Increases curie temperature of $Nd_2Fe_{14}B$ phase, increases Br, decreases iHc
Al	Matrix and grain boundaries	Improves wetting during sintering producing smother grains	Lower Br due to formation of non-magnetic phases, improved iHc due to isolation smoothing
Nb, V	Grain boundaries	Borides formed at grain boundaries	iHc improved due to reduced grain growth in sintering
Dy	Uneven distribution in matrix phase	Substitutes for Nd to greater extent at edges of matrix grains	Improves iHc through grain- isolation, decreases Br through anti ferromagnetic coupling

In addition to classical and widely used dopants, numerous uncommon variations have been recently investigated. MgO and ZrO were reported to improve the remanence and corrosion resistance due to higher densification of the PM during the sintering process [43, 44]. Nano-Dy or nano-DyH_x particles have been added, resulting in higher coercivity at lower Dy input [45, 46]. TiC or Ti with C influences positively the thermal stabilitiy of the magnetic material thanks to smaller and more homogeneous grain size enhancing the exchange coupling pinning field [47, 48, 49]. Combined addition of Dy_2O_3 and Zn increases the coercivity and thermal stability of nanocrystalline PMs prepared by the SPS method [50].
The most challenging and unbeneficial effect of the different additives is their positive influence on one particulate property that is accompanied with deterioration of another one. It is required to determine and consider the optimal conditions.

1.3.7. Domain structure

Domains are small magnetic regions in the grains of magnetic materials separated with domain or Bloch walls. In a non-magnetized state, the magnetization vectors on different domains are randomly oriented in a magnetic material. The total magnetization is zero. During magnetization, magnetic vectors of domains orient in the same direction [51]. Fig. 1.2 in section 1.2.1 presents schematically the change in domain orientation.
Several methods have been found to observe magnetic domains – Kerr and Lorentz microscopy [52, 53, 54, 55], Magnetic Force Microscopy (MFM) [56]. These methods allow recognition of the domains only on the PM surface.

The images obtained with Takezawa's Kerr spectroscopy for the the thermally demagnetized PM allow us to see the presence of interaction domains of the hard phase. When the saturation is achieved, no iteration domains are visible and the material acts as a single domain material. The decreased coercivity of a sintered PM at high temperature is attributed to a decrease of the anisotropy and ineffective pinning of the domain walls at grain boundaries.
A typical Kerr microscopy image is presented in Fig. 1.8. It represents the domain images with an external field of +14 and –14 kOe applied at room temparature along the magnetization axis.

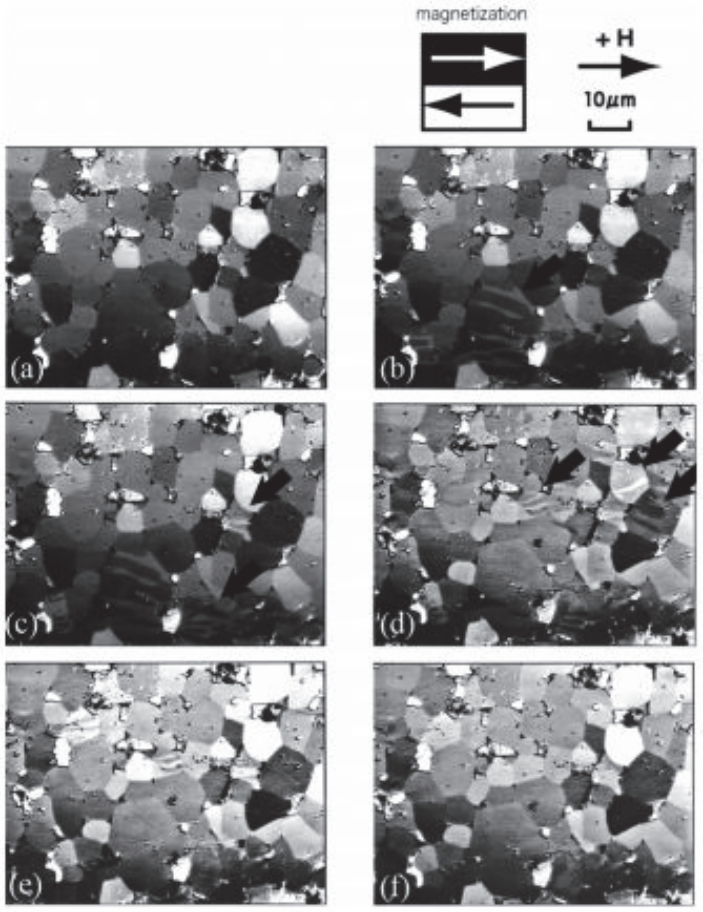

Figure 1.8. Domain images of RE PM at applied external fields: (a) +14 kOe; (b) +1.1 kOe; (c) +0.8 kOe; (d) 0 kOe; (e) –1.4 kOe; (f) –7.2 kOe [52].

MFM images provide information concerning the spike and reversal domains, defect regions and the nucleation area. It is possible to determine the domain wall width and domain wall energy for both surfaces perpendicular and parallel to the alignment axis. MFM technique allows demonstrating the influence of the defects

on the coercivity. Domain structure obtained with the MFM technique is presented in Fig. 1.9.

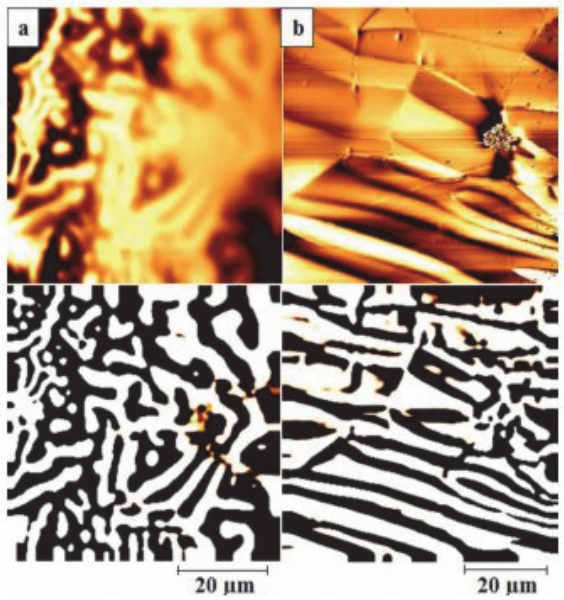

Figure 1.9. Domain structure of sintered RE PM observed with MFM: (a) perpendicular to the alignment axis; (b) paraller to the axis. Upper and lower raws show original MFM images and enhanced MFM images, respectively [56].

1.3.8. Losses

At room temperature, the magnetic properties of Nd-Fe-B PMs are superior in comparison to those of Sm-Co PMs. Magnetization starts to deteriorate with an increasing temperature and losses occur. The total loss includes reversible, irreversible and structural losses. The structural losses are irrecoverable [4].
If the critical temperature is not exceeded, losses will be reversible. The magnetization will recover once the temperature is decreased. These losses are usually characterized with temperature coefficients for both coercivity and remanence for the specific temperature range (for instance, between 20 °C and 100 °C) [4, 19].
Irreversible losses occur due to spontaneous demagnetization in some regions of the material. Irreversible losses are recoverable with the remagnetization of the PM. Due to additional corrosion, some extra non-recoverable losses may appear (structural losses) [19]. It can be concluded that recoverable losses mainly depend on the coercivity [57].
It is essential to control and predict the reversible losses of the material for an application design [58]. To avoid irreversible losses, the maximum operating temperature should not be reached or exceeded. If magnetic material oxidizes, in addition to recoverable losses, permanent structural losses will arise.

1.3.9. Long-term performance

Stable characteristics of a PM material during its lifetime are important in selecting an appropriate material for different applications. Characterization of the long-term stability is difficult as the knowledge of this phenomenon is insufficient and testing is time consuming. Haavisto [59] assumes that for materials with a squarer MH demagnetization curve, losses are very small at temperatures even up to 130 °C and could be neglected. Once the temperature exceeds the critical temperature, significant losses occur. Generally, it is possible to estimate the critical temperature under which even after 30 years, the loss of polarization will not exceed 1%. The rounder the BH curve, the earlier the losses will occur and have a stronger effect on degradation.

1.3.10. Thermal stability

The magnetic behavior of the RE PMs is dependent to the temperature. The polarization and coercivity are decreasing with the increasing temperature. The critical temperature usually called maximum operating temperature T_m should not be exceeded. This will prevent the degradation of the PMs and possible failure of the assembly/machine. Generally, maximum operating temperature increases with the increase of Curie temperature T_C that refers to the temperature at which the ferromagnetic material changes to a paramagnetic. The Curie temperature depends on coercivity. Commonly, higher coercive force results in higher temperature stability of the magnetic material.
The thermal stability is usually characterized with a maximum operating temperature, Curie temperature and two temperature coefficients of the remanent polarization and the coercive field.
For high temperature sintered Nd-Fe-B magnets, the heavy REE Dy is frequently added. Dy increases the coercivity and consequently has a positive impact on the thermal stability of the PMs. Due to Dy availability and high price it is beneficial to reduce the content of Dy in PMs. Recent approaches are targeted towards reduction of Dy content or its total substitution [60, 61, 62, 63].

1.3.11. Corrosion resistance

REMs belong to the group of highly reactive elements. Frequently, RE PMs are exposed to hot and humid environments. Under such conditions, in case the protective coating is damaged, the surface of the PM can be corroded and RE regions oxidized. The PM material will degrade and lose its magnetic properties. The reactivity of REMs is rapidly accelerated at higher temperatures [5].
To protect magnetic materials from corrosion, two methods have been applied. In the first technique, additives are introduced to influence the chemical composition and in the second, protective layers are deposited on the surface of the sintered PMs. Adding alloying elements often has a negative effect on the

magnetic properties of PMs. Therefore, corrosion resistance studies are mainly focused on the development of protective coatings [64].
Standard coatings include nickel, copper nickel and zinc plating, which however, often have insufficient adhesion on the surface [65]. Resulting from the analysis of magnetron sputtering of aluminum and cobalt based coatings, a higher anti-corrosion effect was found [66, 64, 67].

1.4. Recent trends in Nd-Fe-B magnets

The trends in the development of magnetic materials can be divided into three main categories. Firstly, to decrease the amount of heavy REMs so that competitive magnetic characteristics remain unchanged. Secondly, the aim is to improve the processing technology towards enhanced performance of the magnets and to reduce the costs. Thirdly, efforts are made to recycle the Nd-Fe-B magnets, especially hard duty RE magnets with a high content of heavy REEs. All of these objectives are challenging. It is difficult to find an additive as useful and effective as Dy to improve the coercivity and consequently thermal stability of the sintered magnets. Secondly, most of the developed processing technologies tend to be uneconomical or unsuitable for mass production and thirdly, in regard to recycling, the most difficult part at present is to collect and separate the magnetic scrap prior to the reprocess cycle.
Although remanence and maximum energy product of the magnets reach over 90% of the maximum theoretical values, the coercivity a lot of potential to be improved [1]. The grain refinement is one possibility to enhance the coercive force, while the grain boundary diffusion is the other [20, 68, 69, 70]. As the main effort is aimed to avoid or minimize the use of heavy REEs, especially Dy, it is reasonable to enrich only grain boundaries with Dy, instead of the whole $Nd_2Fe_{14}B$ grain. The diffusion method allows producing only thin magnets [68]. Addition of several percent nano-Dy particles results in a positive effect on the magnetic properties comparable to 10% of micron sized Dy powder addition as nano-Dy segregates along the grain boundaries [45, 71]. High-speed jet milling in helium and the following PLP processing was developed by Sagawa, allowing to obtain Dy-free magnets with a remarkable improvement of coercivity [72].
Recycling of the PMs is attracting increasing attention as there is no competitive and nature friendly technique to reprocess and reuse the RE based magnets. In most cases, devices containing magnets are not separated but recycled together with steel scrap. The most recent methods proposed for reprocessing the magnetic materials are HD, HDDR and hydrometallurgical methods [73, 74, 75]. It is possible to either manufacture recycled PMs or recover REMs [76, 77, 78].

1.5. Aims of the work

After 30 years of Nd-Fe-B magnets use in computers (hard drive magnets), in the field of healthcare (MRI, orthopedics), automotive (sensors, small motors, ABS systems, etc.) and audio applications (headphones, loudspeakers, microphones),

their utilization turns more and more to high temperature applications such as wind generators, wave power and larger motors for electric vehicles. In a long-term perspective, in addition to magnet performance, the availability and price of the critical RE metals (Nd, Dy) has a strong impact on development of both the magnetic materials and power industries.

The general goal of this PhD research is to reduce the use of critical RE metals in high-performance magnets without compromising magnetic properties or temperature stability of the material.

The main target is to develop advanced permanent magnet materials based on the Nd-Fe-B system.

The main objectives of the research are:

- To develop and produce magnetic alloys with controlled composition and microstructure by substituting partially Nd, Pr with a less critical RE metal;
- To develop a set of methods and procedures for obtaining fine and ultra-fine grained Nd-Fe-B powders with high purity (low level of contaminants – oxygen and α-iron);
- To develop novel micro-alloying techniques for Nd-Fe-B magnets and thus improve the performance at high operating temperatures and reduce the consumption of heavy RE metals (Dy, Tb).

The following challenges were overcome and mastered throughout the work:

- Processing of RE magnets on the laboratory scale;
- Characterization of microstructure, phase analysis;
- Evaluation of magnetic properties;
- Control over impurities during laboratory scale processing;
- Partial substitution of Nd, Pr with other RE;
- Improvement of thermal stability without using heavy REEs;
- Applying a new technique for preparing PMs, including novel hydrogen-vacuum milling and rapid sintering by SPS.

1.6. Structure of the work

Fig. 1.10 represents the structure of the research. The thesis contains four parts. The first part reveals the challenges in the preparation of magnetic alloys (Paper I). The next two parts focus on powder preparation as it is one of the most important steps of PM production and has a significant influence on the final properties (Paper II and III). Then, thermal stability and performance of PMs at higher temperatures via introducing nano-TiC particles into PM material are analyzed (Paper IV). The additional parts not shown in Fig. 1.10 address the results of the study of fine-grained SPSed PMs and the optimization study of jet

milling. These publications are not attached to the current thesis, however are used in the body part of the work.

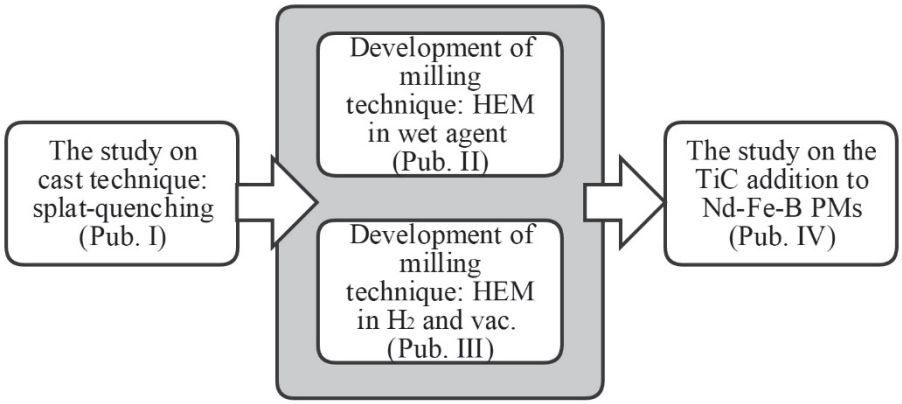

Figure 1.10. Structure of the thesis.

2. EXPERIMENTAL

This chapter describes starting materials and procedures that were used to process the magnets, from alloy preparation and finishing with the characterization of the sintered samples. The chapter is divided into three sections. First, the materials used in this study and their chemical composition are described; second, main processing parameters for the magnet materials are presented; third, the samples are characterized.

2.1. Materials

The experimental magnets were produced mainly from the materials supplied by Molycorp Silmet AS and Neorem Magnets Oy. The research is based partly on book molded alloys, partly on strip casted (SC) alloys and also on alloys produced by splat-quenching method of mixtures of elemental Fe, Nd, Al powders and master alloys FeB, NdFe, NdPrFe, CeFe and DyFe (supplied by Molycorp Silmet AS). Images and microstructures of different raw materials are shown in Fig. 2.1. Some experimental chemical compositions prepared in Tallinn University of Technology are presented in Table 2.1.

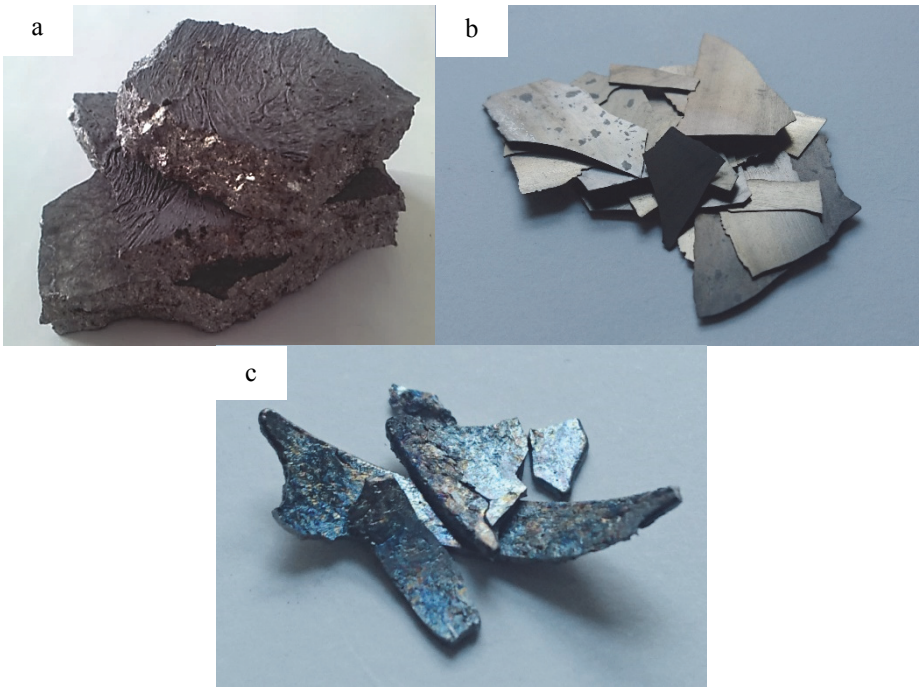

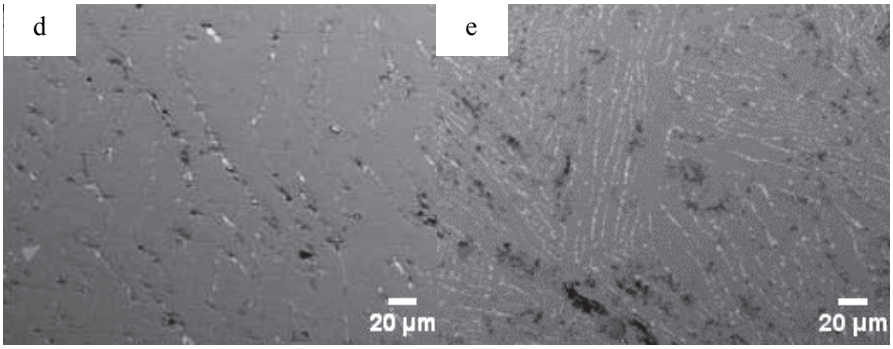

Figure 2.1. Raw materials: (a) book molded alloy; (b) SC material; (c) splat-quenched alloy and microstructures of book molded alloy (d); splat quenched material (e).

Book molded ingot is about 10...15 mm thick. The thickness of the SC flakes is about 0.3...0.5 mm and that of the splat quenched alloy 0.3...4 mm. It can be seen in Fig. 2.1 d and e that the splat-quenched material has finer and more homogeneous structure than the book molded material. Microstructure of SC alloy is similar to that of the splat-quenched material (Fig. 2.1e).

Table 2.1. Chemical compositions of experimental alloys prepared by the splat-quenching technique

Designation	Element, wt%							
	Nd	Pr	Dy	Ce	B	Al	Nb	Fe
A40(Paper I)	22.00	1.80	1.00	8.30	1.20	0.45	0.30	bal
M1	29.34	2.34	1.32	-	1.20	0.45	0.30	bal
M2	32.50	-	-	-	1.20	0.20	-	bal
M3	32.50	-	-	-	1.20	-	0.20	bal
M4	32.20	2.80	-	-	1.20	-	-	bal

2.2. NdFeB magnets preparation route

The block diagram of the preparation process is presented in Fig. 2.2. The classic powder metallurgy route, including a jet mill with high pressure nitrogen gas, external field orientation and vacuum sintering processes, shown as realized in most of the production units, was established on the laboratory scale. The study also analyzed alternative techniques like high-energy ball milling with addition of heptane as a wet agent, dry high-energy attritor milling with hydrogen and vacuum for powder refinement and the following spark plasma sintering (SPS) for samples consolidation. Sections 2.2.1 - 2.2.7 describe each preparation step in detail.

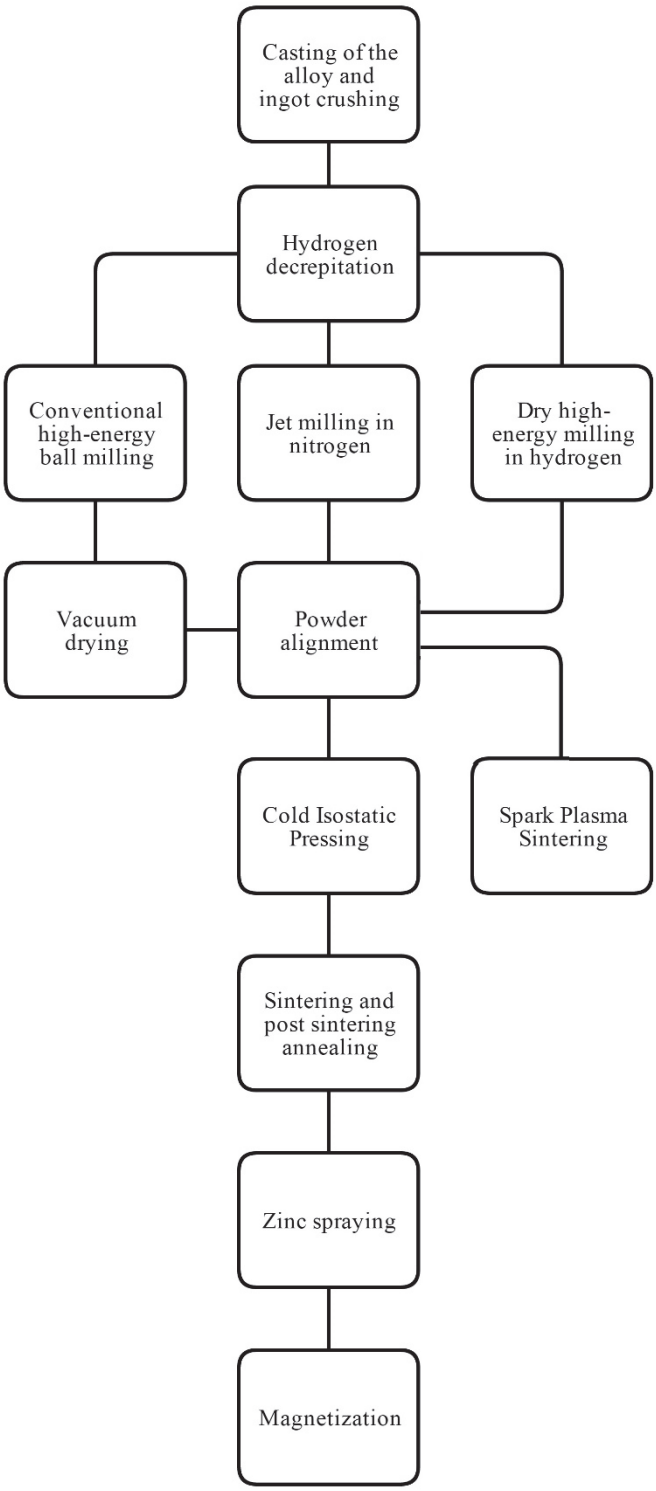

Figure 2.2. Production processes of Nd-Fe-B magnets on the laboratory scale.

2.2.1. Casting of ingots

A laboratory scale magnets preparation line was built up. Centrifugal casting unit *Lifumat Met 3.3 Vac* (Linn GmbH) was used for the splat quenching experiments (see Fig. 2.3). Starting materials (master alloys) were crushed and premix was placed into the tantalum crucible. The mixture was heated under vacuum (10^{-2} mBar) up to 1250 °C within few minutes and held for 5…10 s. Casting was performed into experimental copper mold at the rotating speed of 600 min^{-1} [Paper I].

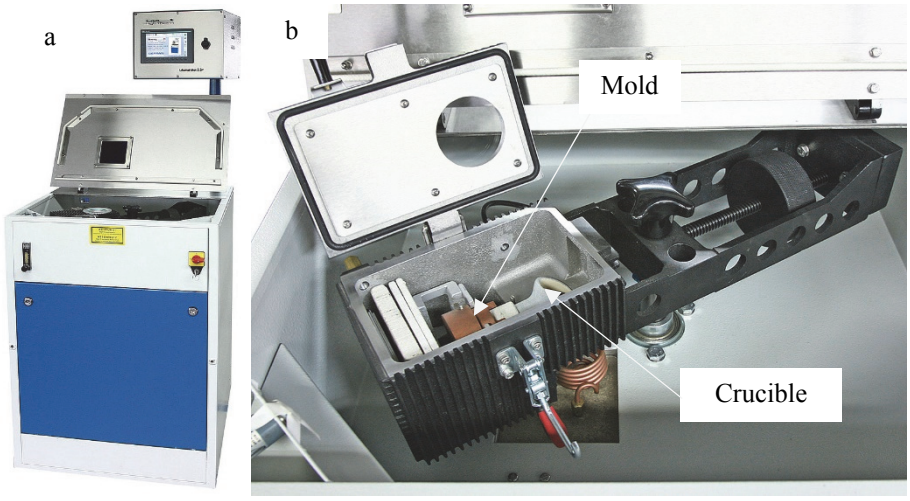

Figure 2.3. Ingot cast: (a) casting unit used for splat quenching experiments; (b) casting arm [79].

The initial experimental quenching of Nd-Fe-B melt was realized onto a copper disc with a thickness of 5 mm. A sketch of the initial casting mold is shown in Fig. 2.4 a.
The cooling rate was not high enough to provide the formation of the required microstructure in the alloy material. In order to decrease the solidified Nd-Fe-B plate thickness (thus increasing the cooling rate), an improved cooling cell was designed. The modified cooling cell is presented in Fig. 2.4 b. The developed mold has a cone shape insert, which first directs the melt towards the outer walls at the angle of 45° (see Fig. 2.4 b). The melt is collected at the thin gap (marked with a in Fig. 2.4 b) between the inner copper insert and the outer copper cylinder [Paper I].

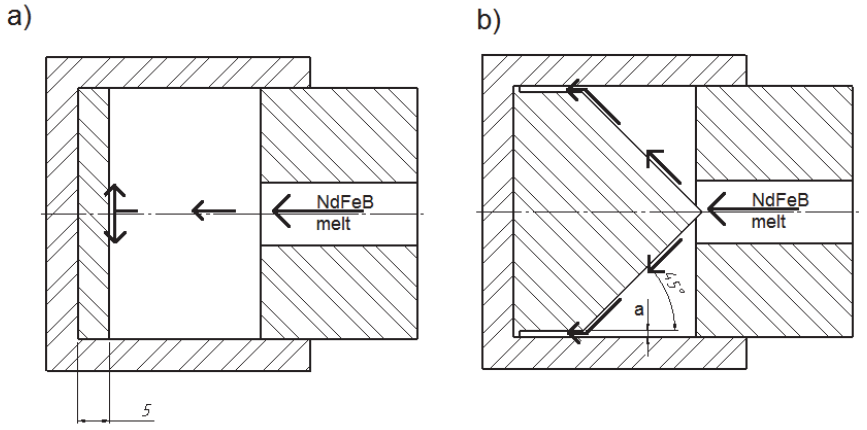

Figure 2.4. Sketch of the centrifugal cast mold design: (a) initial design; (b) modified design. Melt flow is shown with black arrows [Paper I].

2.2.2. Crushing and powder milling

Cast ingots were crushed and processed by the hydrogen decrepitation (HD) technique to fine powders (average particle size less than 400 μm) at room temperature for 2...3 h. Further refinement consisted of conventional high-energy ball milling with addition of wet agent [Paper II], dry high-energy attritor milling in hydrogen and vacuum [Paper III] or jet milling in nitrogen flow [80]. At powder refinement in the attritor filled with hydrogen, raw SC flakes were loaded into the vessel and no hydrogen decrepitation was performed.

2.2.3. High energy wet milling

For ball milling, a 500 ml attritor was used. Milling time varied between 1 and 4 h. Heptane was added as a wet agent to limit the powder oxidation. The solvent was mixed with 20 g of HD powder with the weight ratios of 1:1 and 5:1. The weight ratios of the WC-Co balls to the powders were 5:1 and 10:1. Rotational speed of the attritor varied from 500 to 850 rpm. Refined powders were dried in a vacuum exicator prior to further processing. The attritor used is demonstrated in Fig. 2.5 [Paper II].

Figure 2.5. High energy attritor.

2.2.4. Dry milling in jet mill with nitrogen gas

Nitrogen flow milling was performed by spiral jet mill *MC 44 IR-BD* (Micromazinacione SA). The mill was coupled with a pneumatic powder feeder *P&S IMPAKT-2C* (Powder and Surface GmbH), which allows fully closed-circuit operation (see Fig. 2.6 a and b). The working principle of the powder feeder is based on material transfer by pneumatic pulses (Fig. 2.7). In addition to the ability of grinding gas pressure adjustment, the feed gas pressure and also vacuum pump pressure can be varied.

Vacuum pump pressure influences directly the feed rate (keeping the speed of the particles constant). Within aspiration time limits (pulse duration), the powder feed gas flow rate has no influence on the feed rate but it mainly changes the particle speed injected to the milling chamber. The gas jet stream inside the mill has a certain "stability" threshold and it needs some minimum kinetic energy of the particles to come inside the highly turbulent jet area.

Experiments were designed to vary feed gas pressures between 1 and 5 bar and change the speed of the particles, entering the mill chamber varying vacuum pump pressures between 1 and 4 bar in order to analyze their influence on the final particle size and the feed rate of the powders. Grinding gas was kept constant at the level of 7 bars [80].

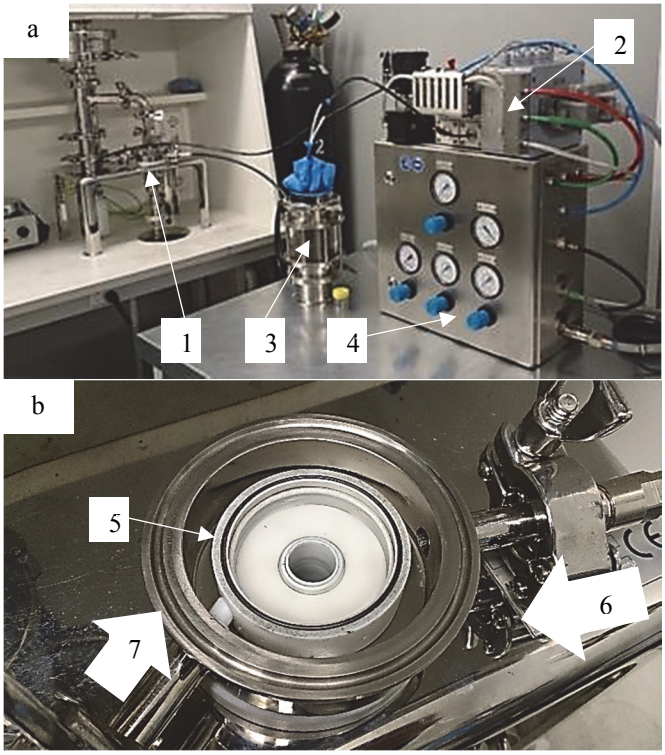

Figure 2.6. Equipment for powder refinement: (a) laboratory scale JM (1) with feeder (2), powder container (3) and controller (4); (b) JM inner (milling) chamber with top cap removed (5), grinding gas inlet (6), feed gas with powder inlet (7).

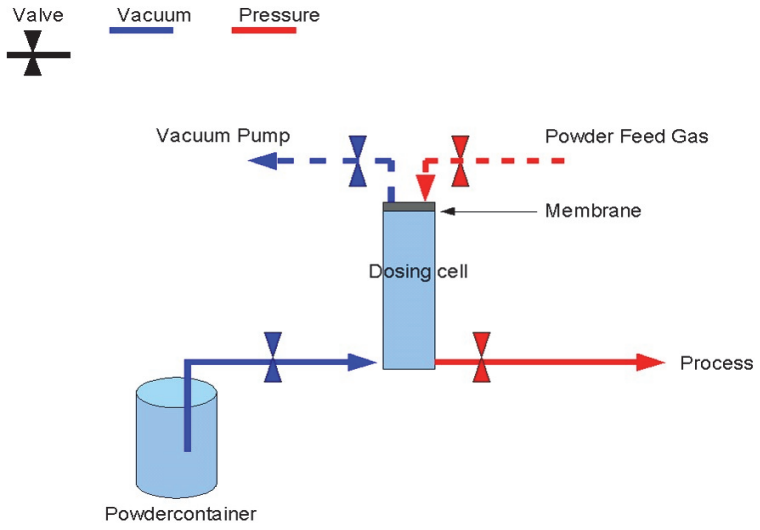

Figure 2.7. Working principle of a pneumatic feeder (feeder shown under 2 in Fig. 2.6a) [81].

2.2.5. High energy milling in hydrogen and vacuum

The high energy attritor for milling in different atmospheres, including hydrogen gas and vacuum, was designed and constructed (see Fig. 2.8). First, the SC flakes and balls were placed inside the milling chamber and the whole system was slowly evacuated to 10^{-3} mbar vacuum. Then, the attritor was filled with hydrogen, keeping the end pressure at 0.3 bar. The pressure was kept constant while hydrogen was reacting with the powder during milling. The scheme of milling consisted of 600 s of dry attritor milling (mill size 2000 mL) with steel balls in hydrogen atmosphere, followed by vacuum milling for 300 s (Fig. 2.9). The weight ratio of the balls to 25 g of the SC flakes was 20:1. [Paper III].

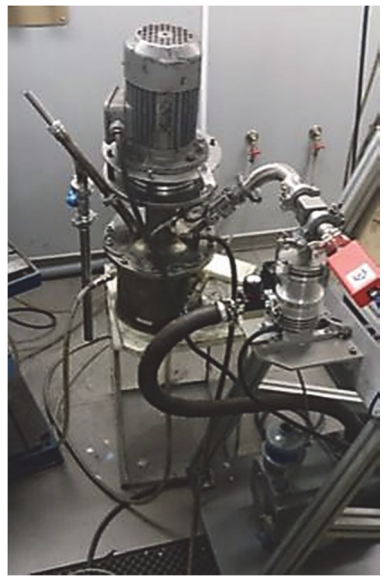

Figure 2.8. Attritor for dry milling in hydrogen and vacuum.

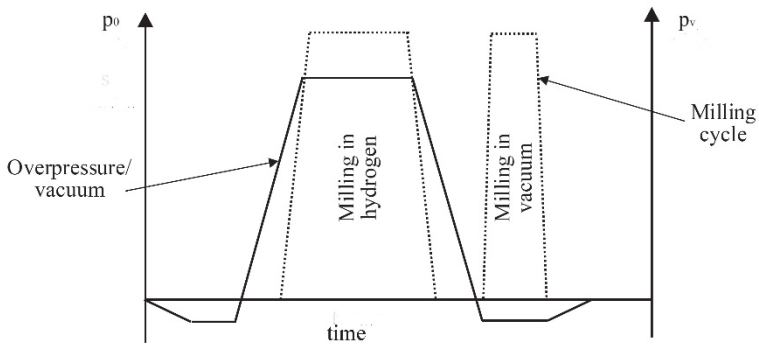

Figure 2.9. Milling sequence.

2.2.6. Orientation, pressing and sintering

The green compacts were aligned by homogeneous external magnetic field generated in 2T coil (designed by Prizztech Oy) and compacted by Cold Isostatic Pressing (CIP) in a rubber mold at a pressure of 100 MPa. Samples with a diameter of 10 mm and height of 5 mm were sintered in high vacuum of at least 10^{-5} mbar for 1…4 h at the temperature range of 1000…1150 °C. Sintering was performed in a stainless steel capsule inserted into the tube furnace (see Fig. 2.10). Sintered magnets were slowly cooled down to room temperature with the furnace in about 3 h [Paper IV].

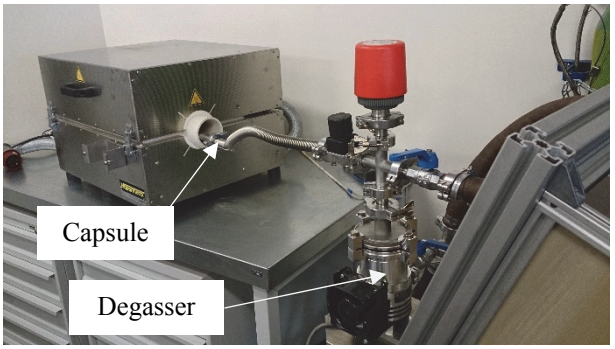

Figure 2.10. Equipment for consolidation: tube furnace with a degassing unit; sintering capsule inserted.

At SPS processing, refined materials were filled into a hardmetal mold and sintered under vacuum of 10^{-2} mbar in a SPS furnace (*FCT Systeme GmbH*). Sintering temperature was 800 °C, holding time 300 s and heating rate 25 °C /min. Pressure of 50 MPa was kept constant during heating and sintering.
The temperature of the sample was measured by a thermocouple placed close to the surface of the mold cavity. After the sintering cycle, the pressure was released and sample cooled to room temperature within 600 s [82].

2.2.7. Protection from oxidation and magnetization

All samples were sprayed with zinc paint to protect them from oxidation. No grinding, machining or slicing was performed. The magnetization was realized in ABB AS with a 14 T external field pulsed magnetizer [Paper IV].

2.3. Characterization of powders and materials

Here only most important analyses or the analyses that are not very common and standard for magnetic materials are described in detail. The most widely used

methods like SEM, EDS, X-ray diffraction, ICP-OES will not be covered. In papers I-IV, all the essential information is provided in detail.

2.3.1. Magnetic properties

The magnetic properties of the samples at room temperature were measured using a vibrating sample magnetometer (VSM) installed either in *Quantum Design Physical Property Measurement System (PPMS)* or in *Cryogenic Limited HTVSM 700* system. Both of them offer a maximum field of 14 T.
High temperature measurements were conducted by a High Temperature VSM Module installed in the *Cryogenic* system that allows a maximum temperature of 425 °C. Fig. 2.11 shows an example of JH and BH curves measured for commercial magnet by PPMS at room temperature. The graph is followed by Table 2.2, showing the measured magnetic properties in comparison to values given by the producer.

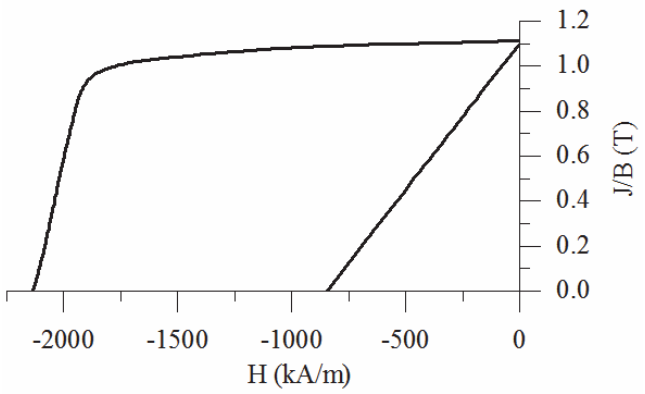

Figure 2.11. 2nd quadrant of JH and BH curves measured at room temperature by PPMS.

Table 2.2. Magnetic properties measured at room temperatures (commercial magnet)

Designation	H_{cj}, kA/m (20 °C)	H_{cb}, kA/m (20 °C)	B_r, T (20 °C)
VSM-PPMS	2132	845	1.11
VSM-Cryogenic	2091	-	1.10
Producer provided	2100	810	1.08

2.3.2. Determination of light impurities

The content of light impurities, especially oxygen, significantly influences magnetic properties of sintered permanent magnets. It is unreasonable to introduce oxygen and moisture to magnetic materials while processing. The most critical production stage is the powder refinemen,t because with increased surface area of the particles, it is more challenging to keep the oxygen level low. In

commercial magnets, oxygen content is about 1000...1200 ppm. Neither should carbon, nitrogen and hydrogen predominate in sintered magnets.
In this work, total contents of oxygen and other light impurities (if necessary) were measured using infrared (IR) spectrometers *Eltra CS800* and *Eltra ONH2000*. The procedure is as follows: a sample (powdered or bulk) is weighed and loaded into carbon or ceramic crucible or sample drop mechanism; the crucible is outgassed to reduce the possible contamination; the sample is evaporated, mixed with carrier gas and the mixture of the sample and carrier gasses are directed through catalysts into infrared/thermal conductivity cells to detect the content of the element. According to the measured element concentration in IR cell/thermal conductivy cell and sample weight, the total weight percentage of the oxygen, for instance, is calculated [83]. The scheme of the oxygen analyzer is shown in Fig. 2.12.
Many measurements were conducted to establish the magnets processing routine on the laboratory scale. Oxygen content was measured after each step to find out "bottlenecks" to improve the system. One of the challenges was the very small amount of the material under processing and a higher possibility for oxidation as a consequence. In Table 2.3, several examples of oxygen, carbon, nitrogen and hydrogen measurements are shown.

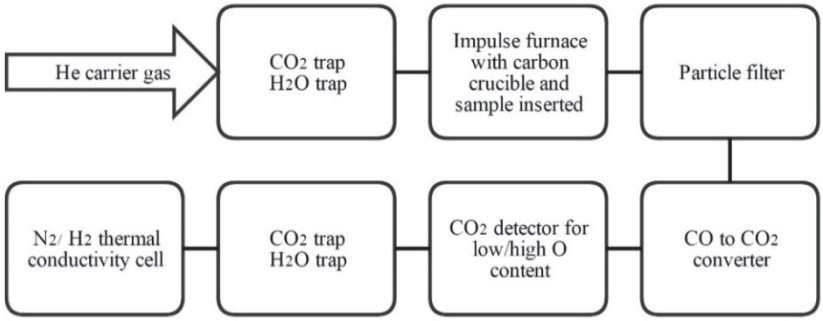

Figure 2.12. Working scheme of the Eltra ONH-2000 analyzer [83].

Table 2.3. Content of light impurities in powders and sintered magnets

Designation	Description	Impurity content			
		O, wt%	C, wt%	N, ppm	H, ppm
Commercial PM 1	sintered, bulk	0.12	0.13	882	76
Commercial PM 2	sintered, bulk	0.14	0.13	400	-
Alloy	book molded, bulk	0.08	0.12	65	30
HD powder 1	hydrogen decrepitated powder	0.09	-	-	-
JM powder	jet milled powder	0.20	-	414	-
Sintered PM	sintered, bulk	0.22	0.12	689	-
HD powder 2	hydrogen milled powder	0.11	-	-	-
SPSed PM	consolidated by spark plasma sintering, bulk	0.19	0.13	346	2472

2.3.3. Characterization of particle and grain size

Besides impurities in the chemical composition of permanent magnets, particle size of the starting powder and grain size of the sintered magnets are very important. To obtain competitive magnetic properties, the grain size of the powder should be equivalent or close to a single domain size. Even more important is the grain size distribution. It is crucial to produce powders with narrow distribution to maximize the properties. Grain growth during sintering is not beneficial. Commercial magnets have particle sizes in the range of 3...5 μm.
At the beginning of the study, a film scanner was used to characterize the particle size. The drawback of the method was the resolution of the machine. Also, laser particle sizer *Analysette 22* (Fritsch) was used. This technique required preparation of the suspension in ethanol. As the magnetic powders were agglomerated, the results were inaccurate.
The most suitable technique for measuring particle and grain size proved to be the statistical analysis of SEM micrographs with ImageJ software. Theoretically, particles or grains should have a circular shape to obtain the highest quality results. The software provides the area occupied by the particle on the micrograph and the diameter can be calculated. With non-round particles, the result is calculated under the estimation that the particle is a circle. As a result, the length of the particle inscribed in a circle rather than the diameter is calculated. An uncertainty occurs but it is not drastic. The analysis made using ImageJ software is exemplified below (Fig. 2.13, Table 2.4). Figure 2.13a shows the appropriate SEM scan of the magnet surface to be processed and analysed. B part of the Figure 2.13 displays modified picture of the same SEM scan prepared for the analysis with ImageJ.

a

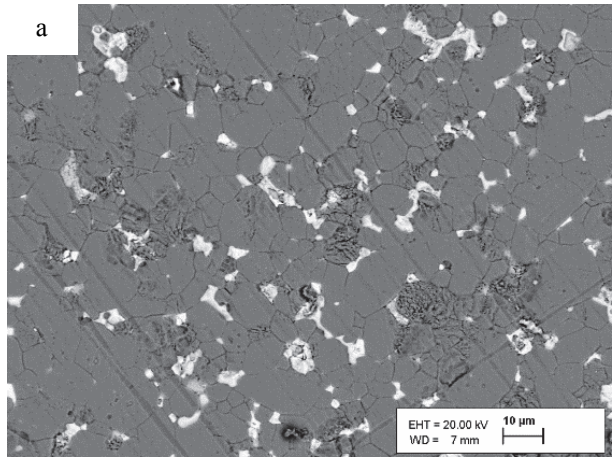

b

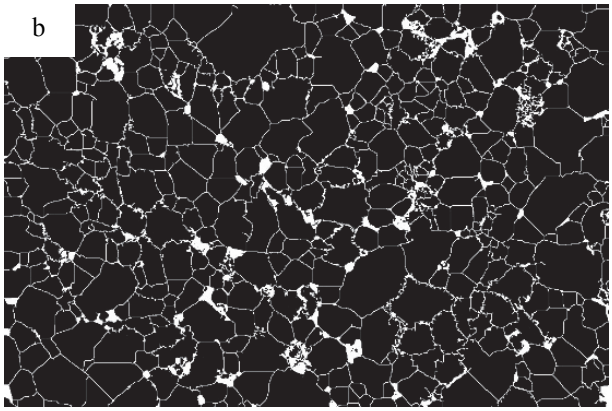

Figure 2.13. Analysis for sintered magnet made with ImageJ software: a) appropriate SEM scan of the magnet surface; b) processed SEM scan, ready for analysis with ImageJ software

Table 2.4. Results from the analyses made with ImageJ

Designation	**Particle/grain size, μm**
Powder 1	1.2
Powder 2	3.3
Powder 3	6.8
NdFeB PM	8.0
NdFeB+1 %TiC PM	6.5

3. TECHNOLOGY, STRUCTURE AND PROPERTIES OF PMs

It was shown in the analysis of recent trends in PM materials based on Nd-Fe-B in section 1.4 that the refinement of the grains and changing the chemical composition influence substantially the resulting properties of PMs. Next, the main achievements of this work will be covered in brief. The replacement of REEs (Nd, Pr, Dy) with Ce and nano-TiC, powder refinement in a high energy attritor with a wet agent, hydrogen and vacuum, and in a jet mill are addressed. Also, the SPS method for consolidation as an alternative method for vacuum sintering and following annealing is discussed.

3.1. Nd and Pr substitution with Ce

The RE-Fe-B alloy where Nd and Pr are partially substituted with Ce was studied to obtain a microstructure free of α-iron with an optimized phase composition. One possibility to avoid α-iron is to introduce a higher content of RE elements. Another route to terminate the α-iron evolvement is a rapid solidification.
According to the experimental results, the cooling rate should be higher than 10^3 °C/s to achieve an α-iron free material. Alloys with thicknesses of 0.3, 0.6, 0.9 and 4 mm were prepared. The cooling rates of the casts were calculated to be equal to $2 \cdot 10^5$, $5 \cdot 10^4$, $2 \cdot 10^4$ and $1 \cdot 10^3$ °C/s, correspondingly.
Fig. 3.1 shows the microstructure of a 4 mm thick sample with an estimated cooling rate of 10^3 °C/s [Paper I].

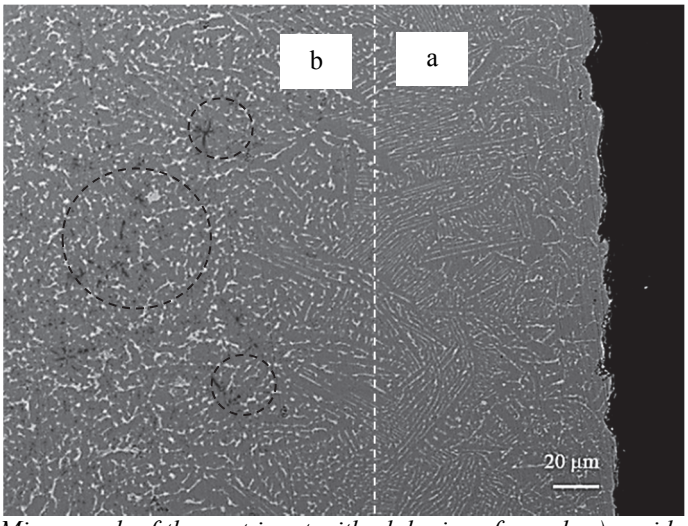

Figure 3.1. Micrograph of the cast ingot with alpha iron formed: a) rapid cooling area that was in contact with the mold; b) area with slower cooling; α-iron areas are shown by dashed circles [Paper I].

Due to relatively slow solidification of the melt, a considerable amount of α-iron was observed, starting from around 100 μm from the contact surface (area b in Fig. 3.1). The α-iron in NdFeB magnets hinders grain alignment and creates Nd-rich regions, which are extremely susceptible to oxidation and therefore magnet degradation. Close-up of the undesired microstructure is shown in Fig. 3.2. Nominations A and B denote the α-iron and oxidation areas, respectively.
It was predicted theoretically that up to 2 mm thick casts with α-iron free microstructure can be produced and a batch size up to 7…8 g with the experimental setup can be increased. For a 0.9 mm thick alloy, the yield is less than 2 g. (For more details see Paper I)
The micrographs of 0.3-0.9 mm thick cast alloys are shown in Fig. 3.3. No α-iron was observed. It is clearly seen that the higher the quenching rate, the finer the microstructure features and the more homogenous the mixture of phases is. The thicknesses of the dendrites (hard phase thickness) vary between 1.08 mm for 0.3 mm alloy and 1.78 mm for 0.9 mm alloy. The thicknesses of dendrite arms (RE-rich phase thickness) are 0.35 and 0.43 mm for 0.3 mm and 0.9 mm alloys, respectively. Also, the contents of hard and soft magnetic phases were calculated. As a renegal rule, the higher the cooling rate, the lower is the content of soft magnetic phase. (More information can be found in Paper I.)

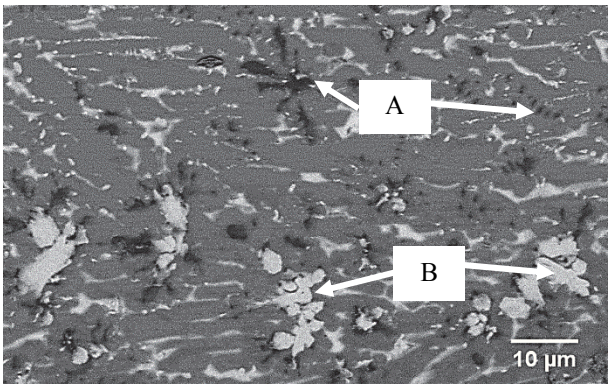

Figure 3.2. Undesired microstructure of the alloy: (A) α-iron; (B) signs of oxidation.

In contrast, SC provides a uniform and α-iron- free dendritic microstructure of the strips with the thickness of 0.2…0.3 mm, hard phase thickness of 4...6 μm and RE-rich phase thickness up to 0.5 μm [36, 26]. In the alloys containing Ce, α-iron dendrites form more easily due to the lower melting point of Ce-Fe-B phase [84].
Generally, PMs prepared from Ce-containing alloys cannot compete with Nd-Fe-B PMs in terms of magnetic properties as the anisotropy of the Ce-Fe-B compound is lower [85]. However, Ce can be a suitable alternative to substitute REEs like Nd and Pr and implement more abundant REM in the manufacturing of cheaper magnetic materials for applications where extremely high magnetic characteristics are not required.

Figure 1.6 in section 1.3.3 compares the bonded and the sintered Nd-Fe-B. There is a gap in the performance between these two types of PMs, and REEs replacement to Ce has a potential to fill it.

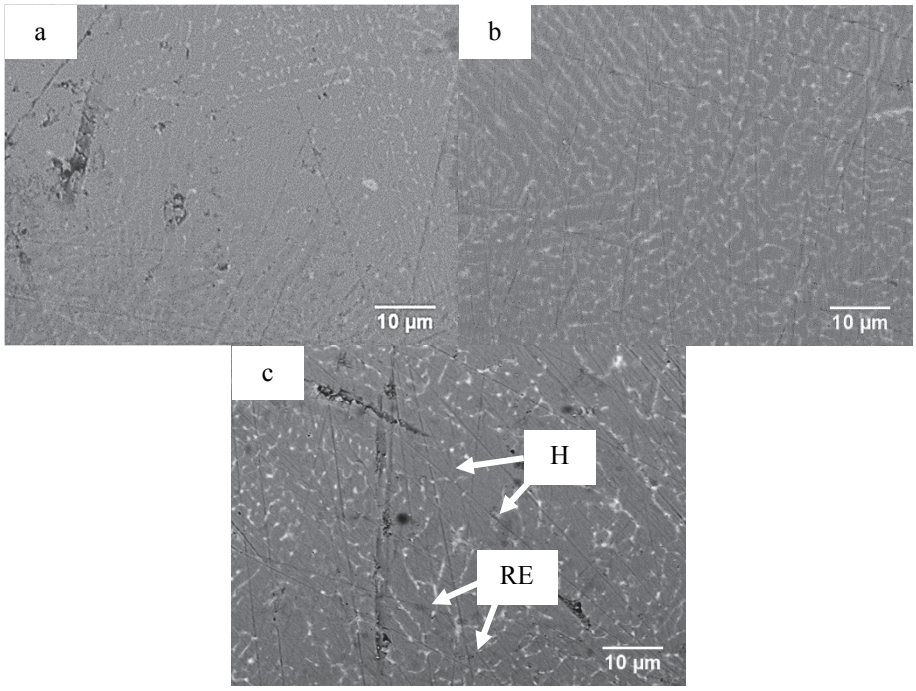

Figure 3.3. Microstructures of the alloys: (a) 0.3 mm, (b) 0.6 mm and (c) 0.9 mm; (H) - hard phase, (RE) – RE-rich phase [Paper I].

3.2. Preparation of the powders

3.2.1. High-energy ball milling in wet agent

As an alternative to jet milling (see section 3.2.2 for more details), to optimize and conduct a preliminary research for the novel ball milling method, the experiments of high-energy milling in wet agent were conducted, using hydrogen and vacuum (see section 3.2.3).

Table 3.1 presents the average particle sizes of the milled powders before the hydrogen desorption according to the input parameters. Final particle sizes vary between 1.2 and 22.5 µm. The morphology of the finest powder is shown in Fig. 3.4. No direct influence of specific parameters can be seen, except for a lower milling speed that yields the largest particle sizes. The particle shapes after milling are angular.

The influence of the milling on grain refinement and phase structure can be separated to two effects – the number of impacts and the kinetic energy of a single impact. As the amount of powder in this study was not varied, the number of impacts at a certain speed of milling can be assumed to be directly related to the

number of balls in the vessel. This was 38 and 72, for BPR of 5:1 and 10:1, respectively. Additionally, the number of impacts is influenced by the milling time and speed of rotation. Different process variables were evaluated according to the estimated total number of the impacts. The speed, BPR and wet agent combined with speed and time showed the highest influence. (For more details check Paper II.)

Table 3.1. High-energy milling parameters and final particle sizes of the powders[Paper II]

Designation	BRP	Wet agent, ml	Time, h	Speed, min^{-1}	Particle size, μm
N1	10:1	100	4	850	3.0
N2	10:1	25	4	850	1.2
N3	10:1	100	1	500	5.0
N4	10:1	100	4	500	8.0
N5	10:1	25	1	850	2.3
N6	5:1	100	1	850	2.2
N7	5:1	25	4	850	5.1
N8	5:1	100	4	850	2.4
N9	10:1	25	1	500	4.5
N10	5:1	25	1	500	13.3
N11	5:1	100	1	500	22.5
N12	5:1	25	4	500	4.8

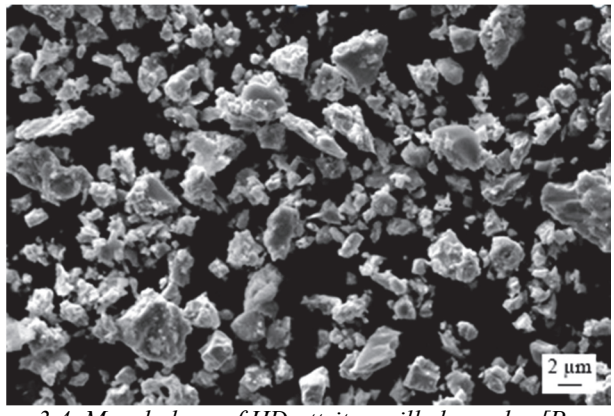

Figure 3.4. Morphology of HD attritor milled powder [Paper II].

The results of average particle sizes of milled powders according to the number of impacts are shown in Fig. 3.5. Higher impact energies (due to higher milling speed – 850 min^{-1}) always yield more refined particles as compared to materials processed with lower impact energies. When milling at 500 rpm, the smallest particle size is at around 5 μm, at approximately one million of impacts. Increased particle size can be observed for materials milled for longer periods. The reason for increased particle size is not well understood, but it could relate to the welding of the particles.

When milling at higher input energies, the particle size is always less than 5 μm. It seems that balance between fracture and welding during milling is achieved already after 1 hour of milling. The smallest particle size, 1.2 μm, was obtained at the highest number of impacts. Powders N1 and N2 (Fig. 3.5) yield high content of α- Fe after the heat treatment. Regarding undesired α-phase, the milling should be performed under small impact energies and small number of impacts. In this regard, material N3 (Fig. 3.5) is the most promising of the studied alloy-powders [Paper II].

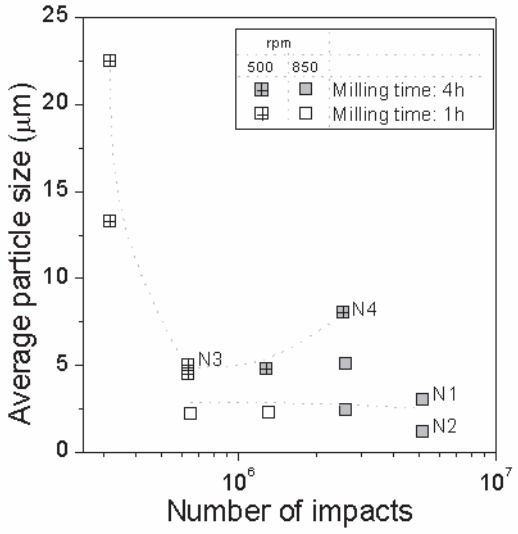

Figure 3.5. Average particle size vs estimated total number of impacts during the milling process [Paper II].

To sum up, attritor milling with wet agent allows us to prepare fine powders of 1.2 μm in size at prolonged milling times and at a high number of impacts. However, to obtain the powders with acceptable quality, the number of impacts should be kept low and in this case, the powders with the maximum particle size of 5 μm can be prepared.

3.2.2. Jet milling in nitrogen gas flow

JM with nitrogen has become a classical way for magnetic powders refinement, as the method allows suppressing the contamination and broadening of the particle size distribution (See section 1.3.2). However, within the JM processing it is difficult to produce pure powders with the particle size below a certain size as the rapid oxidation occurs and degradation of the magnetic properties starts [40].
In the study, the jet mill coupled with a pneumatic feeder was used. To influence the particle size of the powders, in addition to grinding gas pressure, feed gas and

pump supply pressures can be changed. In this study, grinding gas was kept at a maximum possible level [80].
As a result, varying the feed gas pressure between 1…5 bar, the feed rate of the powder changes between 1…5 g/min. Under constant feed gas, when the speed of the particles entering the mill is changing, the feed rate is regularly stable. This means that pump supply pressure has no significant influence on the feed rate.
On the contrary, when it comes to the particle size, the pump supply pressure that is in direct correlation with the speed of flowing particles has a significant influence on the final powder particle size (See Fig. 3.6 a). The results show that it is important to keep the speed of particle entering the milling chamber as low as possible if fine grain size is required. Additionally, the feed gas flow rate influences the particle size as well. In this case, the relation between the particle size and the feed gas pressure is linear (See Fig. 3.6 b). In other words, lower feed gas results in finer powder. The microstructure of the jet milled powder with an average particle size of 2.0 μm is shown in Fig. 3.7. Thus, with JM in nitrogen it is possible to obtain fine powders of 2 μm in size and oxygen content less than 0.2 wt%. However, in most experiments conducted in TUT Powder Metallurgy Laboratory, the particle size was kept in the range of 6…8 μm, as the amounts of the materials used were too small and oxidation had a greater impact [80].

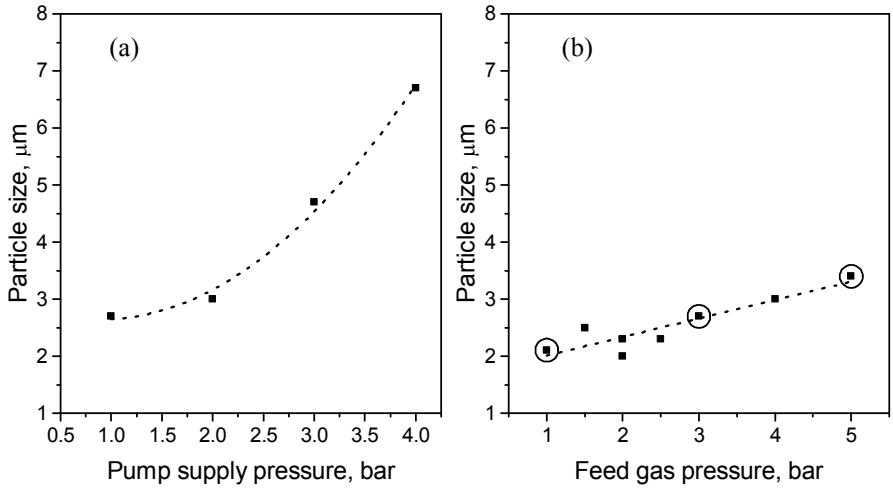

Figure 3.6. Variation of particle size: (a) with pump supply pressure, (b) with feed gas pressure. Marked points are chosen sample/powders for the chemical analysis described in [80].

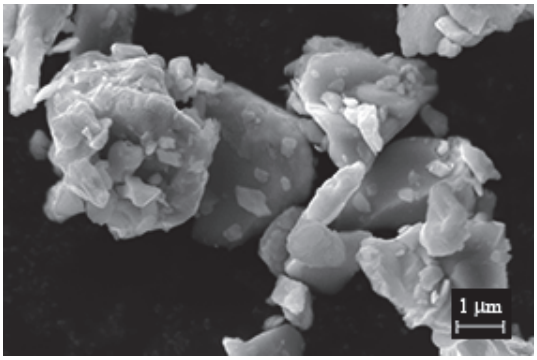

Figure 3.7. The morphology of the powder refined in nitrogen gas flow [80].

3.2.3. High-energy dry milling in hydrogen gas and vacuum

The invented high-energy attritor is intended for synthesis of powder materials, whereas milling of the powders and subsequent handling and consolidation is performed under vacuum atmosphere. The high-energy attritor milling (ABM) method allows reduction of contamination of highly reactive materials, especially with oxygen. The method is applicable for fine pulverizing of easily oxidizing powder materials, like magnet alloys, light metals or ceramic-metal composites and making bulk products from thereof. Sketches of the designed attritor and powder transportation unit can be found in Figs. 1 and 2 in [Paper III].
Morphology of the powder obtained by ABM in subsequent hydrogen and vacuum milling is shown in Fig. 3.8. Generally, refined powder is relatively homogeneous. The average particle size is 0.3 μm. Particles up to 1 μm were observed. Oxygen concentration after ABM did not exceed 0.11 wt%. Thus, powders refined in hydrogen and subsequently in vacuum resulted in lower oxidation level with much finer particles [Paper III]. The absence of jaw crushing or HD processing gives an additional advantange to ABM (See section 2.2.2).

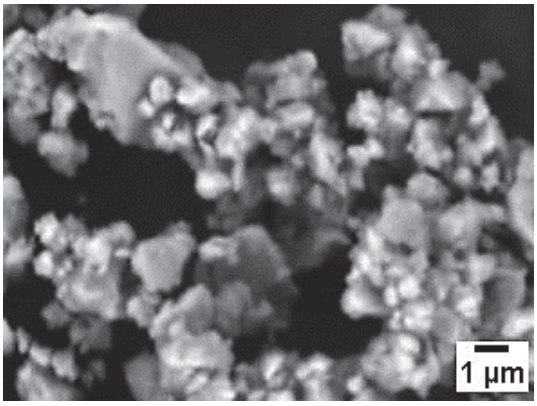

Figure 3.8. Morphology of the powder milled by ABM [82].

3.3. Substitution of Dy with nano-TiC

Commonly, Dy or Co is added into RE magnetic materials to enhance the thermal characteristics, as mentioned in section 1.3.6. In the study presented in Paper IV, TiC nanoparticles were added prior to jet milling into sintered Nd-Fe-B magnets to improve the Curie temperature and the thermal stability. Nano-TiC powder with an average particle size of 20 nm (weighing from 0.1 to 5.0 wt%) was introduced to the HD powder before feeding it into the JM.
The analysis of the XRD patterns showed single low intensity peaks corresponding to the TiC phase that were observed at approximately $2\Theta = 36$ ° and 61° for the samples with higher dopant content (1 and 2 wt%). The single peaks not defined by $Nd_2Fe_{14}B$ and TiC phases were observed at $2\Theta = 27$ °, 30 ° and 52 °. Most probably, the other single peaks correspond to the RE-rich phase at $2\Theta = 27$ ° and TiB_2 minor phase with a maximum peak at $2\Theta = 52$ ° (see Fig. 3.9).

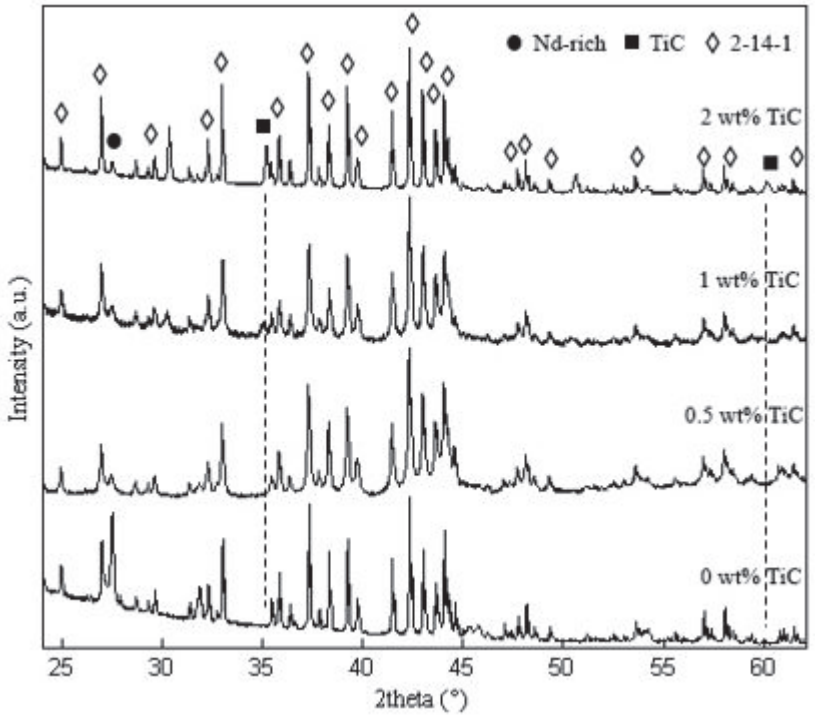

Figure 3.9. X-ray patterns of 0.5, 1 and 2 wt% nano-TiC sintered PMs [Paper IV].

The lattice parameters of the refined hard magnetic phase remained practically unchanged with increasing carbide concentration. This indicates that the hard magnetic phase undoped with TiC and carbide particles behaves as an inclusion between the grains and in the RE-rich phase regions. Also, TiC does not

decompose during the processing and acts as a grain refinement agent in the RE-rich phase.

SEM images of the initial and 1 wt% nano-TiC containing sample are shown in Fig. 3.10 a, b and c, respectively and EDS mapping of a magnet with 1 wt% nano-TiC in Fig. 3.10 d. It can be seen that Ti is concentrated mostly in the RE-rich phase (Fig. 3.10 c).

TiC-free samples have a coarser structure with an average grain size of about 8 μm (Fig. 3.10 a), whereas addition of 1wt% nano-TiC results in a finer structure with an average grain size of about 6.5 μm (Fig. 3.10 b). The proposed mechanism of microstructure development is illustrated in Fig. 3.11. The grain refinement can be explained with the effect of nano-TiC particles acting as grain growth inhibitors. (Supplementary data can be found in Paper IV.)

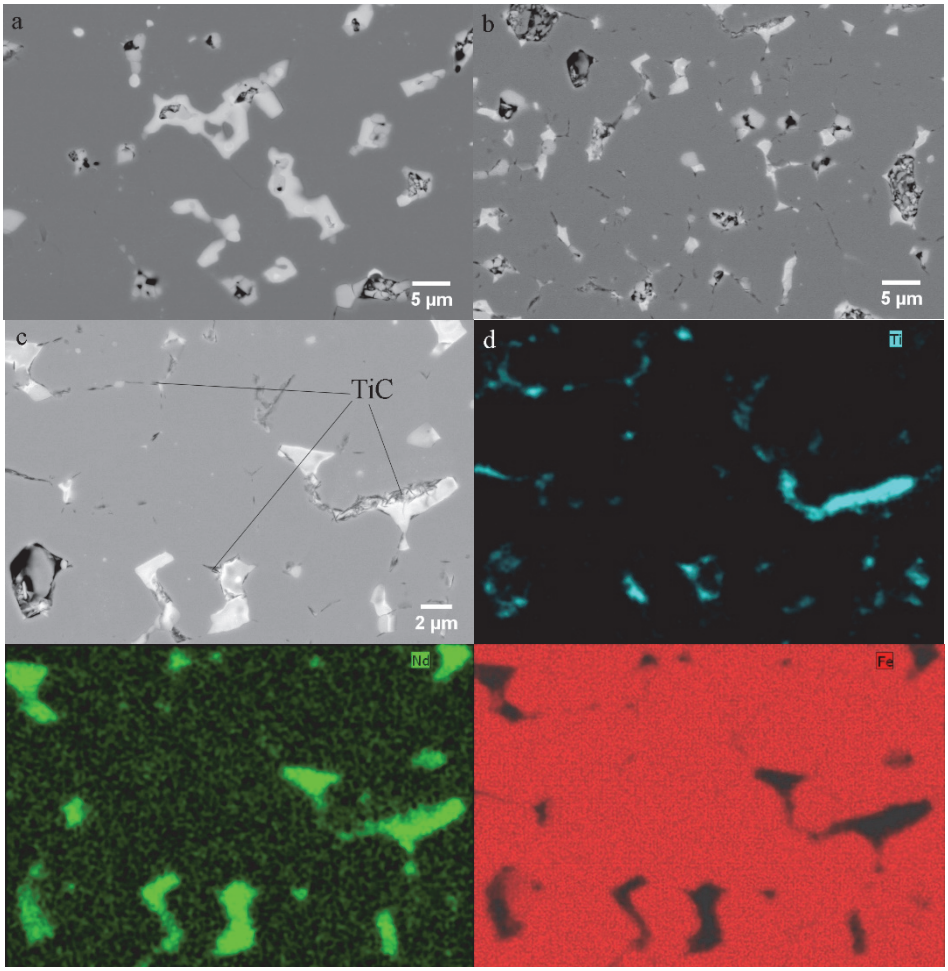

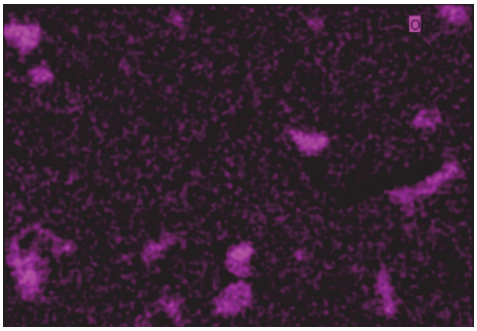

Figure 3.10. Microstructure: a) SEM image of initial sintered magnet without TiC; b) sample with 1wt % of TiC; c) sample with 1 wt% of TiC, TiC particles are visible; d) EDS mapping for Ti, Nd, Fe and O [Paper IV].

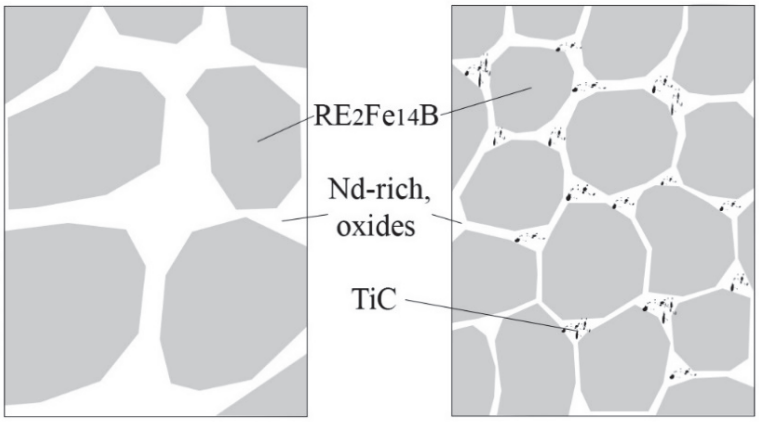

Figure 3.11. Mechanism of microstructure development when the magnet composition is modified by TiC addition. Left figure illustrates schematically microstructure of the initial magnet. On the right, the influence of TiC addition is shown [Paper IV].

In comparison to the samples without carbide introduction, Fig. 3.12 shows the effect of nano-TiC addition on the magnetic properties of remanence (B_r), coercivity (H_{ci}) and maximum energy product (BH_{max}) measured at room temperature. Generally, TiC has a positive influence on coercivity. It increases with higher TiC concentrations and starts to decrease with the TiC concentration exceeding 1 wt%. Remanence value remains almost unchanged and decreases with higher dopant concentrations – at 2 and 5 wt% of carbide addition due to the nonmagnetic TiC phase. The maximum energy product is highest for the magnet with 1 wt% TiC, as seen from Fig. 3.12. (For more details see Paper IV.)
The magnetic properties at elevated temperatures for nano-TiC doped sintered NdFeB magnets were characterized. In comparison to the initial characteristics of 333K for maximum working point and 583 K for Curie temperature, the highest working and Curie temperature of 373 K and 633 K are found for the magnet with 0.5 wt% nano-TiC. The magnet with 1 wt% TiC resulted in 10 K lower Curie temperature.

In terms of stability, at lower temperatures in the range up to 373 K, the difference in remanence is insignificant, but at elevated temperatures, the magnets with nano-carbide are more stable. For coercivity, the picture is quite similar at higher temperatures, however at lower temperatures coercive force decreases slightly faster. (Extra information is provided in Paper IV.)

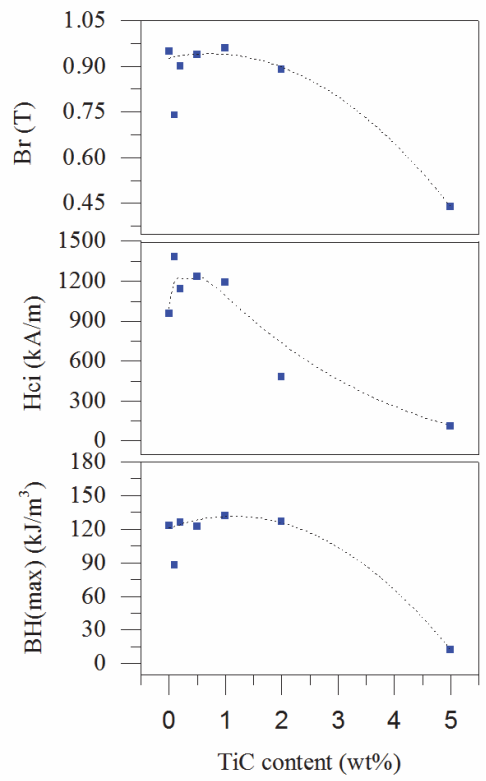

Figure 3.12. Magnetic properties of TiC doped NdFeB magnets at room temperature as the function of TiC content [Paper IV].

3.4. SPS processing of fine-grained Nd-Fe-B powders

Spark Plasma Sintering (SPS) is known as one of the sintering techniques for fine powders. The advantage of SPS is the rapid sintering cycle that allows suppressing the grain growth and achieving full density at relatively low sintering temperatures [86, 87]. Earlier studies on permanent magnets manufactured by the SPS technique showed that fine grained and nanostructured magnets with promising magnetic, thermal properties and higher corrosion resistance can be achieved [88, 89].

Microstructure of spark plasma sintered materials produced from SC flakes is presented in Fig. 3.13. After sintering, the material shows ultrafine structure. X-ray phase analysis revealed the presence of the mixture of Nd and Pr hydrides and iron. Measurement of the hydrogen with an ONH analyzer proved the

presence of hydrides. The theoretical content of hydrogen in Nd_2H_5 and PrH_2 compounds is 1.7 wt% and 1.4 wt%, consequently. Assuming that the powders are fully hydrogenated, it may be possible to desorb all the hydrogen out of the refined powders during prolonged milling in vacuum, as after 15 min the content of hydrogen dropped to 0.25 wt% [82].

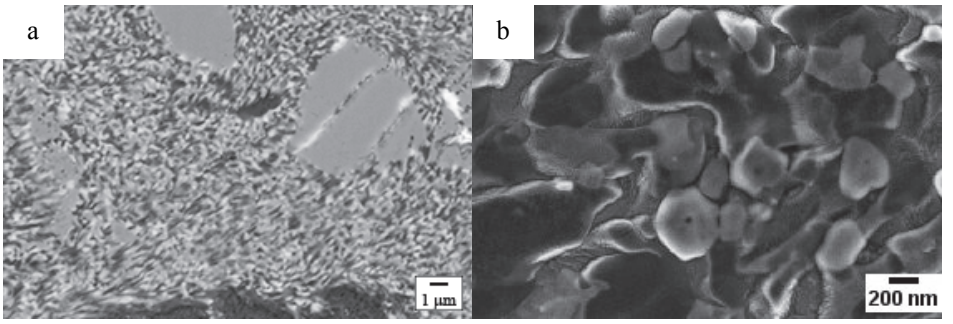

Figure 3.13. Magnet processed with SPS: (a) microstructure of as-sintered material at magnification 10 000x; (b) at magnification 100 000x [82].

After heat treatment of SPS magnets, the microstructure typical for magnets was recovered and showed the presence on the $Nd_2Fe_{14}B$ hard phase. At 575 °C, the reduction of hydrides started and at 650…675 °C, the hydrides were fully reduced. The changes in the microstructures can be seen in Fig. 3.14. In comparison with the microstructure of as-sintered materials, the microstructure of the magnet heat treated at 575 °C showed that the desorption process had started, however typical phases for Nd-Fe-B magnets were not completely formed (Fig. 3.14 a, area marked as 1). The microstructure was similar to that found by Sheridan [90]. He assumed that the material is partially recombinated. Areas of alpha iron (98.9 wt%) were observed and designated as 2 in Fig. 3.14 a. The microstructure similar to that of sintered Nd-Fe-B magnets was obtained at higher temperatures of heat treatment (Fig. 3.4.2 b, c, d). Increasing temperature leads to the grain growth. For the magnet heat treated at 1090 °C, grain size was determined at about 8 μm, which is comparable to the size of the grains in the magnet manufactured by the classical production route (Fig. 3.14 d) [82].
Both the remanence and coercivity increase with the temperature increment of the heat treatment. Higher properties for the magnet heat treated at 1090 °C can be explained by uniform microstructure and decreased content of the Nd-rich phase. Apparently, smaller particle size of the hard phase for 675 °C and 875 °C treated magnets does not have sufficient influence on the magnetic properties when compared to other microstructural features [82].

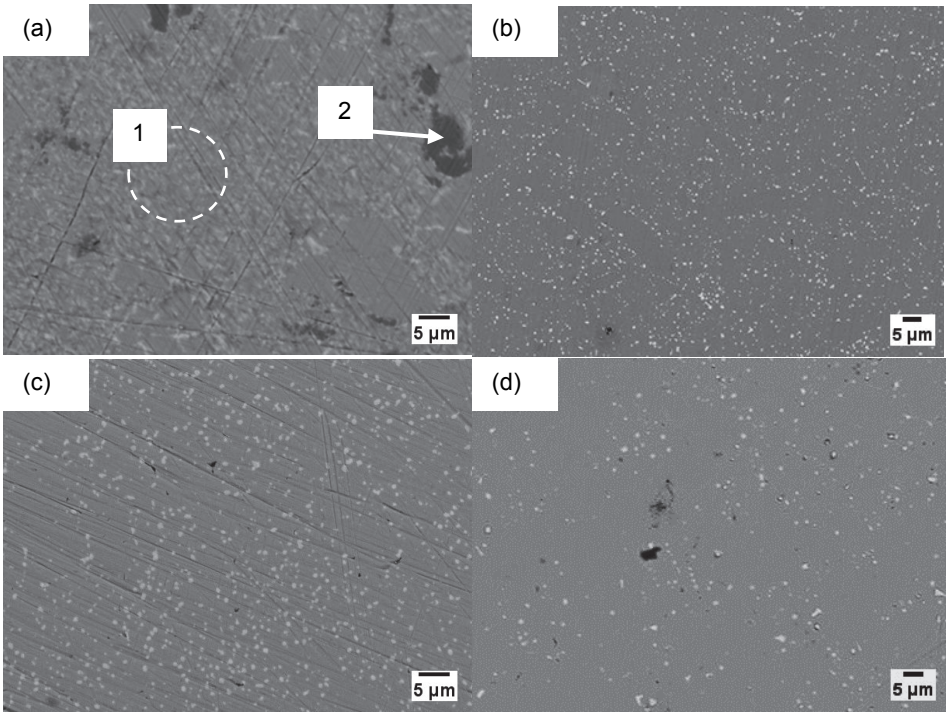

Figure 3.14. Microstructures of SPS magnets after heat treatment at different temperatures: (a) 575 °C, (b) 675 °C, (c) 875 °C and (d) 1090 °C [82].

4. CONCLUSIONS

The main conclusions of the thesis research are as follows:

- For the production of Ce-containing magnetic alloys with the cooling rate up to 10^5 K/s, the splat quenching method was implemented. Tertiary (Nd-Ce-Fe-B) alloy with fine microstructure and free of α-iron was obtained. The coercivity of the Ce-containing magnets reaches 500 kA/m.
- The optimization of the jet-milling parameters for hydrogen decrepitated NdFeB powders showed the smallest average particle size of 2 μm. To achieve fine powders, the velocity of the particles entering the grinding chamber should be decreased.
- Novel ultrafine powder milling procedure was developed. Powders refined in hydrogen and subsequently in vacuum resulted in low oxygen contamination with fine particles of 0.3 μm.
- To enhance thermal properties of PMs, a simplified method was developed by adding titanium carbide nanoparticles into the powder mixture prior to jet milling. TiC particles are concentrated mainly intergranularly in the RE-rich phase and almost do not dissolve in the matrix phase. At concentrations as small as 0.1 wt.% TiC nanopowder additions already lead to finer microstructure and decreased volume fraction of nonmagnetic phase.
- Addition of nano-TiC to the RE magnets by mixing into hydrogen decrepitated strip cast powder resulted in an improvement of the magnetic properties, increase in Curie temperature and thermal stability, especially at a higher temperature range.

The novelty of the present research can be attributed to:

- Application of Ce in magnetic alloys prepared by the splat quenching method;
- Invention of the method for milling of the powders and subsequent handling and consolidation under vacuum atmosphere, which allows reduction of contamination of highly reactive materials and results in submicron powders;
- Improvement of magnetic properties, Curie temperature and thermal stability of the RE magnets introducing nano-TiC powder prior to jet milling by nitrogen gas flow.

REFERENCES

[1] Kaneko, Y., Kuniyoshi, F. and Ishigaki, N. Proven technologies on high-performance Nd–Fe–B sintered magnets. *J. Alloy. Comp.,* 2006, **408-412**, 1344–1349.

[2] Matsuura, Y. Recent development of Nd–Fe–B sintered magnets. *J. Magn. Magn. Mater.,* 2006, **303**, 344–347.

[3] Shi, D., Zhang, W. and Nagata, H. Magnetic Properties and Microstructure of High (BH)max Nd-Fe-B Sintered Magnet with Grain Boundary Diffusion Treatment. - *Proceedings of 2015 IEEE Magnetics Conference (INTERMAG) : 11-15 May 2015*, *Beijing, China*.

[4] Coey, J. *Rare-Earth Iron Permanent Magnets*. Oxford University Press Inc., New York, 2006.

[5] Hilzinger, R. and Rodewald, W. *Magnetic Materials: Fundamentals, Products, Properties, Applications.* Publicis Publishing, 2013.

[6] Getzlaff, M. *Fundamentals of Magnetism*. Springer, 2010.

[7] Jinfang, L., Helie L. and Jiang, W. Discussion of the coercivity mechanism of RE-TM-B permanent magnets. *J. Physics D: Applied Physics,* 1992, **25**, 1238-1242.

[8] Buschow, K. and De Boer, F. *Physics of Magnetism and Magnetic Materials*. Kluwer Academic/Plenum Publishers, New York, 2003.

[9] Durst, K. D. and Kronmüller, H. The coercive field of sintered and melt-spun NdFeB magnets. *J. Magn. Magn. Mater.* 1987, **68**(1), 63-75.

[10] Anderson, J. J. *Structural and Magnetic Properties of Neodymium-Iron-Boron Clusters.* Mechanical (and Materials) Engineering - Dissertations, Theses, and Student Research, Lincoln, 2010.

[11] Bertotti, G. *Hysteresis in magnetism, for physicists, materials scientists and engineers*. Academic Press, 1998.

[12] Gutfleisch, O. Controlling the properties of high energy density permanent magnetic materials by different processing routes. *J. Physics D: Applied Physics,* 2000, **33**(17).

[13] Sagawa, M., Fujimura, S., Togawa, N., Yamamoto, H. and Matsuura, Y. New material for permanent magnets on a base of Nd and Fe. *J. Appl. Phys.,* 1984, **55**, 2083-2087.

[14] Croat, J. J., Herbst, J. F., Lee, R. W. and Pinkerton, F. E. Pr-Fe and Nd-Fe-based materials: A new class of high-performance permanent magnets. *J. Appl. Phys.,* 1984, **55**(6).

[15] Croat, J. J., Herbst, J. F., Lee, R. W. and Pinkerton, F. E. High-energy product Nd-Fe-B permanent magnets. *Appl. Phys. Lett.,* 1984, **44**(1).

[16] Herbst, J. F., Croat, J. J., Pinkerton, F. E. and Yelon, W. B. Relationships between crystal structure and magnetic properties in $Nd_2Fe_{14}B$. *Phys. Rev. B,* 1984, **29**(7), 4176-4178.

[17] *Magnetics Magazine,* [Online] Information to global market of PMs 26.04.2016 http://www.magneticsmagazine.com/main/news/permanent-magnet-market-will-reach-28-70-billion-in-2019/

[18] Benecki, W. T. The Permanent Magnet Market - 2015. - *Magnetics 2013 Conference : 7-8 February 2013, Orlando, USA.*

[19] Brown, D., Ma, B. M. and Chen, Z. Developments in the processing and properties of NdFeb-type permanent magnets. *J. Magn. Magn. Mater.,* 2002, **248**, 432–440.

[20] Bai, G., Gao, R., Sun, Y., Han, G. and Wang, B. Study of high-coercivity sintered NdFeB magnets. *J. Magn. Magn. Mater.,* 2007, **308**(1), 20–23.

[21] Jing, X., Shihong, Y., Dunbo, Y., Zongan, L., Shipeng, L. and Hongwei, L. Influence of Solidification Rate on Microstructures of Cast Strips and Corresponding Sintered NdFeB Magnets. *J. Rare Earths,* 2006, **24**, 306-309.

[22] Bai, G., Gao, R., Sun, Y., Han, G. and Wang, B. Study of high-coercivity sintered NdFeB magnets. *J. Magn. Magn. Mater.,* 2007, **308**(1), 20-23.

[23] Yu, L., Yan, M., Wu, J., Luo, W., Cui, X. and Ying, H. On the cooling rate of strip cast ingots for sintered NdFeB magnets. *Physica B: Condensed Matter,* 2007, **393**(1-2), 1-5.

[24] Scott, D. W., Ma, B. M., Liang, Y. L. and Bounds, C. O. The effects of average grain size on the magnetic properties and corrosion resistance of NdFeB sintered magnets. *J. Appl. Phys.,* 1996, **79**, 5501-5503.

[25] Davies, B., Mottram, R. and Harris, I. Recent developments in the sintering of NdFeB. *Mater. Chem. Phys.,* 2001, **67**(1-3), 272–281.

[26] Vial, F., Joly, F., Nevalainen, E., Sagawa, M., Hiraga, K. and Park, K. Improvement of coercivity of sintered NdFeB permanent magnets by heat treatment. *J. Magn. Magn. Mater.,* 2002, 242-245, 1329–1334.

[27] Mitarai, H., Noguchi, K., Mishima, C., Matsuoka, H., Yamazaki, M. and Kawasugi, Y. Development of Compound for Anisotropic Bonded Nd Magnets Using d-HDDR Magnet Powder. *IEEE T. Magn.,* 2014, **50**(11).

[28] Morimoto, K., Kaneko, S., Katayama, N. and Shigeoka, K. Effect of substituting Pr for Nd on magnetic properties of Nd-Fe-B HDDR powder. *J. Alloy. Comp.,* 2016, **666**, 118-121.

[29] Ma, B., Herchenroeder, J., Smith, B., Suda, M., Brown, D. and Chen, Z. Recent development in bonded NdFeB magnets. *J. Magn. Magn. Mater.,* 2002, **239**, 418–423.

[30] Gutfleisch, O., Kirchner, A., Grünberger, W., Hinz, D., Schäfer, R., Schultz, L., Harris, I. and Müller, K. Backward extruded NdFeB HDDR ring magnets. *J. Magn. Magn. Mater.,* 1998, **183**(3), 359–364.

[31] Ormerod, J. and Constantinides, S. Bonded permanent magnets: Current status and future opportunities. *J. Appl. Phys.,* 1997, **81**.

[32] Woodcock, T., Zhang, Y., Hrkac, G., Ciuta, G., Dempsey, N., Schrefl, T., Gutfleisch, O. and Givord, D. Understanding the microstructure and coercivity of high performance NdFeB-based magnets. *Scr. Mater.,* 2012, **67**(6), 536–541.

[33] Sagawa, M., Fujimura, S., Yamamoto, H. and Matsuura, Y. Permanent Magnet Materials Based on the Rare Earth-Iron-Boron Tetragonal Compounds," *IEEE T. Magn.,* 1984, **20**(5).

[34] Gao, R., Zhang, D., Li, H. and Zhang, J. Effects of the degree of grain alignment on the hard magnetic properties of sintered NdFeB magnets. *Appl. Phys. A,* 1998, **67**, 353–356.

[35] Scott, D. W., Ma, B. M., Liang, Y. L. and Bounds, C. O. Microstructural control of NdFeB cast ingots for achieving 50 MGOe sintered magnets. *J. Appl. Phys.,* 1996, **79**.

[36] Yan, G. H., Chen, R. J., Ding, Y., Guo, S., Lee, D. and Yan, A. R. The preparation of sintered NdFeB magnet with high-coercivity and high temperature-stability. - *Proceedings of the 2nd Int. Symp. on Advanced*

Magnetic Materials and Applications (ISAMMA2010) : 12-16 July 2010, *Sendai, Japan.*

[37] Hiraga, K., Hirabayashi, M., Sagawa, M. and Matsuura, Y. A Study of Microstructures of Grain Boundaries in Sintered Fe77Nd15B8 Permanent Magnet. *Japanese J. Appl. Phys.,* 1985, **24**(6).

[38] Woodcock, T. and Gutfleisch, O. Multi-phase EBSD mapping and local texture analysis in NdFeB sintered magnets. *Acta Mater.,* 2011, **59**, 1026–1036.

[39] Mo, W., Zhang, L., Liu, Q., Shan, A., Wu, J. and Komuro, M. Dependence of the crystal structure of the Nd-rich phase on oxygen content in an Nd–Fe–B sintered magnet. *Scr. Mater.,* 2008, **59**(2), 179–182.

[40] Li, W., Ohkubo, T., Hono, K. and Sagawa, M. The origin of coercivity decrease in fine grained Nd–Fe–B sintered magnets. *J. Magn. Magn. Mater.,* 2009, **321**(8), 1100–1105.

[41] Pandian, S., Chandrasekaran, V., Markandeyulu, G., Iyer, K. J. L. and Rama Rao, K. V. S. Effect of Al, Cu, Ga, and Nb additions on the magnetic properties and microstructural features of sintered NdFeB. *J. Appl. Phys.,* 2002, **92**(10).

[42] Ohmori, K., Li, L. and Graham, C. D. Effect of added Cu on the Nd-rich phase in hot-deformed NdFeB magnets. *IEEE T. Magn.,* 1992, **28**(5).

[43] Mo, W., Lantin, Z., Liu, Q., Shan, A., Wu, J., Komuro, M. and Shen, L. Microstructure and corrosion resistance of sintered NdFeB magnet modified by intergranular additions of MgO and ZnO. *J. Rare Eerths,* 2008, **26**(2).

[44] Mo, W., Zhang, L., Shan, A., Cao, L., Wu, J. and Komuro, M. Improvement of magnetic properties and corrosion resistance of NdFeB magnets by intergranular addition of MgO. *J. Alloy. Comp.,* 2008, **461**, 351–354.

[45] Liu, W., Sun, H., Yi, X., Liu, X., Zhang, D., Yue, M. and Zhang, J. Coercivity enhancement in Nd-Fe-B sintered permanent magnet by Dy nanoparticles doping. *J. Alloy. Comp.,* 2010, **501**(1), 67–69.

[46] Wang, C., Yue, M., Zhang, D., Liu, W. and Zhang, J. Structure and magnetic properties of hot deformed $Nd_2Fe_{14}B$ magnets doped with D_yH_x nanoparticles. *J. Magn. Magn. Mater.,* 2016, **404**, 64–67.

[47] Branagan, D. and McCallum, R. Precipitation phenomenon in stoichiometric Nd2Fe14B alloys modified with titanium and titanium with carbon. *J. Alloy. Comp.,* 1995, **230**(2), 67–75.

[48] Cong, W., ZhiMeng, G., YanLi, S., XiaoQian, B. and ZhiAn, C. Effect of Titanium Substitution on Magnetic Properties and Microstructure of Nanocrystalline Monophase Nd-Fe-B Magnets. *J. Nanomater.,* 2012, 2012, **2012**.

[49] Zhang, R., Liu, Y., Li, J., Gao, S. and Tu, M. Effect of Ti&C substitution on the magnetic properties and microstructures of rapidly-quenched NdFeB alloy. *Mater. Charact.,* 2008, **59**(5), 642–646.

[50] Liu, Z. W., Zhao, L. Z., Hu, S. L., Yu, H. Y., Zhong, X. C. and Gao, X. X. Coercivity and Thermal Stability Enhancement for Spark-Plasma-Sintered Nanocrystalline NdFeB Magnets With Dy_2O_3 and Zn Additions. *IEEE T. Magn.,* 2015, **51**(11).

[51] Spaldin, N. A., *Magnetic Material: Fundamentals and Applications*. Cambridge University Press, Cambridge, 2011.

[52] Takezawa, M., Nagashima, Y., Morimoto, Y. and Yamasaki, J. Magnetic Domain Observation of Nd-Fe-B Sintered Magnets at Elevated Temperatures by Using Kerr Microscope. *IEEE T. Magn.,* 2011, **47**(10).

[53] Thielsch, J., Hinz, D., Schultz, L. and Gutfleisch, O. Magnetization reversal in textured NdFeB–Fe composites observed by domain imaging. *J. Magn. Magn. Mater.,* 2010, **322**(20), 3208–3213.

[54] Takezawa, M., Shimada, T., Kondo, S., Mimura, S., Morimoto, Y., Hidaka T. and Yamasaki, J. Domain observation technique for Nd–Fe–B magnet in high magnetic field by image processing using liquid crystal modulator. *J. Appl. Phys.,* 2007, **101**.

[55] Mishra, R. K. and Lee, R. W. Microstructure, domain walls, and magnetization reversal in hot-pressed Nd-Fe-B magnets. *Appl. Phys. Lett.,* 1986, **48**.

[56] Yazid, M., Olsen, S. and Atkinson, G. MFM study of a sintered Nd-Fe-B magnet: analysing domain structure and measuring defect size in 3D view. *IEEE T. Magn.,* 2016, **PP**.

[57] Narasimhan, K. S. V. L. Iron-based rare-earth magnets. *J. Appl. Phys.,* 1985, **57**.

[58] Trout, S. R. Material Selection of Permanent Magnets, Considering Thermal Properties Correctly. - *Proceedings of Electrical Insulation*

Conference and Electrical Manufacturing & Coil Winding Conference : 18 October 2001, *Cincinnati, USA*.

[59] Haavisto, M., Tuominen, S., Santa-Nokki, T., Kankaanpää, H., Paju, M. and Ruuskanen, P. Magnetic Behavior of Sintered NdFeB Magnets on a Long-Term Timescale. *Adv. Mater. Sci.,* 2014.

[60] Liu, Z., Qian, D., Zhao, L., Zheng, Z., Gao, X. and Ramanujan, R. Enhancing the coercivity, thermal stability and exchange coupling of nano-composite (Nd,Dy,Y)–Fe–B alloys with reduced Dy content by Zr addition. *J. Alloy. Comp.,* 2014, **606**(5), 44–49.

[61] Liu, Z., Qian, D. and Zeng, D. Reducing Dy Content by Y Substitution in Nanocomposite NdFeB Alloys With Enhanced Magnetic Properties and Thermal Stability. *IEEE T. Magn.,* 2012, **48**(11).

[62] Li, X., Liu, S., Cao, X., Zhou, B., Chen, L., Yan, A. and Yan, G. Coercivity and thermal stability improvement in sintered Nd–Fe–B permanent magnets by intergranular addition of Dy–Mn alloy. *J. Magn. Magn. Mater.,* 2016, **407**, 247–251.

[63] Ding, G., Guo, S., Cai, L., Chen, L., Yan, C., Lee, D. and Yan, A. Enhanced Thermal Stability of Nd–Fe–B Sintered Magnets by Intergranular Doping $Y_{72}Co_{28}$ Alloys. *IEEE T. Magn.,* 2015, **51**(8).

[64] Chen, E., Peng, K, Yang, W. L., Zhu, J. J., Li, D. Y. and Zhou, L. P. Effects of Al coating on corrosion resistance of sintered NdFeB magnet. *Trans. Nonferrous Met. Soc. China,* 2014, **24**, 2864−2869.

[65] Blackwood, D., Balakrisnan, B., Huang, Y. and Tan, C. Influence of the chemical composition of the plating solution on the ability of nickel coatings to protect $Nd_2Fe_{14}B$ magnets against corrosion. *J. Magn. Magn. Mater.,* 2001, **223**(2), 103–111.

[66] Di, J., Guo, S., Cai, L., Chen, L., Ding, G., Liu, J. and Yan, A. Enhanced corrosion resistance of sintered NdFeB magnets by diffusion of Co film prepared by direct current magnetron sputtering deposition. - Proceedings of *2015 IEEE Magnetics Conference (INTERMAG) : 11-15 May 2015*, Beijing, China.

[67] Huang, Y., Li, H., Zuo, M., Tao, L., Wang, W., Zhang, J. and Tang, Q. Corrosion resistance of sintered NdFeB coated with SiC/Al bilayer thin films by magnetron sputtering. *J.Magn. Magn. Mater.,* 2016, **409**, 39–44.

[68] de Castro, J. A. and de Campos, M. F. Influence of the Grain Size on the Dysprosium Diffusion in NdFeB Magnets. *Mater. Sci. Forum,* 2014, **802**, 546-551.

[69] Yu, L., Wen, Y. and Yan, M. Effects of Dy and Nb on the magnetic properties and corrosion resistance of sintered NdFeB. *J. Magn. Magn. Mater.,* 2004, **283**(2), 353–356.

[70] Goto, R., Sugimoto, S., Matsuura, M., Tezuka, N., Une, Y. and Sagawa, M. Nd-Fe-B sintered magnets fabrication by using atomized powders. - Proceedings of the *2nd Int. Symp. on Advanced Magnetic Materials and Applications (ISAMMA 2010) : 12-16 July 2010* , *Sendai, Japan.*

[71] Liu, Z. and Davies, H. The practical limits for enhancing magnetic property combinations for bulk nanocrystalline NdFeB alloys through Pr, Co and Dy substitutions. *J. Magn. Magn. Mater.,* 2007, **313**(2), 337–341.

[72] Sepehri-Amin, H., Une, Y., Ohkubo, T., Hono, K. and Sagawa, M. Microstructure of fine-grained Nd–Fe–B sintered magnets with high coercivity. *Scr. Mater.,* 2011, **65**(5), 396–399.

[73] Gutfleisch, O., Güth, K., Woodcock, T. G. and Schultz, L. Recycling Used Nd-Fe-B Sintered Magnets via a Hydrogen-Based Route to Produce Anisotropic, Resin Bonded Magnets. *Adv. Energy Mater.,* 2013, **3**, 151–155.

[74] Zakotnik, M., Harris, I. and Williams, A. Multiple recycling of NdFeB-type sintered magnets. *J. Alloy. Comp.,* 2009, **469**, 314–321.

[75] Önal, M. A. R., Rao Borra, C., Guo, M., Blanpain, B. and Van Gerven, T. Recycling of NdFeB Magnets Using Sulfation, Selective Roasting, and Water Leaching. *J. Sustainable Metallurgy,* 2015, **1**(3), 199-215.

[76] Dhammika Bandara, H. M., Field, K. D. and Emmert, M. H. Rare earth recovery from end-of-life motors employing green chemistry design principles. *Green Chem.,* 2016, **18**, 753-759.

[77] Riaño, S. and Binnemans, K. Extraction and separation of neodymium and dysprosium from used NdFeB magnets: an application of ionic liquids in solvent extraction towards the recycling of magnets. *Green Chem.,* 2015, **17**, 2931-2942.

[78] Sun, M., Hu, X., Peng, L., Fu, P., Ding, W. and Peng, Y. On the production of Mg-Nd master alloy from NdFeB magnet scraps. *J. Mater. Process. Technol.,* 2015, **218**, 57–61.

[79] *Linn High Therm*, [Online] Information to centrifugal furnace, 9 May 2016, http://www.linn-high-therm.de/products/details/pid/lifumat-met-model.html

[80] Mural, Z., Kollo, L. and Veinthal, R. Jet Milling of the Powders for Nd-Fe-B Sintered Magnets. *Proceedings of 2014 International Conference on NdFeB Magnets: Supply Chain, Critical Properties & Applications (NdFeBpm2014) : 2-5 March 2014, Ningbo, China.*

[81] *P&S GmbH*, [Online] Information to feeder (jet mill), 9 May 2016, http://www.powderandsurface.de/eng%20P&S/feed-pumps.html

[82] Mural, Z., Kollo, L. and Veinthal, R. Spark Plasma Sintered Nd-Fe-B Magnets from High-Energy Ball Milled Powders. - *Proceedings of the 24th International Workshop on rare-Earth and Future Permanent Magnets and Their Applications (REPM 2016) : 28 August-1 September 2016, Darmstadt, Germany* (accepted).

[83] *Eltra GmbH*, [Online] Information to IR analyser Eltra ONH, 26 April 2016 http://www.eltra.com/eltra-elemental-analyzers

[84] Yan, C., Guo, S., Chen, R., Lee, D. and Yan, A. Enhanced Magnetic Properties of Sintered Ce-Fe-B-Based Magnets by Optimizing the Microstructure of Strip-Casting Alloy. *IEEE T. Magn.,* 2014, **50**(11).

[85] Wang, X., Zhu, M., Li, W., Zheng, L., Zhao, D., Du, X. and Du, A. The Microstructure and Magnetic Properties of Melt-Spun CeFeB Ribbons with Varying Ce Content. *Electron. Mater. Lett.,* 2015, **11**(1), 109-112.

[86] Chen, W., Anselmi-Tamburini, U., Garay, J., Groza, J. and Munir, Z. Fundamental investigations on the spark plasma sintering/synthesis process: I. Effect of dc pulsing on reactivity. *Mater. Sci. Eng.: A,* 2005, **394**(1), 132-138.

[87] Anselmi-Tamburini, U., Garay, J. and Munir, Z. Fundamental investigations on the spark plasma sintering/synthesis process: III. Current effect on reactivity. *Mater. Sci. Eng.: A,* 2005, **407**(1), 24-30.

[88] Huang, Y., Wang, Y., Hou, Y., Wang, Y., Wu, Y., Ma, S., Liu, Z., Zeng, D., Tian, Y., Xia, W. and Zhong, Z. Magnetic microstructure and magnetic properties of spark plasma sintered NdFeB magnets. *J. Magn. Magn. Mater.,* 2016, **399**, 175-178.

[89] Wuest, H., Bommer, L., Weissgaerber, T. and Kieback, B. Magnetic and structural properties of spark plasma sintered nanocrystalline NdFeB-powders. *J. Magn. Magn. Mater.,* 2015, **392**, 74–78.

[90] Sheridan, R., Harris, I. and Walton, A. The development of microstructure during hydrogenation–disproportionation–desorption–recombination

treatment of sintered neodymium-iron-boron-type magnets. *J. Magn. Magn. Mater.,* 2016, 401, 455–462.

ABSTRACT
Technology and properties of fine-grained NdFeB magnets

In the current state, the Rare-Earth (RE) permanent magnets (PM) have nearly reached their theoretical limits of a maximum energy product (BHmax). On the other hand, none of PMs provide all the properties required for effective applications. Moreover, processing procedures for PMs are often costly and difficult to implement on industrial scale. Therefore, it is highly desirable to develop an ideal PM that will possess high magnetization, coercivity and thermal stability. At the same time, all these properties should be achieved at a possibly low cost.

Microstructure and properties of the magnets are strongly connected to the preparation route. The most crucial parameters influencing the quality of the PM are chemical composition, grain size and distribution of the magnetic powders, sintering regimes and contamination rate, especially with oxygen.

Focus in the PhD research is on the development and preparation of magnetic alloys with controlled composition and microstructure, optimization of milling techniques to obtain powders with fine grains and narrow distribution. Design of magnets with improved magnetic behavior and more effective performance at relatively high temperatures is a key aspect along with the establishment of a laboratory scale magnet production route.

Classic production route of sintered RE magnets is used as the main fabrication technology. Alternatively, high-energy milling in wet agent or in hydrogen and vacuum were implemented. Splat quenching was used to prepare small amounts of Ce-containing alloys with fine and homogeneous microstructure free of α-iron. In the present study, nano-TiC powder addition to NdFeB powders is suggested to enhance the magnetic properties, Curie temperature and thermal stability. This could be regarded as the main novelty point of the current work.

Results show that implementing the splat quenching method for the cooling rate of Ce-containing magnetic alloys amounting up to 10^5 K/s was achieved; an alloy with fine microstructure and free of α-iron was obtained. Quenching technique also resulted in more homogeneuos magnetic alloy with a lower Nd-rich phase present in the microstructure. The optimal parameters implementing HD and JM of NdFeB powders provided the lowest average particle size of 2 μm. In comparison to JM, high-energy milling in attritor with hydrogen gas and vacuum resulted in 0.3 μm sized powders with lower oxidation. Testing magnets with nano-TiC added at elevated temperatures, they proved to be more stable and possess higher Curie temperature. Addition of nano-TiC to the RE magnets by mixing into hydrogen decrepitated strip cast powder resulted in an improvement of their magnetic properties.

The general goal of the PhD research was to gain deeper insights into RE permanent magnets, their magnetic properties and also promote expertise in the characterization of magnetic materials. In addition, the aim was to develop criteria for selection of suitable compositions and microstructures to enhance the properties of Nd-Fe-B magnets.

The following challenges were overcome and mastered throughout the work:

- Processing of RE magnets;
- Characterization of microstructure;
- Evaluation of magnetic properties;
- Control over impurities level;
- Partial substitution of Nd,Pr with other RE;
- Improvement of thermal stability.

Keywords: magnetic materials, Nd-Fe-B permanent magnets, $Nd_2Fe_{14}B$, Ce containing magnetic alloys, jet mill, thermal stability

KOKKUVÕTE
Nd-Fe-B peenteramagnetite tehnoloogia ja omadused

Haruldaste muldmetallide baasil püsimagnetite hetkeolukord on selline, et ühelt poolt püsimagnetite maksimaalne energia (BHmax) läheneb teoreetilisele piirile, teiselt poolt aga ei paku ükski NdFeB baasil püsimagnet korraga kõiki vajalikke omadusi magnetite efektiivseks rakendamiseks. Peale selle on püsimagnetite valmistamine kulukas ja sageli alternatiivseid ja uuenduslikke meetodeid on keeruline rakendada tööstuslikult. Seetõttu on oluline välja arendada püsimagneteid, millele oleksid kõrged magnetomadused (magnetiseerumine, koertsitiivsus ja termostabiilsus). Samal ajal peavad need omadused olema saavutatavad võimalikult madalate materjali- ja töötlemiskuludega.

Püsimagnetite ja mikrostruktuuride lõppomadused sõltuvad otseselt valmistamisviisist. Kõige olulisemad parameetrid, mis mõjutavad magneti kvaliteeti, on keemiline koostis, magnetpulbrite terasuurus ja jaotus, paagutusrežiimid ja materjali puhtusaste (eelkõige hapnikusisaldus).

Käesolev uurimistöö keskendub kontrollitud koostise ja mikrostruktuuriga magnetsulamite arendamisele, valmistamisele ning jahvatustehnoloogiate optimeerimisele, et tagada kitsa osiselise jaotusega peent pulbrit. Olulisteks aspektideks on püsimagnetite tehnoloogia juurutamine laboratoorsel tasemel ning paremate magnet- ja termopüsivuse omadustega magnetite arendamine.

Doktoritöös on peamise valmistamistehnoloogiana kasutatud klassikalisi pulbermetallurgia meetodeid paagutatud püsimagnetite saamiseks. Alternatiivina on kasutatud kõrgenergeetilist märgjahvatust vedelikus (heptaanis) või kuivjahvatust vesinikus ja vaakumis. Lamepulbri sulametallist tootmisprotsess (*splat-quenching*) võimaldab valmistada väikestes kogustes Nd-Ce-Fe-B magnetsulameid ning tagab peene ja homogeense mikrostruktuuri ilma α-raua tekketa. Käesolevas töös näidatakse, et nano-TiC osakeste lisamine NdFeB magnetpulbrisse tõstab paagutatud magnetite magnetomadused, Curie' temperatuuri ja termostabiilsust. Seda võib lugeda doktoritöö peamiseks uudsuse momendiks.

Lamepulbri sulametallist tootmisprotsessi korral tardub väike kogus vedelmetalli kokkupuutel jahutatud vormipinnaga. Tulemused näitavad, et selle meetodi puhul saavutatakse jahutumisekiirus kuni 10^6 K/s. See võimaldab saada α-raua vaba ja peene mikrostruktuuriga magnetsulami. Samuti on sulami mikrostruktuuris vähem Nd-rikast faasi, mis on ühtlasemalt jaotatud. Optimeeritud hüdrogeenimine ja jugajahvatus kindlustavad pulbri madalaima keskmise osakeste suuruse (2 μm). Võrdluseks – kõrgenergeetiline jahvatus vesinikus ja vaakumis tagab keskmise osakestesuuruse 0,3 μm ja pulbri madalama oksüdeerimise. NdFeB-TiC magnetid on osutunud termostabiilsemaiks

suhteliselt kõrgetel temperatuuridel. Neil on kõrgem Curie' temperatuur ja TiC lisamine hüdrogeenitud ribavalusse mõjutab positiivselt materjali magnetomadusi.

Töö põhieesmärgiks oli saada sügavamaid teadmisi haruldaste muldmetallide baasil püsimagnetitest, nende magnetomadustest ja magnetmaterjalide karakteriseerimisest; välja töötada mikrostruktuure ja keemiliste koostiste valikukriteeriumid paremate magnetomaduste tagamiseks.

Käesolevas töös on lahendatud ja ületatud järgmised teaduslikud ja tehnoloogilised väljakutsed:

- püsimagnetite valmistamine;
- mikrostruktuuri iseloomustamine;
- magnetomaduste mõõtmine ja hindamine;
- kahjulike lisandite kontroll;
- Nd ja Pr osaline asendamine teiste haruldaste muldmetallidega;
- magnetite termostabiilsuse parandamine.

Võtmesõnad: magnetmaterjalid, Nd-Fe-B püsimagnetid, $Nd_2Fe_{14}B$, Ce-ga magnetsulamid, jugajahvatus, termostabiilsus

Other publications

Mural, Z., Kollo, L. and Veinthal, R. (2014). Jet Milling of the Powders for Nd-Fe-B Sintered Magnets. *2014 International Conference on NdFeB Magnets: Supply Chain, Critical Properties & Applications (NdFeBpm2014)*, Ningbo, China, 02-05.03.2014, 181−183.

Mural, Z., Kollo, L. and Veinthal, R. (2016). Spark Plasma Sintered Nd-Fe-B Magnets from High-Energy Ball Milled Powders. *The 24th International Workshop on Rare-Earth and Future Permanent Magnets and Their Applications (REPM 16)*, Darmstadt, Germany, 28.08-01.09.2016

Approbation

Scientific results presented in the thesis have been presented at the following international conferences:

1. Applied Magnetic Materials 2013, Pori, Finland (2013) – *High-energy ball milling of Nd-Fe-B powders* (oral presentation)
2. 22nd International Baltic Conference: Engineering materials and tribology, Riga, Latvia (2013) – *Structure and Magnetic Properties of NdFeB Powder Prepared by Hydrogen Decrepitation and High-energy Ball Milling* (oral presentation)
3. 2014 International Conference on NdFeB Magnets: Supply Chain, Critical Properties & Applications, Ningbo, China (2014) – *Jet Milling of the Powders for Nd-Fe-B Sintered Magnets* (oral presentation)
4. Junior Euromat 2014, Lausanne, Switzerland (2014) – *Microstructure and magnetic properties of cerium alloyed sintered Nd-Fe-B magnets* (oral and poster presentation)
5. 23rd International Baltic Conference on Materials Engineering, Kaunas, Lithuania (2014) – *Influence of Optimised Jet Milling Parameters to the Magnetic Properties of Nd-Fe-B Sintered Magnets* (poster presentation)
6. 20th International Conference on Magnetism, Barcelona, Spain (2015) – *TiC Additive in Neodymium Iron Boron Magnets* (poster presentation)
7. The 24th International Workshop on Rare-Earth and Future Permanent Magnets and Their Applications (REPM 16), Darmstadt, Germany (2016) - *Spark Plasma Sintered Nd-Fe-B Magnets from High-Energy Ball Milled Powders* (poster presentation)

Acknowledgements

I wish to express my sincere gratitude to my supervisors Professor Renno Veinthal and Senior Research Scientist Lauri Kollo from the Department of Materials Engineering of Tallinn University of Technology (TUT) for providing me an opportunity to do my doctoral study and work under the project "Permanent magnets for sustainable energy application (MagMat)".

I sincerely thank Hans Vallner, TUT engineer, for his continuous effort related to technical issues and rescue the laboratory from several fireworks initiated by me. My thanks are due to MSc. student Yusuf Ilke Čakmakoglu for his assistance in preparing and conducting the experiments.

During my PhD studies I had a pleasure of collaboration with scientists from Technical University of Denmark (DTU). The efforts of Senior Research Scientists Christian Bahl and Asger Bech Abrahamsen are highly appreciated.

I would like to thank all my colleagues in the TUT Department of Materials Engineering for their assistance and support. The teams of Molycorp Silmet AS, Neorem Magnets OY and Prizztech OY are recognized for their helpful hints and tips. The Archimedes Foundation is acknowledged for covering my travel costs. National Institute of Chemical Physics and Biophysics, especially Joosep Link, and TUT Department of Fundamentals of Electrical Engineering and Electrical Machines deserve my thanks as well.

Finally, I would like to thank my family and friends for their everyday support and encouragement. Belly rubs to my four-legged buddy Karabas for being by my side and accepting shorter walks while I was concentrated on the work.

APPENDICES

Curriculum Vitae

Personal information:
Name: Zorjana Mural
Date and place of birth: 30.06.1988 Tallinn, Estonia
E-mail: zorjana.mural@ttu.ee

Language skills (mother tongue, fluent, average, basic skills)

Language	Level
Russian	Mother tongue
Estonian	Fluent
English	Fluent
Ukranian	Fluent
German	Basic

Career:
Careers and positions:

Period	Organisation	Position
01.05.2016–...	Ingenium Baltic OY	Engineer
11.01.2016–...	Tallinn University of Technology	Engineer
01.09.2012–30.06.2015	Tallinn University of Technology	Early Stage Researcher
01.04.2012–31.05.2012	Ingenium Baltic OY	Trainee
01.03.2010–01.04.2010	Ensto Ensek Ltd	Trainee

Education:

Period	Institution	Education (field of study, degree)
2012–2016	Tallinn University of Technology	Materials Engineering, PhD studies
2010–2012	Tallinn University of Technology	Production Engineering, M. Sc.
2007–2010	Tallinn University of Technology	Product Development, B. Sc.
1995–2007	Tallinn Central Russian Gymnasium	Secondary Education

Qualifications:
Academic degrees:
Master's Degree, 2012, supervisor Prof. Renno Veinthal, Gaseous impurities in the metallic niobium, Tallinn University of Technology, Faculty of Mechanical Engineering, Department of Materials Engineering.

Research fields:
Field of research: 4. Natural Sciences and Engineering; 4.12. Process Technology and Materials Science; CERCS speciality: T150 Material technology; Speciality: Magnetic materials (Nd-Fe-B)

Projects:
2012–2015 Permanent magnets for sustainable energy application (MagMat). Tallinn University of Technology, Faculty of Mechanical Engineering, Department of Materials Engineering. Project nr AR12131

Elulookirjeldus

Isiku- ja kontaktandmed:
Nimi: Zorjana Mural
Sünniaeg ja -koht: 30.06.1988 Tallinn, Eesti
E-post: zorjana.mural@ttu.ee

Keelteoskus (emakeel, alg-, kesk- või kõrgtase):

Keel	Tase
Vene	emakeel
Eesti	kõrgtase
Inglise	kõrgtase
Ukraina	kõrgtase
Saksa	algtase

Teenistuskäik:
Töökohad ja ametid:

Periood	Organisatsioon	Ametikoht
01.05.2016–...	Ingenium Baltic OÜ	Insener
11.01.2016–...	Tallinna Tehnikaülikool	Insener
01.09.2012–30.06.2015	Tallinna Tehnikaülikool	Nooremteadur
01.04.2012–31.05.2012	Ingenium Baltic OÜ	Praktikant
01.03.2010–01.04.2010	Ensto Ensek AS	Praktikant

Haridustee:

Periood	Õppeasutus	Haridus (eriala, kraad)
2012–2017	Tallinna Tehnikaülikool	Materjalitehnika, doktoriõpe
2010–2012	Tallinna Tehnikaülikool	Tootmistehnika, magistrikraad
2007–2010	Tallinna Tehnikaülikool	Tootearendus, bakalaureusekraad
1995–2007	Tallinna Kesklinna Vene Gümnaasium	Keskkool

Kvalifikatsioon:
Teaduskraadid:
Magistrikraad, 2012, juhendaja prof. Renno Veinthal, Gaasilised lisandid metallilises nioobiumis, Tallinna Tehnikaülikool, mehaanikateaduskond, materjalitehnika instituut.

Teadustöö põhisuunad:
Valdkond: 4. Loodusteadused ja tehnika; 4.12. Protsessitehnoloogia ja materjaliteadus; CERCS eriala: T150 materjalitehnoloogia; põhisuund: magnetmaterjalid (Nd-Fe-B)

Projektid:
2012–2015 Püsimagnetid jätkusuutliku energeetika rakendustes (MagMat). Tallinna Tehnikaülikool, mehaanikateaduskond, materjalitehnika instituut. Projekti nr AR12131

PUBLICATIONS

Paper I **Mural, Z**., Kolnes, M., Afshari, H., Kollo, L., Link, J. and Veinthal, R. Fabrication and microstructural analysis of didymium-iron-boron magnet alloys with cerium additions. *Proceedings of the Estonian Academy of Sciences*, 65 (2), 2016, 166 – 171.

Proceedings of the Estonian Academy of Sciences,
2016, **65**, 2, 166–171
doi: 10.3176/proc.2016.2.02
Available online at www.eap.ee/proceedings

MATERIALS
ENGINEERING

Fabrication and microstructural analysis of didymium–iron–boron magnet alloys with cerium additions

Zorjana Mural[a*], Märt Kolnes[a], Hosein Afshari[a], Lauri Kollo[a], Joosep Link[b], and Renno Veinthal[a]

[a] Department of Materials Engineering, Tallinn University of Technology, Ehitajate tee 5, 19086 Tallinn, Estonia
[b] National Institute of Chemical Physics and Biophysics, Akadeemia tee 23, 12618 Tallinn, Estonia

Received 7 September 2015, revised 30 October 2015, accepted 16 November 2015, available online 17 March 2016

Abstract. A common industrially accepted method for producing magnetic alloys with fine, α-iron-free microstructure is strip casting. Small amounts of alloys can be rapidly solidified with the method called splat quenching. In both cases the quenching rate can reach 10^6 K/s. This work reports the results of using a method for producing small amounts of NdFeB magnetic alloys with Ce additions. The aim of the study was to determine the influence of the cooling rate on the microstructure of the cast. Implementing centrifugal casting in vacuum resulted in NdFeB alloys with the following optimal parameters: sample thickness 0.3 mm, cooling rate 10^5 K/s, rare earth-rich phase content about 4%, thickness of dendrites 1.1 μm, arm spacing of dendrites 0.35 μm, and oxygen content not more than 650 ppm. Theoretically, it is possible to increase the alloy thickness up to 2 mm. Decreasing the cooling speed to the critical level 4×10^3 K/s completely prevented the formation of the undesired features in the microstructure of the cast.

Key words: magnetic alloy, didymium–iron–boron, cerium, microstructure, centrifugal induction casting, cooling rate.

1. INTRODUCTION

Neodymium–iron–boron (NdFeB) alloys can be processed into magnets by several different routes [1,2]. Common methods include classical powder metallurgy, comprising jet milling, orienting the refined powder, compaction, and sintering [3]. Prior to these steps the starting alloy is usually manufactured by rapid solidification: strip casting or ingot casting. In both cases the starting elemental powders or master alloys are induction melted under a protective atmosphere. If ingot casting is used, the mixture of the master alloys is melted and poured into a flat mould. In case of a relatively slow cooling, α-iron precipitation may occur during solidification [2,4]. The α-iron in NdFeB magnets hinders grain alignment and creates Nd-rich regions, which are extremely susceptible to oxidation and therefore to magnet degradation [5]. A possible way of avoiding α-iron is to increase the content of rare earth (RE) elements (Nd, Dy ~15 at%). Another route to terminate the α-iron evolvement is rapid solidification.

Today's standard industrial practice for producing starting powders for powder metallurgy processing is mainly based on strip casting. This method uses a rapidly spinning copper wheel, which contacts with the alloy melt, quenches the melt, and ribbon-shaped particles are formed. Although it has some drawbacks for investigating alloy composition and solidification kinetics, strip casting suits well for standard magnet industry. To get an initial strip cast material with acceptable homogeneity, a relatively large amount of material (up to at least 10 kg per batch) is needed for each experiment.

One route for obtaining rapidly solidified NdFeB alloys is by the method called splat quenching. In case of this method small quantities of molten alloy are directed into contact with a cooled plate. This can be done in different ways, whether by direct casting to the plate, casting between plates, or casting through holes

* Corresponding author, zorjana.mural@ttu.ee

in the plate to cause rapid solidification [6,7]. One of the objectives of the present study was to further develop the splat quenching method in order to produce small quantities (in the range of 10 g) of NdFeB material with a controlled cooling rate. A commercial centrifugal casting device was used to cast the molten metal into experimental moulds. A new cooling cell was designed for the centrifugal casting unit.

Materials based on NdFeB are widely used in the fields of energy, automotive, medical, and computer equipment. In most RE ores, the content of Nd is quite small compared to cerium or lanthanum. Due to the increasing demand for RE elements applicable in the magnet industry, overcapacities of and a non-parallel increase in the demand for Ce or La are seen. Therefore new applications for Ce and La are currently researched. A potential use of Ce is its introduction into the NdFeB magnet composition. Yan et al. [8] showed that up to 25 wt% of REs could be replaced by Ce without significant decrease in magnetic properties. Nevertheless, the development of the microstructure during rapid solidification and the effect of alloying elements on magnetic properties of Ce-containing NdFeB magnets are not extensively investigated.

We studied a NdFeB alloy where Nd and Pr were partially substituted with Ce to obtain an α-iron-free microstructure with an optimized phase composition. In this paper the relationships between the cooling rate and microstructures, chemical composition, and phase contents of Ce-containing alloys are reported.

2. EXPERIMENTAL

A didymium magnetic alloy (Nd and Pr were not separated during extraction) with the chemical composition $Nd_{22}Pr_{1.8}Dy_1Nb_{0.3}Al_{0.45}Ce_{8.3}B_{1.2}Fe_{bal}$ was prepared by centrifugal induction melting of mixtures of elemental powders Fe, Nd, Al and master alloys FeB, NdFe, NdPrFe, CeFe, and DyFe. In all the initial materials the oxygen content was below 600 ppm and the carbon content was below 400 ppm. A centrifugal casting unit Lifumat Met 3.3 Vac (Linn GmbH) was used for the splat quenching experiments. Starting materials were crushed and the premix was placed into a tantalum crucible. The mixture was heated under vacuum (10^{-2} mBar) up to 1523 K within few minutes and held for 5–10 s. Casting was performed into an experimental copper mould when the rotating speed of 600 rpm was reached. The microstructures of the as-cast materials were identified by scanning electron microscopy (SEM). Quantitative microstructure analysis for determining phase content, dendrite thickness, and dendrite arm spacing was carried out using ImageJ software. Oxygen content was determined using an Eltra ONH-2000 spectroscope. Inductively coupled plasma optical emission spectrometry (ICP–OES) was used to characterize the chemical composition of cast alloys. Differential scanning calorimetry (DSC) was applied to obtain the melting temperature and crystallization characteristics of the material.

3. RESULTS AND DISCUSSION

3.1. Production of NdFeB alloys by rapid solidification

3.1.1. Design of the cooling cell

The cooling of the NdFeB melt was first accomplished by splat quenching it onto a copper disc with a thickness of 5 mm. The face of the plate was aligned perpendicular to the direction of the melt (Fig. 1a). The thickness of the solidified material plate was approximately 4 mm. In order to decrease the thickness of the solidified NdFeB plate (hence increasing the cooling rate), a new

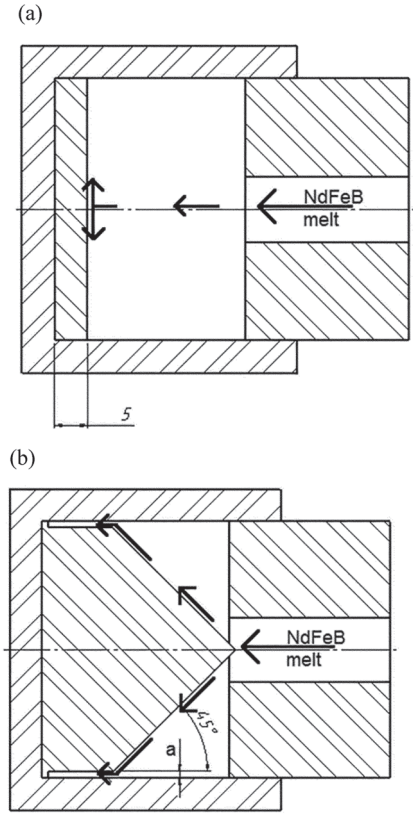

Fig. 1. Sketch of the centrifugal casting mould design: (a) initial version, (b) modified version. The black arrows show melt flow.

cooling cell was designed. This cell had a cone-shaped insert, which first directs the melt towards the outer walls at an angle of 45° (see Fig. 1b). The melt was collected at the thin gap between the inner copper insert and the outer copper cylinder. The gap thickness a was varied between 0.3 and 0.9 mm.

3.1.2. Estimation of the cooling rate

For estimating the cooling capability of the newly designed cooling cells in centrifugal casting, first the cooling rates of the cast NdFeB alloys were calculated. The heat flux calculations were performed using the unsteady heat conduction formula [9] for plate geometry. First, the time needed for the middle of the plate to reach the crystallization temperature was calculated using the following formula:

$$t = \frac{F_0 \rho C_p x_m^2}{k}, \quad (1)$$

where t represents time and x is the distance from the surface to the centre, C_p is specific heat, ρ is density, k is thermal conductivity, and F_0 is the dimensionless Fourier number obtained from the plot in Fig. 2.

Temperature is a function of time after the temperature of two surfaces has been rapidly increased to T_0, which is the temperature at which the crystallization stage is completed. In our calculations, 973 K was used as T_0. Temperature T_i is the initial temperature of the mid-plane of the plate. The cooling rate ε for each sample was calculated using the following formula:

$$\varepsilon = \frac{\Delta T}{t}, \quad (2)$$

where ΔT is the temperature change between 1523 K and 973 K and t is time [9].

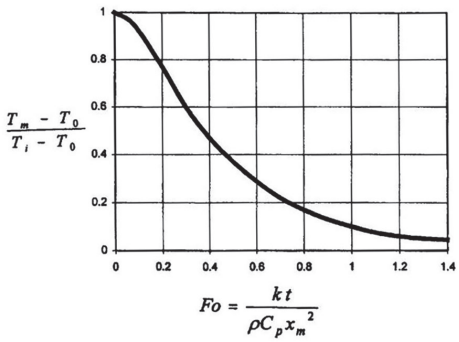

Fig. 2. Plot for calculating the temperature T_m at the centre of a plate [9].

Table 1. Experimentally determined thermal specification of the NdFeB alloy

Density ρ, g/cm^3	Thermal conductivity k, W/m K	Melting point T_{melt}, K	Specific heat c, J/kg K	T_0, K
6.7	9.0	1469	521	973

Table 2. Cooling rates and batch sizes per cast

Sample	Sample thickness, mm	Cooling rate, K/s	Batch size, g
A40	4.0	1×10^3	6.0
B03	0.3	2×10^5	0.5
B06	0.6	5×10^4	1.0
B09	0.9	2×10^4	1.6

For the calculation of the cooling rate, a control volume inside the mould was chosen. It had a plate with the surface area of 1 cm^2 and different thicknesses in different moulds.

Experimentally obtained information concerning thermal properties of the alloys and density are reported in Table 1. The cooling rate for the alloy quenched onto the disc was determined to be 10^3 K/s. The sample thickness is about 4 mm. Batch size is 5–6 g/cast.

Quenching rates for the modified cooling unit, calculated applying the above-described procedure, were estimated as 2×10^5, 5×10^4, and 2×10^4 K/s, respectively (see Table 2). As all the samples had identical chemical composition, the alloys' designations A40 and B03–B09 follow the version of the cooling unit design.

The batch size for alloys cast into the modified mould varied between 0.5 and 1.6 g in a 5 g sample. According to experimental results, the cooling rate should be higher than 10^3 K/s to achieve an α-iron-free alloy. Sample thickness can be calculated using this value in Eqs (1) and (2). This allows predicting that it is possible to go up to 2 mm thick casts to obtain an α-iron-free microstructure and increase the batch size up to 7–8 g in a 10 g sample.

3.2. Development of the RE–Ce alloy

3.2.1. Stability of the alloy composition

The chemical composition and distribution of the alloying elements were studied to verify the uniformity, possible changes in the chemical composition during casting, and sensitivity to oxygen contamination. Firstly, the premixed starting powders were crushed and held in air for one week in order to initiate partial oxidation of RE elements. The experiments showed low sensitivity of splat quenching towards oxidation. The oxides were

Table 3. Example of boron loss during melting and casting

	B content in starting mixture, wt%	B content in cast alloy, wt%	B loss, wt%
A40	0.60	0.26	58.00
A40	1.80	0.71	61.00
Average loss			59.50

found to be removed with the slag, and the oxygen content of the resulting alloy was less than 700 ppm. The difference between the calculated and measured content of RE and other elements did not exceed 1.5%.

Secondly, the stability of boron during casting was estimated. A significant loss of the boron content was observed after casting. Table 3 shows the boron content in the starting mixtures and cast alloys. The average boron loss was about 60%. It can be due to the reactions between boron, oxygen, and nitrogen impurities and the consequent removal of the compounds with the slag. Boron loss was taken into account when designing the alloy composition so that the final cast alloy has 1.2 wt% of boron.

3.2.2. Effect of the cooling rate on the alloy microstructure

The microstructure of sample A40 with the estimated cooling rate of 10^3 K/s is shown in Fig. 3.

A considerable amount of α-iron was observed starting from around 100 μm from the contact surface (area b in Fig. 3). This is due to the relatively slow solidification of the melt. From standard strip casting, the cooling rate is known to dramatically influence the microstructure and magnetic properties of the alloys [10].

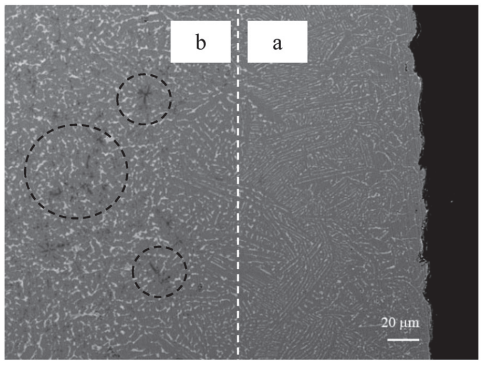

Fig. 3. Micrograph of the cast ingot with the formed α-iron: (a) rapidly cooling area that was in contact with the mould; (b) more slowly cooled area. Dashed circles show α-iron areas.

Clearly, for cerium alloyed neodymium magnets under-quenching occurs when a cooling rate below 10^3 K/s is used. Under-quenching refers to the critical point of cooling speed at which α-iron dendrites start to occur. This shows that magnet alloys applicable for standard powder metallurgy processing can be processed only in thin layered forms.

Micrographs of cast alloys B03, B06, and B09 are presented in Fig. 4. No α-iron was observed.

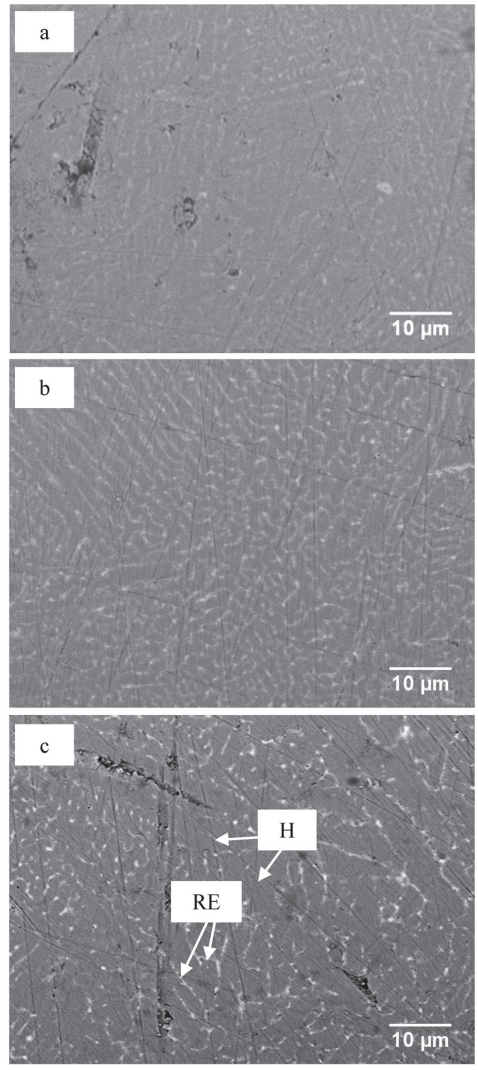

Fig. 4. Microstructures of the alloys: (a) B03, (b) B06, and (c) B09. H – hard phase, RE – rare earth-rich phase.

The thicknesses of the dendrites (hard phase thickness) and dendrite arms (RE-rich phase thickness) between them are presented in Table 4, where also the contents of the phases are shown for comparison. It is clearly seen that the higher the quenching rate, the finer the microstructure features and the more homogeneous the mixture of phases. The difference between the thicknesses of the dendrites of samples B09 and B03 is more than 60% and between dendrite arm spacings about 25%. Figure 5 re-plots the data presented in Table 4 to show the correlation between the cooling rate, thickness of dendrites, and arm spacing of dendrites.

For comparison, strip casting provides a uniform and α-iron-free dendritic microstructure of the strips with the thickness of 0.2–0.3 mm, hard phase thickness of 4–6 μm, and RE-rich phase thickness up to 0.5 μm [11,12]. In case of Ce-containing alloys, α-iron dendrites form more easily due to the lower melting point of the CeFeB phase [13]. Gao et al. [14] showed that when the drop tube technique is used most small drops of NdFeB alloy are free from the α-iron phase because of the high under-cooling prior to solidification. However, the droplet size should stay below 0.6 mm for the alloys with lower RE content and below 2 mm for the alloys that are rich in RE. These authors also claim that lower cooling rates result in a coarse microstructure. Our results are in a good agreement with those provided by Gao et al. [14] for the Ce-free alloy.

Table 4. Microstructure of the melts

Sample	RE-rich phase, %	Hard phase, %	Dendrite thickness, μm	Dendrite arm spacing, μm
B03	3.90	96.10	1.08	0.35
B06	6.70	93.30	1.36	0.37
B09	12.50	87.50	1.78	0.43

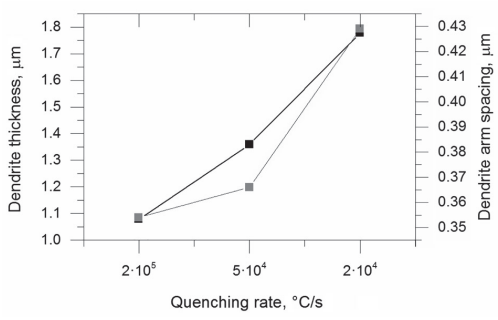

Fig. 5. Correlation of quenching rate and parameters of microstructure.

4. CONCLUSIONS

Magnetic NdFeB alloys were prepared by centrifugal induction casting to study the influence of quenching rate on the microstructure of the castings. By implementing this method it is possible to achieve a cooling rate up to 10^5 K/s and obtain an alloy with a fine microstructure free from α-iron with a smaller Nd-rich phase that is distributed more homogeneously. However, the batch size in this case is only 0.5 g per melt. Increasing the cast thickness up to 0.9 mm gives a maximum of 1.6 g. Theoretically, it is possible to increase the amount of the molten alloy flown into the mould up to 8 g per cast. In this case the gap between the inner insert and the outer cylinder should be 2 mm. Generally, to eliminate the formation of α-iron the cooling speed should be higher than 1×10^3 K/s.

ACKNOWLEDGEMENT

This work was partially supported by the project ‘Permanent magnets for sustainable energy application (MagMat)’ funded from the European Regional Fund under project 3.2.1101.12-0003 in Estonia.

REFERENCES

1. Hilzinger, R. and Rodewald, W. *Magnetic Materials: Fundamentals, Products, Properties, Applications*. Publicis Verlag, 2013.
2. Coey, J. M. D. *Rare-Earth Iron Permanent Magnets*. Oxford University Press Inc., New York, 1996.
3. Kaneko, Y., Kuniyoshi, F., and Ishigaki, N. Proven technologies on high-performance Nd–Fe–B sintered magnets. *J. Alloy. Comp.*, 2006, **408–412**, 1344–1349.
4. Wang, X., Minggang, Z., Wei, L., Liyun, Z., Dongliang, Z., Xiao, D., and An, D. The microstructure and magnetic properties of melt-spun CeFeB ribbons with varying Ce content. *Electron. Mater. Lett.*, 2015, **11**(1), 109–112.
5. Scott, D. W., Ma, B. M., Liang, Y. L., and Bounds, C. O. Microstructural control of NdFeB cast ingots for achieving 50 MGOe sintered magnets. *J. Appl. Phys.*, 1996, **79**, 4830–4832.
6. Harada, T., Ando, T., O’Handley, R. C., and Grant, N. J. Microstructures and magnetic properties of anisotropic Nd–Fe–B magnets produced by splat-quenching. *J. Appl. Phys.*, 1991, **70**, 6468–6470.
7. Nagashio, K., Mingjun, L., and Kazuhiko, K. Containerless solidification and net shaping by splat quenching of undercooled $Nd_2Fe_{14}B$ melts. *Mater. T. JIM*, 2003, **44**(5), 853–860.
8. Yan, C., Guo, S., Chen, R., Lee, D., and Yan, A. Effect of Ce on the magnetic properties and microstructure of sintered didymium–Fe–B magnets. *IEEE T. Magn.*, 2014, **50**(10), article No. 2102605.
9. Vlachopoulos, J. and Strutt, D. Basic heat transfer and some applications in polymer processing. *Plastics Technician’s Toolbox*, 2002, **2**, 21–33.

10. Yu, L. Q., Yan, M., Wu, J. M., Luo, W., Cui, X. G., and Ying, H. G. On the cooling rate of strip cast ingots for sintered NdFeB magnets. *Physica B*, 2007, **393**, 1–5.
11. Yan, G. H., Chen, R. J., Ding, Y., Guo, S., Lee, D., and Yan, A. R. The preparation of sintered NdFeB magnet with high-coercivity and high temperature-stability. *J. Phys. Conf. Ser.*, 2011, **266**, 012052.
12. Vial, F., Joly, F., Nevalainen, E., Sagawa, M., Hiraga, K., and Park, K. T. Improvement of coercivity of sintered NdFeB permanent magnets by heat treatment. *J. Magn. Magn. Mater.*, 2002, **242–245**, 1329–1334.
13. Yan, C., Guo, S., Chen, R., Lee, D., and Yan, A. Enhanced magnetic properties of sintered Ce–Fe–B-based magnets by optimizing the microstructure of strip-casting alloys. *IEEE T. Magn.*, 2014, **50**(11), article No. 2104604.
14. Gao, J., Volkmann, T., Roth, S., Löser, W., and Herlach, D. M. Phase formation in undercooled NdFeB alloy droplets. *J. Magn. Magn. Mater.*, 2001, **234**, 313–319.

Tseeriumiga NdFeB magnetsulamite valmistamine

Zorjana Mural, Märt Kolnes, Hosein Afshari, Lauri Kollo, Joosep Link ja Renno Veinthal

Levinuimaks magnetsulamite valmistamise meetodiks on tänapäeval ribavalu. Antud meetodiga toodetud sulamid ei sisalda mikrostruktuuris α-rauda ja on peene struktuuriga tänu suurtele allajahutamiskiirustele. Väikese koguse sulami eksperimentaalseks valmistamiseks saab pidevprotsessi (ribavalu) asendada tsüklilisega, mida inglise keeles tähistab mõiste *splat quenching*. Antud juhul tardub väike kogus kokkupuutel jahutatud vormipinnaga. Mõlema meetodi puhul saavutatakse jahtumiskiirus kuni 10^6 K/s. Artiklis on kirjeldatud tsentrifugaalvalumeetodit, mis võimaldab väikestes kogustes NdFeB magnetsulamite valmistamist. Töö eesmärgiks oli uurida jahtumiskiiruse mõju magnetsulami mikrostruktuurile. Töö tulemusena saadi optimaalsete parameetritega NdFeB sulam: jahtumiskiirus 10^5 K/s, lamelli paksus 0,3 mm ja hapnikusisaldus alla 650 ppm.

Paper II **Mural, Z**., Kollo, L., Traksmaa, R., Kallip, K., Link, J. and Veinthal, R. Structure and Magnetic Properties of NdFeB Powder Prepared by Hydrogen Decrepitation and High-energy Ball Milling. *Key Engineering Materials*, 604, 2014, 262 – 266.

Key Engineering Materials Vol. 604 (2014) pp 262-266

doi:10.4028/www.scientific.net/KEM.604.262

Structure and Magnetic Properties of NdFeB Powder Prepared by Hydrogen Decrepitation and High-energy Ball Milling.

Zoryana Mural[1a], Lauri Kollo[1b], Rainer Traksmaa[2], Kaspar Kallip[1], Joosep Link[3] and Renno Veinthal[1c]

[1]Department of Materials Engineering, Tallinn University of technology, Estonia
[2]National Institute of Chemical Physics and Biophysics, Estonia
[3]Centre for Materials Research, Faculty of Chemical and Materials Technology, Tallinn University of Technology, Estonia,
[a]zorjana.mural@ttu.ee, [b]lauri.kollo@ttu.ee, [c]renno.veithal@ttu.ee

Keywords: NdFeB powder; Hydrogen decrepitation; High–Energy Ball Milling; Attritor milling; Magnetic properties; Microstructure

Abstract. An ingot of NdFeB alloy was disintegrated by hydrogen decrepitation (HD). High-energy ball milling technique with hard metal milling elements and balls was employed to refine HD powders down to particle size optimum for magnet processing. The experiments were performed according to experimental plan to optimize the milling parameters regarding particle size, contamination and magnetic properties of the powder. The effect of milling time, speed of rotation, ball-powder weight ratio (BPR) and amount of wet agent was investigated. The highest influence was shown to be from attritor speed of rotation, ball-to powder ratio and combined effect of milling wet agent and rotating speed. Unified parameter of estimated number of total ball impacts was calculated, which allows predicting the final particle size of the powder at different milling speeds. Magnetic moments of powders were measured.

Introduction

Permanent magnets based on NdFeB have been used in various applications for their superior magnetic properties, since they were discovered in 1983 [1]. The conventional production route of sintered rare-earth magnets begins with coarse and fine crushing of ingot material. Hydrogen Decrepitation (HD) procedure can be used to replace energy consuming crushing operations [2]. Industrially, prior to aligning and pressing, jet milling for particle size refinement is performed. An alternative to the jet miller is high-energy ball milling. The advantages of attritor milling are simplicity, inexpensiveness and high efficiency in reducing the particle size [3]. Batch production, drying procedure of the powder prior to pressing and possible contamination with milling media are main disadvantages of milling in attritor [4]. In the present work experimental space was defined to reveal the effect of milling time, speed of rotation, ball to powder weight ratio (BPR) and amount of wet agent on particle size of the milled powder.

Materials and methods

The alloy with nominal composition of $Nd_{36,9}Fe_{61,5}B_{1,1}Al_{0,5}$ was supplied by Molycorp Silmet AS. A microstructure of polished as-cast alloy is shown in Figure 1. It consists of two phases: hard $Nd_2Fe_{14}B$ phase (a) and soft Nd-rich phase (b).

Alloy was crushed into 1-2 cm^3 pieces and placed into stainless steel container for hydrogenation at 350 °C for 1 h. Irregular Fraction Array was used to design the experimental space for fine crushing of these particles using 500 mL attritor (utility model EE00507U1) [5]. The experimental plan is shown in Table 1. The input parameters were chosen to influence the number of impacts during the milling (milling time, ball to powder ratio and rotational speed) and energy of impact (rotational speed). Additionally, amount of heptane was varied in order to evaluate the effect of amount of wet agent on the particle size. Milling periods of 1 and 4 hours were used. Heptane was used as wet agent to limit the powder oxidation. The solvent was mixed with 20 g of powder with weight ratio of 1:1 and 5:1 (25 and 100 ml of heptane accordingly). The weight ratios of the WC-Co balls (diameter 7 mm) to the powders were 5:1 and 10:1. Rotational speed of the attritor varied from

500 to 850 rpm. Milled powder was dried in vacuum evaporator and stored in glove-box under nitrogen atmosphere. The heat treatment of the HD attritor milled powder was performed in high vacuum at temperature of 650 °C for 4 h to desorb the hydrogen from powder.

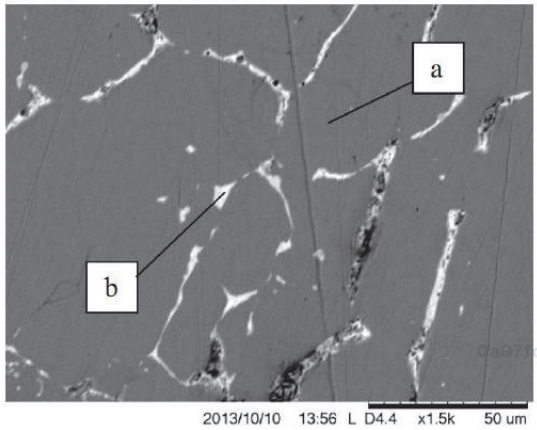

Figure 1. SEM image showing as-cast structure of the NdFeB alloy, x500. Observed phases: a) $Nd_2Fe_{14}B$ pha–se, b) Nd-rich phase.

Results and discussion

Table 1 represents the average particle size of the milled powders before the hydrogen desorption according to the input parameters. With some exceptions, the desired particle size for commercial scale magnet production (2-5 μm) was obtained [6]. Final particle size varies between 1.2 and 22.5 μm. Particle size was measured using software ImageJ. No direct influence of specific parameters can be seen, except for that lower milling speed yields the largest particle sizes. An example of the morphology of the HD attritor milled powder is shown in Figure 2. The particle shape after milling is angular.

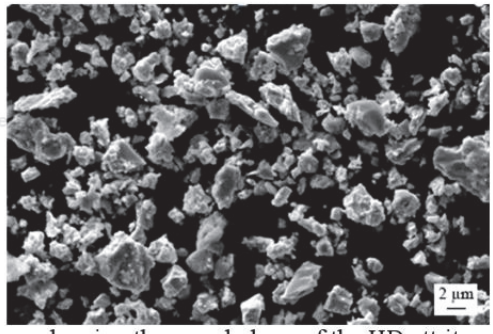

Figure 2. SEM image showing the morphology of the HD attritor milled powder N2.

Phase composition studies were performed on chosen samples. Figure 5 shows the diffraction patterns of the HD powder and attritor milled powders after hydrogen absorption. The samples with coarse grain sizes (N3 and N4) show crystalline phase structure after milling. On the other hand, after milling for extended times at high speeds (N1 and N2) the powder is in majority amorphous.

Figure 6 shows the XRD patterns of the as-cast alloy and N2 powder before and after hydrogen desorption. Tungsten carbide peak has evolved due to the wear of the milling media. Estimated amount of tungsten carbide in the material is ~20 vol%. After dehydrogenation $Nd_2Fe_{14}B$ peaks are distinguishable. In addition α-Fe peak has evolved. Magnetic moment of 70…90 Am^2/kg was measured using 14T VSM that is a part of Physical Properties Measurement System (PPMS).

Table 1. Experimental plan employed for high-energy ball milling.

ID	BPR	Wet agent [ml]	Time [h]	Speed [rpm]	Particle size [μm]
N1	10:1	100	4	850	3.0
N2	10:1	25	4	850	1.2
N3	10:1	100	1	500	5.0
N4	10:1	100	4	500	8.0
N5	10:1	25	1	850	2.3
N6	5:1	100	1	850	2.2
N7	5:1	25	4	850	5.1
N8	5:1	100	4	850	2.4
N9	10:1	25	1	500	4.5
N10	5:1	25	1	500	13.3
N11	5:1	100	1	500	22.5
N12	5:1	25	4	500	4.8

The influence of the milling to grain refinement and phase structure can be separated to two effects – number of impacts and the kinetic energy of single impact. As the amount of powder in this study was not varied, the number of impacts at certain speed of milling can be assumed to be directly related to the number of balls in the vessel. This was 38 and 72, for BPR of 5:1 and 10:1 respectively. Additionally, the number of impacts is influenced by milling time and speed of rotation. The estimated total number of impacts N during attritor milling was calculated by formula

$$N = t \cdot n \cdot f, \tag{1}$$

where t is time of milling, n is number of balls. Impact frequency of single ball f was estimated using experimental study for ball dynamics in attritor mill. It was calculated as a percentage of rotational speed, being 2.3 Hz for 500 rpm and 4.8 Hz for 850 rpm [7].

Different process variables were evaluated according to the estimated total number of the impacts. The highest influence was by the speed, BPR and wet agent combined with speed and time (see Figure 1).

The results of average particle size of milled powders according to number of impacts is shown in Figure 4. Higher impact energies (due to higher milling speed – 850 rpm) always yield more refined particles when compared to materials processed with lower impact energies. When milling at 500 rpm, the lowest particle size achieved lays at around 5 μm, at approximately one million of impacts. Increase in particle size can be observed for materials milled for longer periods.

When comparing milling IDs N3 and N4, the only varied parameter is time of milling, which directly relates to the number of impacts. The reason for increased particle size is not well understood, but it could relate to welding of particles.

When milling at higher input energies, the particle size is always less than 5 μm. It seems that balance between fracture and welding during milling is achieved already after 1 hour of milling.
The smallest particle size, 1.2 μm, was obtained for the highest number of impacts. The powders (N1 and N2) exhibit amorphous structure after milling, and yield high content of α- Fe after the heat treatment (See Figure 6). Regarding undesired α-phase the milling should be performed under small impact energies and small number of impacts. In this regard material N3 is most promising of the studied alloys. The material is crystalline and contains insignificant amount of tungsten carbide (See Figure 5).

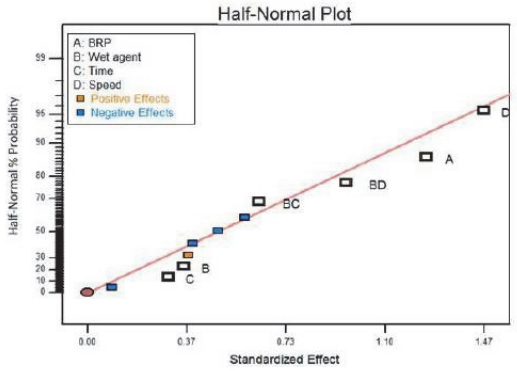

Figure 3. Most significant influence from milling speed (D), BPR (A) and combined effects wet agent +speed(BD) and wet agent + time(BC).

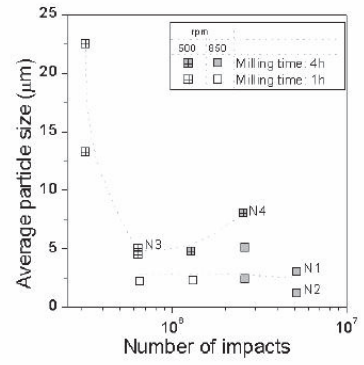

Figure 4. Average particle size versus estimated total number of impacts during the milling.

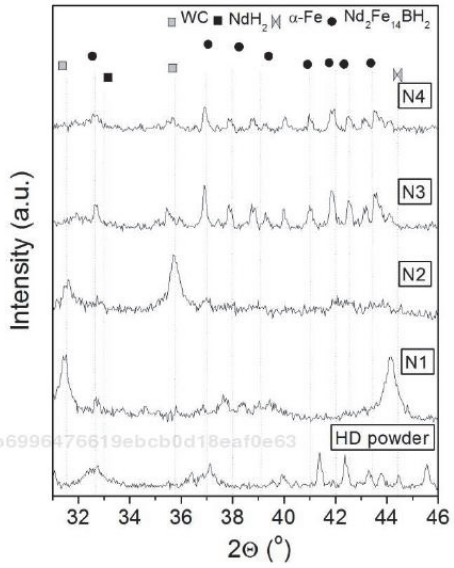

Figure 5. XRD patterns of the HD powder and attritor milled powders after hydrogen absorption,

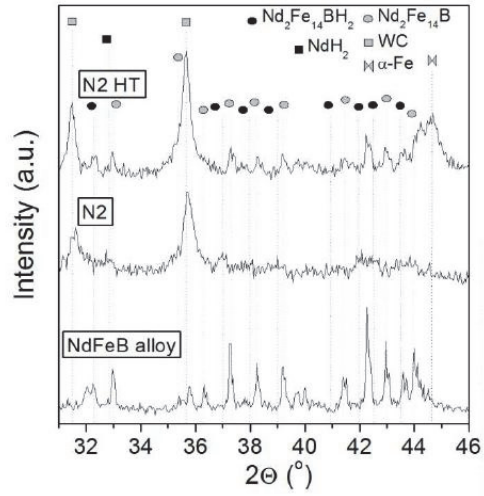

Figure 6. XRD patterns of the as-cast alloy and N2 powder before and after hydrogen desorption.without desorption.

The influence of amount of heptane as milling liquid medium is noticeable, but remains not understood. When milling with highest number of impacts (N1 and N2), higher amount of heptane yields decreased particle size. In the case of smaller number of impacts ($3x10^5$) the influence is opposite – smaller content of heptane yields decreased particle size. After milling HD powder at different milling times, rotation speeds, BPRs and amounts of wet agent average particle sizes varied between 1.2...22.4 μm. After holding powders in the furnace at temperature 650 °C for 4 h the size of the particles increased noticeably. The increased particle size after annealing could be attributed to the formed debris on the particle surface. As the powders were manipulated under protective atmosphere, the oxidation is not believed to be the reason for growth. The particles were screened with EDS in SEM and insignificant content of oxygen was observed for both, milled HD powders and additionally dehydrogenated powders.

Magnetic properties of chosen powders were also investigated. Magnetic moment of 70…90 Am^2/kg for powders N3 and N4 was measured.

Summary

The present study demonstrates that:
(1) It is possible to obtain powder particle size about 1.2 μm implementing HD and high-energy milling using heptane as wet agent to protect the powder from oxidation.
(2)Milling parameters, like BPR, speed of rotation, amount of the wet agent combined with time and wet agent combined with speed have a great influence on the properties of final powder.
(3)After prolonged milling time at high energy input the powder is fine, but contaminated and amorphous.
(4)Number of impacts is in correlation with average particle size. Powder was refined after small number of impacts (~$6x10^5$) and particle size was not decreased after further milling (up to ~$5x10^6$ impacts).
(5)Marked influence from the wet process control agent, heptane was observed. Mechanisms of these effects remain not understood. It was noticed, that in case of highest number of impacts, higher amount of heptane yields decreased particle size and otherwise, in the case of smaller number of impacts, smaller content of heptane yields decreased particle size.
(6) Regarding undesired contamination, amorphization and formation of α-phase the milling should be performed under small impact energies and small number of impacts.

Acknowledgments

This work has been partially supported by project “Permanent magnets for sustainable energy application (MagMat)” receiving funding from the European Regional (Social) Fund under project 3.2.1101.12-0003 in Estonia.

References

[1] M. Sagawa, S. Fujimura, N. Togawa, H. Yamamoto and Y. Matsuura, New material for permanent magnets on a base of Nd and Fe, Journal of Applied Physics, 55(1984) 2083-2087.
[2] P. J. McGuiness, I.R.Harris., E. Rozendaal, J. Ormerod, M. Ward, The production of a Nd-Fe-B permanent magnet by a hydrogen decrepitation/attritor milling route, Journal of Materials Science 21(1986) 4107-4110.
[3] K. Simeonidis, C.S., E. Papastergiadis, M. Angelakeris, I. Tsiaoussis, O. Kalogirou, Evolution of Nd2Fe14B nanoparticles magnetism during surfactant-assisted ball-milling, Intermetallics, 19(2011) 589-595.
[4] J.M.D. Coey, Rare-Earth Iron Permanent Magnets, Clarendon Press, 1996.
[5] D.J. Street, D.J., L. Burgess, The Construction of Optimal Stated Choice Experiments: Theory and Methods, Wiley, 2007.
[6] D. Brown, Bao-Min Ma and Zhongmin Chen, Developments in the processing and properties of NdFeB-type permanent magnet, Journal of magnetism and magnetic materials, 248(2002) 432-440.
[7] R. W. Rydin, D. Maurice and T.H. Courtney, Milling Dynamics: Part 1. Attritor, Metallurgical transactions, 24(1993).

Paper III Kollo, L., Kallip. K., **Mural, Z**., Vallner, H., Veinthal, R., Kolnes, M., Tarraste, M. and Jõeleht, M. (2016). Method and device for manufacturing sintered material products. Patent number: EE 05786 B1. Publication date: 27.01.2017.

EE 05786 B1

(19) EESTI VABARIIK
PATENDIAMET

(11) **EE 05786 B1**

(51) Int.Cl.
B22F 3/12 (2015.01)
B22F 9/04 (2015.01)
C22C 1/04 (2015.01)

(12) PATENDIKIRJELDUS

(21) Patenditaotluse number: **P201500021**

(22) Patenditaotluse esitamise kuupäev: **13.05.2015**

(24) Patendi kehtivuse alguse kuupäev: **13.05.2015**

(43) Patenditaotluse avaldamise kuupäev: **15.07.2016**

(45) Patendikirjelduse avaldamise kuupäev: **16.01.2017**

(73) Patendiomanik:

Tallinna Tehnikaülikool
Ehitajate tee 5, 19086 Tallinn, EE

(72) Leiutise autorid:

Lauri Kollo
Ehitajate tee 5, 19086 Tallinn, EE

Kaspar Kallip
Ehitajate tee 5, 19086 Tallinn, EE

Zorjana Mural
Ehitajate tee 5, 19086 Tallinn, EE

Hans Vallner
Ehitajate tee 5, 19086 Tallinn, EE

Renno Veinthal
Ehitajate tee 5, 19086 Tallinn, EE

Märt Kolnes
Ehitajate tee 5, 19086 Tallinn, EE

Marek Tarraste
Ehitajate tee 5, 19086 Tallinn, EE

Marek Jõeleht
Ehitajate tee 5, 19086 Tallinn, EE

(54) Meetod ja seade pulbermaterjalist toodete valmistamiseks

(57) Käesolev leiutis käsitleb meetodit ja seadet pulbermaterjalide valmistamiseks, kus pulbrite jahvatamine, sellele järgnev käitlemine ning konsolideerimine toimub vaakumikeskkonnas. Leiutisekohase meetodiga vähendatakse töödeldava kergesti reageeriva pulbermaterjali saastumist eelkõige hapnikuga. Meetod on kasutatav kergelt oksüdeeruvatest materjalidest nagu magnetsulamitest, kergmetallidest või karbiidkermistest peenpulbrite ja neist valmistatud toodete saamiseks.

(57) The present invention aims at providing a method and device for manufacturing sintered material products, whereas milling of the powders and subsequent handling and consolidation is performed under vacuum atmosphere. The presented method allows reduction of contamination of highly reactive materials, especially with oxygen. The method is applicable for fine pulverising of easily oxidising powder materials, like magnet alloys, light metals or ceramic-metal composites and making bulk products from thereof.

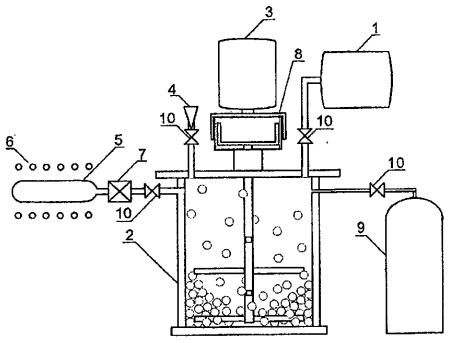

MEETOD JA SEADE PULBERMATERJALIST TOODETE VALMISTAMISEKS

Tehnikavaldkond

Leiutis kuulub masina, metalli- ja aparaaditööstuse valdkonda ning täpsemalt on leiutis ette nähtud pulbritest tahkiste valmistamiseks jahvatamise ja kuumkonsolideerimise teel.

Tehnika tase

Peeneteraliste ning nanostruktuursete materjalide valmistamise meetoditeks on üldiselt pulbermetallurgia meetod, nanostruktuursete materjalide sadestamise meetod ning struktuurse peenendamise meetod kasutades süvaplastset deformatsiooni. Pulbermetallurgia meetod koosneb pulbrite segamisest/aktiveerimisest ning sellele järgnevast kompakteerimisest ning paagutamisest. Jahvatamine viiakse läbi reeglina kuulveskis, kompakteerimine mehhaanilise pressi abil ning paagutamine ülerõhu all või rõhuta kaitsekeskkonnas.

Materjalide valmistamisel peeneteraliste ja nanostruktuursete metallide baasil pulbermetallurgia meetodil tuleb protsessi etappidel reeglina vältida pulbrite oksüdeerumist. Hapniku olemasolu valmisdetailis võib olla soovimatu neodüümmagnetite, supersulamite, titaani, alumiiniumi, magneesiumi jt metalle sisaldavate komposiitide või toodete puhul. Oksüdeerimise vältimiseks viiakse protsessi erietapid läbi kaitsekeskkonnas.

Ühe hapniku vältimise tehnoloogia puhul võidakse kasutada kapseldusmeetodit. Jahvatamine võidakse teostada inertgaasis, vedelikus või vaakumis. Jahvatatud pulber transporditakse inertgaasi keskkonnas kaitsekapslisse, kapsel vakumeeritakse. Vajadusel kuumutatakse kapsel koos selles sisalduva pulbriga vaakumis, et eemaldada soovimatud lisandid (nt vesinik, hapnik). Eelnevalt kompakteerimisele võidakse kapsel sulgeda mehhaaniliselt ning hermeetilisuse tagamiseks see keevitatakse. Kompakteeritakse reeglina pulbrite külmisostaat-pressimisega (CIP), pulbrite valtsimisega, kuumisostaatpressimisega (HIP), kuumpressimisega jt meetoditega. Dokumendis US7354490B2 kirjeldatakse pulbermaterjalide valmistamise meetodit alumiiniumi baasil. Alumiiniumi baasil olevad komposiidipulbrid jahvatatakse vedeliku- keskkonnas vedelas lämmastikus ja järgnevalt konsolideeritakse kuumisostaatpressimisel. Antud tehnoloogiad nõuavad pulbrite degaseerimist, et eemaldada materjalist gaasid, mis takistavad efektiivset konsolideerumist. Antud meetodi puhul toimub kapseldamine kaitsegaasikeskkonnas. Jahvatatud pulber kuivatatakse argoonis, et võimaldada pulbrite transportimist veskist kapslisse. Antud meetodi puudus on, et pulbri transportimise käigus on võimalik pulbrite saastumine hapnikuga.

Teise pulbrite oksüdeerumise vältimise meetodi puhul kasutatakse traditsioonilist pulbermetallurgia meetodit - jahvatamine, pressimine, paagutamine, kus kõik etapid on kaitsekeskkonnas. Jahvatatakse inertgaasi-kaitsekeskkonnas – argoonis või lämmastikus. Jahvatatud pulbrite edasine töötlemine – pressimine, paagutamine toimub samuti inertgaasi-kaitsekeskkonnas. Pulbrite transpordiks eri etappide vahel kasutatakse hermeetilisi, inertgaasiga täidetud kambreid. Dokumendis US6491765B2 kirjeldatakse meetodit magnetite tootmiseks haruldaste muldmetallide baasil. Metalli- või metallihüdriidi pulbrid jahvatatakse jugaveskis lämmastiku keskkonnas. Sellele järgneb magnetpulbrite pressimine ning paagutamine kaitsegaasikeskkonnas. Pulbrid transporditakse kaitsekeskkonnas ning paagutatakse reeglina vaakumis. Antud meetodi puuduseks on, et tööstuslikult on raskendatud magnetite valmistamine pulbritest, mille terasuurus on väiksem kui 1 µm. Tööstusliku puhtusega argoonis (puhtusaste 4N ehk 99,99%) on hapniku sisaldus suurusjärgus 40 ppm ja kastepunkt 72 ppm. Peened metallipulbrid oksüdeeruvad antud tingimustes oma suure eripinna tõttu. Kõrgema puhtusastmega argooni kasutamisega või gaasipuhastite kaasamisega kaasneb protsessi kõrgem hind.

Tuntud on ka pulbrite oksüdeerumise vältimise meetod, mis baseerub märgjahvatusel. Dokumendis WO2010071580A1 kirjeldatakse kõvasulamist materjalide valmistamise pulbersurvevalumeetodit. Antud meetodi puhul jahvatatakse pulbrisegud inertses vedelikus (nt heptaan, isopropanool). Jahvatuse käigus või pärast jahvatamist lisatakse vedelikku plastifikaator, nt parafiinvaha või kautšuk. Jahvatamisele järgnevalt pulbrid kuivatatakse. Kuivamisel vedelik aurustub, plastifikaator sadestub pulbriosakeste pinnale ning moodustab kaitsva kile. Protsessi järgmised etapid – pressimine, paagutamine ning nendevaheline transport toimuvad reeglina õhukeskkonnas. Vaatamata inertsele vedelikule toimub jahvatamisel pulbrite osaline oksüdeerumine, mistõttu antud meetodiga ei saa valmistada saastumiseta kergesti reageerivaid materjale (nt neodüümi baasil magnetid). Samuti lisandub lisaetapp plastifikaatori väljapõletamiseks. Peeneteraliste materjalide valmistamise puhul on vaja eriahjusid, mis võimaldavad plastifikaatori väljapõletamist ning lõpp-vedelfaas paagutust ühes tsüklis.

Juhul kui kogu pulbermetallurgia tootmisprotsess viia alates jahvatamisest kuni konsolideerimiseni läbi vaakumikeskkonnas, on võimalik pulbriosakeste oksüdeerumist tõhusamalt vältida. Tööstuslike vaakumpumpadega on võimalik tekitada vaakum sügavusega kuni *ca* 10^{-8} mbar. Antud sügavusega vaakum on kordades puhtam kõige puhtamatest saadaolevatest inertgaasidest.

Seega, on olemas nõudlus meetodile, millega saab tööstuslikult toota suure puhtusastmega hapnikuvabasid ülipeeni või nanostruktuurseid metall-, keraamilisi või metall-keraamilisi materjale.

Leiutise eesmärk ja olemus

Leiutise esimene eesmärk on täiustada hapnikutundlike pulbrite jahvatuse ja kompakteerimise tehnoloogiaid selliselt, et see vähendaks tootmisprotsessis jahvatuse käigus toimuvat ning jahvatamisele järgnevat pulbrite oksüdeerumist, mis omakorda võimaldab toota kõrge puhtusastmega ning kvaliteetsemaid produkte.

Püstitatud eesmärk saavutatakse meetodiga pulbermaterjalist toodete valmistamiseks, mille kohaselt jahvatatav pulbrisegu sisestatakse veskisse ja jahvatatakse, jahvatatud pulbrisegu teisaldatakse pulbrimahutisse. Pulbrimahutit kuumutatakse väljastpoolt kuumutusallika abil, paagutades nii pulbrisegu. Pulbrimahuti transporditakse pressi juurde ja seda konsolideeritakse avaldades pulbrimahutile välist survet, pulbrimahuti avatakse ja toode eemaldatakse. Seejuures pulbrisegu jahvatamine, teisaldamine, paagutamine ja konsolideerimine ehk pressimine viiakse läbi vaakumikeskkonnas, vaakumis sügavusega $10^{0} - 10^{-8}$ mbar. Jahvatatud pulber on kogu tehnoloogilise protsessi vältel kinnises süsteemis ja kogu tehnoloogiline operatsioon alates pulbrite asetamisest veskisse kuni paagutatud detaili eemaldamiseni kaitsekapslist toimub vaakumikeskkonnas.

Eelistatavalt kasutatakse veskina kuulveskit, millesse sisestatakse enne jahvatamist teraskuulid kui jahvatuselemendid. Kui on saavutatud soovitud vaakum, kiirendatakse kuule labadega või vibratsiooniga, et tekitada kuulidevahelised ning kuulide ja veskiseina vahelised ja/või kuulide ja labade vahelised kokkupõrked. Jahvatusprotsessi ajal säilitatakse aktiivne vaakumi tekitamine vaakumpumba või pumpade abil, et eemaldada jahvatusprotsessis tekkivad gaasilised ühendid.

Eelistatult on temperatuur jahvatuse ajal -190 kuni 600 °C, veelgi eelistatumalt 20 kuni 100 °C.

Teatud materjalide puhul on soodne see, kui jahvatuse ajal lisatakse tsükliliselt reageeriva gaasina vesinikku, lämmastikku või süsinikku ja nende ühendeid või süsinikmonooksiidi, kusjuures jahvatus lõpetatakse vaakumikeskkonnas. Antud protseduur võimaldab tekitada gaasikeskkonnas jahvatamisel metalli reageerimise gaasiga ning järgnevalt vaakumi ning temperatuuri koosmõjul taandatakse jahvatamise viimases etapis tekkinud ühendid.

Sellega võimaldatakse materjalide puhastamine saastavatest ainetest, mida ilma reageeriva gaasi lisamiseta ei saa vaakumis jahvatamisega eraldada.

Üks võimalus on see, et pulbrisegu teisaldamine kuulveskist pulbrimahutisse viiakse läbi kuulveskit kallutades. Pulbrisegu võidakse teisaldada pulbrimahutisse ka pulbri teisaldamise sõlmes, kasutades pulbri kogumiseks magnetit.

Leiutise teine eesmärk on uue meetodi realiseerimiseks vajaliku seadmestiku loomine, vältimaks tootmisprotsessi käigus pulbrite oksüdeerumist. Meetod realiseeritakse seadmega pulbermaterjalist toodete valmistamiseks, see sisaldab vaakumpumpa, veskit, veski ajamit, veskiga ühendatud pulbrimahutit ja pulbrimahutit ümbritsevat kuumutusallikat, kusjuures vaakumpumbad on ühendatud veskiga ja pulbrimahutiga.

Eelistatavalt on veski hermeetiline kuulveski, mis on kõrgenergeetiline veski. Magnetiliste omadustega pulbrite teisaldamiseks on kuulveski ühendatud pulbrimahutiga pulbri teisaldamise sõlme kaudu, mis sisaldab magnetit ja mittemagneetuvat kesta. Et tagada kuulveski hermeetilisust, on kuulveski ajamiks eelistavalt magnetajam.

Pulbrianumat kuumutatakse välise kuumutusallika abil, et kiirendada jääkgaaside eraldumist. Kuumutamise ajal säilitatakse aktiivne vaakumeerimine. Pärast kuumutamist eemaldatakse materjal kapslist juhul, kui temperatuuri ja vaakumi mõjul on toimunud vedelfaaspaagutus ja materjal on tihenenud. Samuti võib konsolideerida materjali vaakumikeskkonnas koos anumaga, kasutades nt. kuumisostaatpressimist. Pulbrimahuti koos jahvatatud pulbriga kuumutatakse vaakumikeskkonnas. Seejärel suletakse mahutit ja veskit ühendav toru mehhaaniliselt, et tagada anuma hermeetilisus ning vaakumi säilimine anumas. Pulbrianum transporditakse kuumisostaatpressi ning konsolideeritakse temperatuuri ja ülerõhu koosmõjul. Meetodi abil on võimalik saada lõppkujule lähedase kujuga nn *near-net-shape* tooteid.

Jooniste lühikirjeldus

Joonisel fig 1 on kujutatud leiutisekohane jahvatus- ja kompakteerimissüsteem.

Joonisel fig 2 on kujutatud pulbrite vaakumis teisaldamise sõlm, mis on mõeldud ferromagnetiliste pulbrite teisaldamiseks leiutisekohases seadmes.

Joonisel fig 3 on joonisel fig 2 kujutatud pulbrite vaakumis teisaldamise sõlme suurendus. Näidatakse magneti asukoht pulbrite kogumise etapil.

Leiutise üksikasjalik kirjeldus teostusnäidetega

Meetod pulbermaterjalist toodete valmistamiseks on realiseeritud seadmega, mis sisaldab vaakumpumpa 1, kuulveskit 2, ajamit 3, pulbri etteandeseadet 4, pulbrimahutit 5 ehk kapslit, kuumutusallikat 6, pulbri teisaldussõlme 7, hermeetilist sidurit 8 kuulveski 2 ja ajami 3 vahel, gaasiballooni 9, ventiile 10, magnetit 11, milleks on püsimagnet, ja mittemagneetuvat kesta 12 ümber magneti 11.

Pulbritest tahkete materjalide valmistamine leiutisekohase meetodiga toimub järgnevalt.

Esmalt valmistatakse ette pulbrite segu, milleks segatakse kokku pulbrite osised. Jahvatatavate materjalidena võidakse valida grupi 2A metall, kaasa arvatud Be ja Mg ja nende segud, grupi 3A metall, kaasa arvatud Al ja nende segud, grupi 4A metall, kaasa arvatud Sn või Pb ja nende segud, grupi V metall, kaasa arvatud V või Nb ja nende segud, grupi VI metall, kaasa arvatud Cr, W, Mo ja nende segud, grupi VII metallid, kaasa arvatud Mn või Re, grupi VIII metallid, kaasa arvatud Co, Ni, Ru, Rh, Pd, Os, Ir, Pt ja nende segud, lantaniidid nagu Ce, La, Nd, Pr, Dy, Tb, Y, Er, Gd, Sm ja nende segud või siirdemetallid nagu Cu, Ag, Au, Zn, Cd, Sc ja nende segud. Jahvatatavad materjalid, mida lisatakse metallipulbritele, on poolmetallid, näiteks boor, räni või mittemetallid süsinik, fosfor ja halogeenid. Segatavad materjalid võivad olla lisatud elementaarosadena või eellegeeritult.

Metallisüsteemide näidetena võivad olla, aga ei piirdu Nd-Fe-B, Al-Mg, Al-Fe, Ti-Al-V, Ti-Fe, Mg-Zn, Sm-Co, Al-Li.

Metallilistele lähtepulbritele võib lisada tugevdavat faasi, milleks võib olla keraamiline pulber (oksiidid, karbiidid, nitriidid, boriidid ja nende segud), intermetalliidne pulber (aluminiidid, silitsiidid).

Samuti võib metallipulbreid segada faasidega, mis ei ole keraamilised. Antud ühendid võivad sisaldada metalli alkoksiide, aga ka nitraate, karbonaate, sulfaate ja hüdroksiide. Need võivad olla segades nii vedelal kujul kui pulbrina.

Pulbritena (nii lähtepulbrid kui juurdelisatavad armeerivad faasid) käsitletakse ühedimensionaalseid materjale (fiibrid, torud), kahedimensionaalseid materjale (liistakud, helbed, laminaadid) ning kolmedimensionaalseid materjale (sfäärilise, koonilise, silindrilise, hulknurkse, ebaregulaarse kujuga ja sarnased).

Keraamilise faasi molaarkogus metallilise faasi suhtes ei ole käesoleva patendiga limiteeritud.

Kui sisendmaterjalid on välja valitud, sisestatakse pulbrid kuulveskisse 2 ja kuulveski 2 suletakse hermeetiliselt. Vaakumi tekitamise allika abil, milleks on vaakumpump 1, tekitatakse vaakum nii kuulveskis 2 kui ka sellega ühenduses olevas pulbrimahutis 5. Jahvatamine toimub vaakumikeskkonnas. Jahvatamise kestel võib jahvatusanumasse ehk kuulveskisse 2 suunata näiteks gaasiballoonist 9 gaase või gaasilisi ühendeid (näiteks H_2, N_2, CH_4, CO), et esile kutsuda pulbrite reageerimist antud gaasiga. Vaakumi sügavus jahvatamisel on eelistatult vahemikus 10^0 kuni 10^{-8} mbar, soovitatavalt 10^{-3} kuni 10^{-6} mbar. Kui jahvatamisel lisatakse kuulveskisse 2 pulbritega reageerivat gaasi, võib vaakumi katkestada. Reageeriva gaasi keskkonnas jahvatamisel tekitatakse kuulveskis 2 eelistatult rõhk 10^{-1} kuni 10^2 bar. Jahvatamise viimane etapp ja jahvatamine lõpetatakse vaakumikeskkonnas.

Jahvatamise võib läbi viia atriitor-tüüpi veskis, planetaartüüpi veskis, pöörlevas kuulveskis või raputatavas kuulveskis (*shaker type mill*). Eelistatult viiakse jahvatamine läbi atriitorveskis. Atriitor on tüüpiliselt silindriline anum. Anumas olevad keraamilised või metallist kuulid kiirendatakse pöörlevate labade abil. Atriitor võib olla asetatud horisontaalselt, vertikaalselt või teatud nurga all. Atriitori hermeetilisus tagatakse võlli pöörlemise tekitamisel hermeetilise siduriga 8, milleks võib olla magnetsidur, ferrovedelik sidur, mehhaaniline sidur. Eelistatult kasutatakse magnetsidurit. Samuti võib võlli pöörlemise tekitada lahendusega, kus ajam 3 on ühendatud otse atriitori külge, kusjuures väljaspool veskit on staator, mis tekitab pöörleva liikumise veskis asuvale rootorile.

Jahvatamise käigus avaldatakse pulbriosakestele deformatsioone, mille tõttu osakesed deformeeruvad plastselt, kalestuvad ja purunevad. Pulbripinna oksüdeerumist välditakse pideva vakumeerimisega ning kergemini lenduvad gaasilised ühendid eemalduvad jahvatamise käigus. Pulbrite puhastamiseks võib kasutada ka gaasikeskkonna tsüklilist tekitamist, kus ühes jahvatamise tsüklis sisestatakse reageeriv gaas ning järgmises tsüklis eemaldatakse vaakumiga metallipulbrist gaasiühend, mille üheks koostisosaks on sisestatud gaas.

Jahvatustemperatuur on eelistatult vahemikus -190 °C kuni 600 °C. Tüüpiliselt toimub jahvatamine temperatuuril 20 °C kuni 100 °C.

Jahvatatava pulbri hulka võib lisada orgaanilisi polümeere nagu polüvinüülalkohol, polüetüleenglükool või orgaanilisi happeid nagu steariinhape, dodekaan või süsivesinikühendeid nagu parafiin. Orgaaniliste ühendite lisamine takistab metallipulbrite adhesiooni jahvatusvahenditele ja kuulidele ning soodustab osakeste purunemist.

Jahvatuskiirus sõltub atriitori mahust ja labade pikkusest. Näiteks 5-liitrise mahuga ja labade pikkusega 150 mm atriitori pöörlemiskiiruseks on eelistatult 300 kuni 1500 $p \cdot min^{-1}$. Atriitorisse sisestatav pulbrikogus sõltub kuulide arvust ja nende läbimõõdust. 5-liitrise mahuga atriitorisse, kus on 5 kg 10 mm läbimõõduga teraskuule, sisestatakse eelistatult 500 grammi jahvatatavat pulbrit.

Pärast jahvatamist suunatakse pulbrid konsolideerimisele sel viisil, et säilib vaakumikeskkond. Pulbrite transpordiks saab kasutada näiteks kuulveski 2 kallutamist, kus pulber voolab läbi avause (ei ole näidatud) pulbrimahutisse 5 ning jahvatuskuulid jäävad kuulveskisse 2 tänu avausel olevale sõelale (ei ole näidatud). Jahvatatud pulbreid võib koguda pulbri teisaldussõlmega 7, mis on liigutatav kuulveski 2 ja pulbrimahuti 5 vahel. Näiteks võib ferromagnetilisi pulbreid koguda magnetiga 11 (näidatud joonisel fig 2), mis on eraldatud mittemagneetuva kestaga 12. Pulbrite kogumiseks viiakse magnet koos mittemagneetuva kestaga 12 vaakumis kuulveskile 2 piisavalt lähedale (joonisel fig 2, pos 1), et pulbriosakesed liituksid mittemagneetuva kestaga 12. Kui vajalik pulbrikogus on kogutud, viiakse magnet 11 koos mittemagneetuva kestaga 12 kuulveskist 2 kaugemale (joonisel fig 2, pos 2). Pulbri suunamiseks pulbrimahutisse 5 eemaldatakse magnet kestast 12. Vastu mittemagneetuva kesta 12 otspinda (ei ole näidatud) jäänud pulber ei saa enam magnetiga 11 kaasa liikuda ning pulbriosakesed kukuvad pulbrimahutisse 5.

Kogutud pulbrite konsolideerimiseks võib kasutada nii lisarõhuga kui lisarõhuta konsolideerimismeetodeid. Konsolideerimisel säilitatakse pulbrimahutis 5 vaakumikeskkond. Lisarõhuga konsolideerimise puhul deformeeritakse pulbrimahutit 5 selliselt, et selle seinad suruvad välisrõhu mõjul pulbriosakesed kokku. Parema tiheduse saavutamiseks kasutatakse reeglina lisaks rõhule ka temperatuuri. Rõhuga konsolideerimisel võib kasutada näiteks kuumisostaatpressimist, kapsliga sepistamist, kapsliga valtsimist ja kapsliga kuumpressimist. Rõhuta konsolideerimisel võib kasutada näiteks vaba pulbri paagutamist. Nii rõhuga kui ka rõhuta konsolideerimise puhul kuumutatakse pulbrimahutis olevat pulbrit väljastpool mahutit, kasutades näiteks konvektsioon-, mikrolaine või induktsioonkuumutust. Eelistatult kasutatakse konvektsioonkuumutamist. Juhul kui materjal paagutatakse ilma vedela faasi moodustumiseta, valmistatakse poorseid materjale. Vedelfaaspaagutamisega on võimalik valmistada kõrge tihedusega materjale. Paagutustemperatuur on tahkefaaspaagutuse puhul eeldatavalt 60% kuni 95% materjali sulamistemperatuurist. Vedelfaaspaagutuse puhul on paagutustemperatuur eeldatavalt 10 °C kuni 150 °C üle süsteemis oleva metalli või sulami madalaima sulamistemperatuuri.

Konsolideerimisele järgnevalt eemaldatakse kapsel ehk pulbrimahuti 5 eelistatult mehhaaniliselt ning vajadusel teostatakse materjali termotöötlus ning lõppkuju andmine mehhaanilise töötlemisega.

Näide 1

Alumiiniumisulam Al_5Mg sünteesiti pulbritest vaakumjahvatuse ja kapslis sepistamise teel. Jämedateraline Al_5Mg algpulber (35 grammi) sisestati vaakumattriitorisse ning jahvatati toatemperatuuril. Jahvatuselementidena kasutati teraskuule, kuulide ja pulbri suhe oli 20:1, jahvatusaeg 12 h, labade pöörlemiskiirus 960 $p \cdot min^{-1}$. Jahvatuslisandina lisati atriitorisse väike kogus (0,4 kaalu%) polüetüleenglükooli, et vältida alumiiniumi pulbrite adhesiooni kuulide ning labade külge. Jahvatatus viidi läbi 2×10^{-3} mbar vaakumis. Jahvatusjärgselt teisaldati jahvatatud pulber läbi atriitori küljes oleva lüüsi pulbrimahutisse (teraskapsel siseläbimõõduga 20 mm, pikkus 60 mm). Teisaldamine viidi läbi atriitorit kallutades, kuulid jäid lüüsi ava ees olevale sõelale. Pulbrite teisaldamisel säilitati pumpadega vaakumi tekitamine. Pulbriga täidetud pulbrimahuti kuumutati väljastpoolt 600 °C-ni toruahjus. Kuumutuskiirus oli 5 $°C \cdot min^{-1}$ ning hoidmine temperatuuril 4 tundi. Pulbrimahuti koos jahvatatud pulbriga transporditi kuumalt, 5 sekundi jooksul, hüdropressi juurde ning pulber konsolideeriti sepistamise teel. Kapslile avaldatud jõud oli 1000 kN.

Sünteesitud Al_5Mg tahkisel mõõdeti hapnikusisaldus ning mehaanilised omadused – tõmbetugevus, voolavuspiir ja purunemissitkus. Hapnikusisalduseks algpulbris mõõdeti 0,11% ning kasutatud polüetüleenglükool lisandist arvutati hapnikulisandiks 0,21%. Sünteesitud tahkisel mõõdeti hapnikusisalduseks 0,40%. Arvestades maha algpulbrist tulenev ja plastifikaatorist lisanduv hapnik, on hapnikulisand vaakumis jahvatamisest ning konsolideerimisest 0,08%. Võrdluseks valmistati katsekehad samast materjalist ja teadaolevatel meetoditel – märgjahvatus vaakumis (Kollo, Lauri, et al. "Investigation of planetary milling for nano-silicon carbide reinforced aluminium metal matrix composites." Journal of Alloys and Compounds 489.2 (2010): 394-400.) ja argooni kaitsegaasis (Kollo, L., et al. "Nano-silicon carbide reinforced aluminium produced by high-energy milling and hot consolidation" Materials Science and Engineering: A 528.21 (2011): 6606-6615). Pulbrite transport jahvatamiselt sepistamisele viidi läbi argooni kaitsegaasi keskkonnas. Hapniku lisandumine pärast jahvatamist ja sepistamist oli vastavalt 1,06% märgjahvatuse ning 0,13% argoonis jahvatamise puhul, mis on kõrgemad kui vaakumis jahvatamisel ja sepistamisel.

Vaakumis jahvatatud ja sepistatud Al_5Mg tõmbetugevuseks mõõdeti 505 MPa, voolavuspiiriks 480 MPa ja purunemissitkuseks 5,5%.

Tabel 1. Hapnikulisand Al_5Mg valmistamisel

Meetod	Mõõdetud hapnik		Hapnikulisand		
	Jahvatatud pulber, %	Tahkis, %	Plastifikaatorist, %	Algpulbrist, %	Lisand jahvatus- ja konsolideerimisprotsessist (=% tahkis – % plastifikaatorist - % algpulbrist)
Vaakumjahvatus ja sepistamine (käesolev leiutis)	-	0,40	0,21	0,11	0,08
Märgjahvatus heptaanis, degaseerimine ja sepistamine vaakumis	0,55	1,17	-	0,11	1,06
Jahvatamine argoonis ja sepistamine vaakumis	0,21	0,27	0,03	0,11	0,13

Näide 2

NdFeB ribavalu pulber (25 grammi) jahvatati atriitorveskis sarnaselt näites 1 kirjeldatud parameetritega. Algselt tekitati atriitorveskis vaakum sügavusega 10^{-3} mbar. Seejärel suunati veskisse reageeriva gaasina vesinik. Vesiniku keskkonnas jahvatati NdFeB pulbrit 15 min. H_2 ülerõhul 0,2 bar. Jahvatusel reageeris jahvatatav pulber vesinikuga ning faasidena tekkisid NdH ja FeB. Vesinikuga jahvatamisele järgnes veski vakumeerimine, kuni saavutati vaakum 10^{-3} mbar. Seejärel jahvatati 5 minutit vaakumikeskkonnas, millega vesinik taandus hüdriidifaasist. Jahvatusjärgselt mõõdeti NdFeB osakeste suurus ning mõõdeti hapnikusisaldus. Pulber transporditi ferromagnetiliste pulbrite teisaldamise sõlmega (näidatud joonisel fig 2) pulbrimahutisse, pulbriosakesed suunati 2 T magnetväljas ning paagutati kasutades sädeplasma paagutusseadet temperatuuril 800 °C ning 50 MPa ülerõhul.

Algpulbri hapnikusisaldus jahvatusele eelnevalt oli 0,08%. Sünteesitud materjalis mõõdeti pärast jahvatust 0,11% ning pärast paagutust 0,19% hapnikku.

Valmistatud NdFeB magnet oli täistihedusega (7,5 $g \cdot cm^{-3}$) ning struktuur ülipeen (0,1–0,3 μm). Võrdlusena jahvatati samast algmaterjalist pulbrid standardsete pulbermetallurgia meetoditel ning sarnaselt eeltoodud näitega paagutati sädeplasma paagutuse seadet kasutades. NdFeB pulbrid hüdrogeeniti toatemperatuuril vesinikus, seejärel hüdreeritud pulbrid jahvatati jugaveskis lämmastikukeskkonnas. Jahvatatud pulbrid suunati 2T magnetväljas. Jahvatatud pulbrid transporditi puhta lämmastiku keskkonnas ($O < 0,1$ ppm, $H_2O < 0,1$ ppm) sädeplasmaseadmesse ning paagutati vedelfaaspaagutusega temperatuuril 800 °C ning 50 MPa ülerõhul. Hapnikusisaldus mõõdeti pärast hüdrogeenimist (0,11%), peale jugajahvatamist (0,2%) ning pärast sädeplasma paagutust (0,23%).

Käesolevas patendis kirjeldatud meetodiga lisandus protsessi jooksul 0,11% hapnikku, standardtehnoloogiat kasutades lisandus 0,15% hapnikku. Samas, käesoleva meetodiga valmistatud materjali terasuurus oli 0,1–0,3 μm ning standardmaterjali terasuuruseks mõõdeti 5–8 μm.

Tabel 2. Hapnikulisand NdFeB magneti valmistamisel

Meetod	Mõõdetud hapnik, %			Lisand jahvatus- ja konsolideerimisprotsessist (=% tahkis – % algpulbrist), %
	Algpulber	Pärast jahvatamist	Lõppdetailis	
Käesolev leiutis	0,08	0,11	0,19	0,11
Standard-tehnoloogia	0,08	0,20	0,23	0,15

PATENDINÕUDLUS

1. Meetod pulbermaterjalist toodete valmistamiseks, mille kohaselt
- jahvatatav pulbrisegu sisestatakse veskisse ja jahvatatakse,
- jahvatatud pulbrisegu teisaldatakse pulbrimahutisse (5),
- pulbrimahutit (5) kuumutatakse väljastpoolt kuumutusallika (6) abil, paagutades nii pulbrisegu,
- pulbrimahuti (5) transporditakse pressi juurde ja seda konsolideeritakse avaldades pulbrimahutile välist survet, pulbrimahuti (5) avatakse ja toode eemaldatakse, **erineb** selle poolest, et pulbrisegu jahvatamine, teisaldamine, paagutamine ja konsolideerimine ehk pressimine viiakse läbi vaakumikeskkonnas, vaakumis sügavusega $10^{0} - 10^{-8}$ mbar.

2. Meetod vastavalt nõudluspunktile 1 **erineb** selle poolest, et veskina kasutatakse kuulveskit (2), millesse sisestatakse enne jahvatamist teraskuulid kui jahvatuselemendid.

3. Meetod vastavalt nõudluspunktile 1 **erineb** selle poolest, et temperatuur jahvatuse ajal on -190 kuni 600 °C, eelistatult 20 kuni 100 °C.

4. Meetod vastavalt nõudluspunktile 1 **erineb** selle poolest, et jahvatuse ajal lisatakse tsükliliselt reageeriva gaasina vesinikku, lämmastikku või süsinikku ja nende ühendeid või süsinikmonooksiidi, kusjuures jahvatus lõpetatakse vaakumikeskkonnas.

5. Meetod vastavalt nõudluspunktile 1 **erineb** selle poolest, et pulbrisegu teisaldamine kuulveskist (2) pulbrimahutisse (5) viiakse läbi kuulveskit (2) kallutades.

6. Meetod vastavalt nõudluspunktile 1 **erineb** selle poolest, et pulbrisegu teisaldamine pulbrimahutisse (5) viiakse läbi pulbri teisaldussõlmes (7), kasutades pulbri kogumiseks magnetit (11).

7. Seade pulbermaterjalist toodete valmistamiseks, mis sisaldab vaakumpumpa (1), veskit, ajamit (3) veski käitamiseks, veskiga ühendatud pulbrimahutit (5), pulbrimahutit (5) ümbritsevat kuumutusallikat (6), **erineb** selle poolest, et vaakumpumbad (1) on ühendatud veskiga ja pulbrimahutiga (5).

8. Seade vastavalt nõudluspunktile 7 **erineb** selle poolest, et veski on hermeetiline kuulveski (2).

9. Seade vastavalt nõudluspunktile 8 **erineb** selle poolest, et kuulveski (2) on ühendatud pulbrimahutiga (5) pulbri teisaldussõlme (7) kaudu, mis sisaldab magnetit (11) ja mittemagneetuvat kesta (12).

10. Seade vastavalt nõudluspunktile 7 **erineb** selle poolest, et ajamiks (3) on magnetajam.

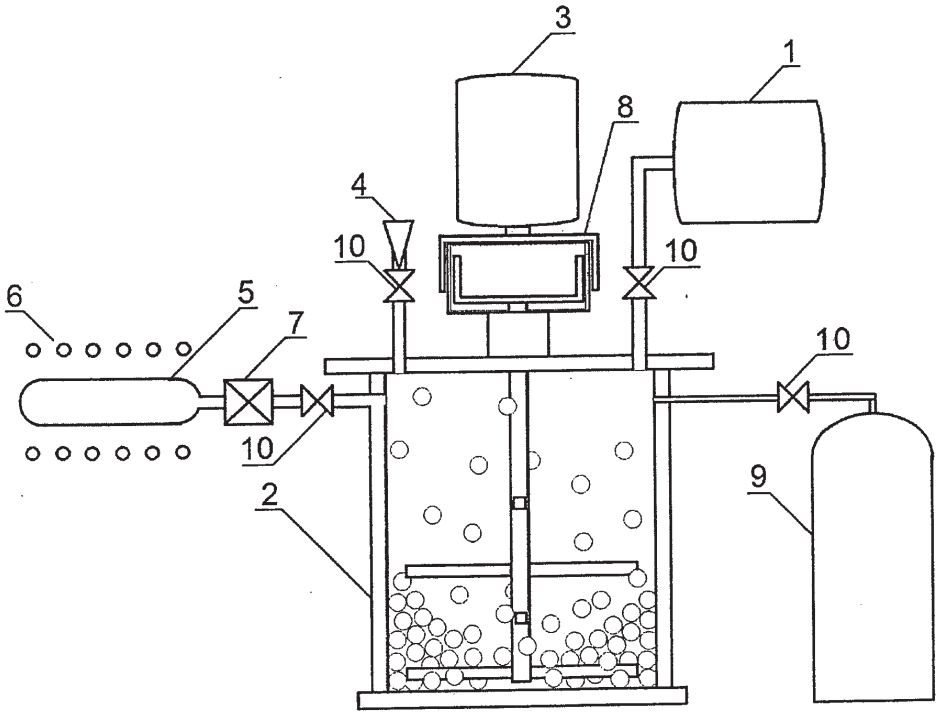

FIG 1

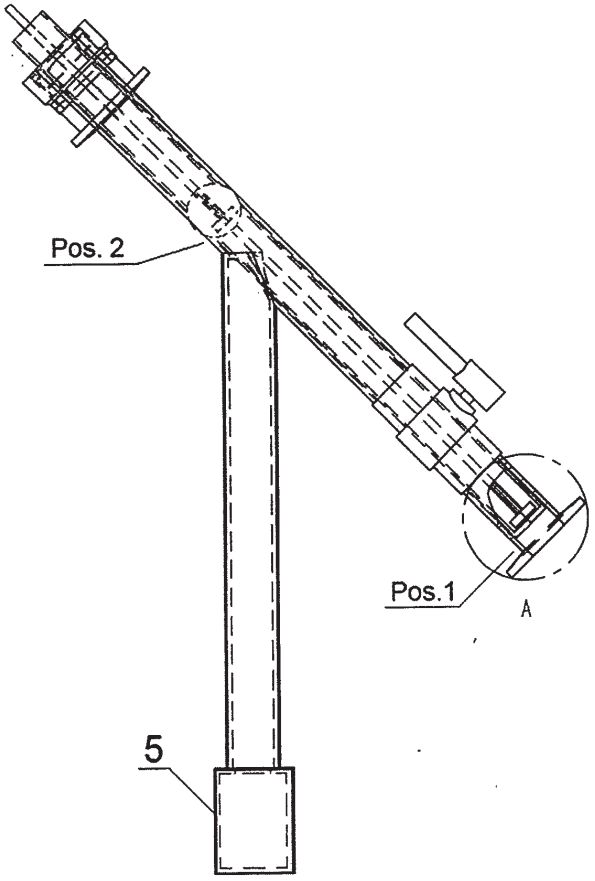

FIG 2

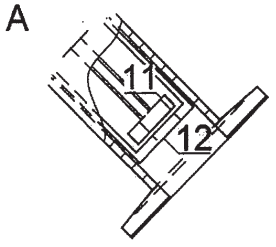

FIG 3

Paper IV **Mural, Z**., Kollo, L., Veinthal, R., Xia, M., Bahl, C., Abrahamsen, A.B. and Neves Bez, H. The Effect of Nano-TiC Addition on Sintered Nd-Fe-B Permanent Magnets. *Journal of Magnetism and Magnetic Materials*, 429, 2017, 23-28 (in press).

Journal of Magnetism and Magnetic Materials 429 (2017) 23–28

Contents lists available at ScienceDirect

Journal of Magnetism and Magnetic Materials

journal homepage: www.elsevier.com/locate/jmmm

The effect of nano-TiC addition on sintered Nd-Fe-B permanent magnets

Zorjana Mural[a,*], Lauri Kollo[a], Manlong Xia[b], Christian R.H. Bahl[b], Asger Bech Abrahamsen[c], Henrique Neves Bez[b], Joosep Link[d], Renno Veinthal[a]

[a] Department of Materials Engineering, Tallinn University of Technology, Ehitajate tee 5, 19086 Tallinn, Estonia
[b] Department of Energy Conversion and Storage, Technical University of Denmark, Frederiksborgvej 399, 4000 Roskilde, Denmark
[c] Department of Wind Energy, Technical University of Denmark, Frederiksborgvej 399, 4000 Roskilde, Denmark
[d] National Institute of Chemical Physics and Biophysics, Akadeemia tee 23, 12618 Tallinn, Estonia

ARTICLE INFO

Keywords:
Sintered Nd-Fe-B magnets
Magnetic properties
Thermal stability
TiC

ABSTRACT

This paper addresses the effect of nano-TiC addition on sintered Nd-Fe-B permanent magnets. TiC nanoparticles were added to sintered Nd-Fe-B magnets with a specific aim to improve the Curie temperature and thermal stability. A standard powder metallurgy route was adopted to prepare the magnets. It was found that introducing nano-TiC prior to jet milling was effective as the nanoparticles dispersed in the final alloy, concentcalcrating in the neodymium-rich phase of the magnets. Magnets with optimal properties were obtained with the addition of 1 wt% TiC nanoparticles. The hysteresis loop for such magnets showed an improved shape and VSM analysis a coercivity value of 1188 kA/m, a remanence value of 0.96 T and a maximum energy product of 132 kJ/m^3. The maximum working point and the Curie temperature of the developed magnets were 373 K and 623 K respectively.

1. Introduction

Since the discovery of the $Nd_2Fe_{14}B$ compound in the 1980s [1], continuous efforts have been made to enhance not only the magnetic properties but also the thermal stability and corrosion resistance of Rare-Earth (RE)-based magnets. This aim can be reached by optimizing the microstructure and chemical composition of the magnets [2–5].

The largest application segments for Nd-Fe-B permanent magnets are expected to be those related to electric motors and power generation. These application areas require magnets that in addition to a reduced size and higher performance have an ability to work at high temperatures. Neodymium and iron are usually substituted by different elements to influence the properties of Nd-Fe-B magnets. In order to improve coercivity, anisotropy, corrosion behaviour or thermal stability of these magnets, various minor additives have been investigated. While a significant enhancement of coercivity occurs with the addition of Al, Cu, Nb, Tb, Ga, Dy_2O_3 or ZrO_2 to magnets, most of these elements lead to a decrease in remanence or thermal stability of the magnetic material [2–5]. Microalloying magnets with Co, V, Cr or Ni surpasses the corrosion issue of magnets but degrades their magnetic properties in some cases [6,7].

Commonly, Dy is added to Nd-Fe-B magnetic material to ensure higher thermal stability. For Dy nanoparticle addition, the maximum effect of coercivity increase was reached at 1.5 wt%. A further addition of Dy appears not to remarkably increase the properties of Nd-Fe-B [8]. In case of micrometer-sized Dy powders, up to 10 wt% can be added to reach the same effect. Co is also known to positively influence the Curie temperature. Alloying with not more than 0.2% of Co is recommended; otherwise, the saturation magnetization and anisotropy energy decreases. In order to supress the decrease in magnetic properties, it is recommended that apart from Co, other elements like copper or niobium should be added to the material. The replacement of Fe for Co improves the temperature coefficient, which will allow using such magnets in high temperature applications [9–13].

Most investigations in alloying have been focused only on the manufacturing stage of magnetic alloys, including strip casting and rapid quenching. Ti and C have been used separately or together to modify the Nd-Fe-B alloys. Minor additions of Ti and C resulted in an increase in coercivity with a modest decrease in remanence [14,15]. The content of Ti and C should not exceed 3 at%; otherwise, the TiB_2 phase will appear instead of the TiC phase and decrease the volume of the hard phase [14,16]. TEM analysis showed Ti or Ti and C addition to produce finer and more homogeneous grains, which is beneficial for the coercivity of the magnet [17,18]. Adding TiC to Nd-Fe-B alloys results in a more uniform microstructure with a strengthened exchange coupling effect [17,19]. It was also found that due to a smaller grain size Nd-Fe-B-TiC bonded magnets absorb less hydrogen and have higher corrosion resistance characteristics [20].

* Corresponding author.
E-mail address: zorjana.mural@ttu.ee (Z. Mural).

http://dx.doi.org/10.1016/j.jmmm.2016.12.115
Received 18 April 2016; Received in revised form 28 October 2016; Accepted 23 December 2016
Available online 24 December 2016
0304-8853/

This paper is aimed at analysing the effect of nano-TiC addition to sintered Nd-Fe-B magnets prior to the refining stage of a hydrogenated alloy with focus on the microstructure, thermal stability and magnetic properties of the doped Nd-Fe-B sintered magnets. To the authors' knowledge, this approach has not been reported in any previous research in the field.

2. Experimental

The conventional powder metallurgical route was adopted to produce sintered RE magnets. Commercial strip cast alloy in the form of flakes with the total RE content of 32 wt%, 67% Fe and about 1% B was applied as a starting material. The magnet alloy was Hydrogen Decrepitated (HD) at atmospheric pressure, and at room temperature with a holding time of 120 min. Jet milling (JM) under nitrogen atmosphere was performed, using the *Micromazinacione* spiral jet mill equipped with the *Impakt*^{TM} powder feeder by *Powder and Surface GmbH*. Nano-TiC powder with the average particle size of 20 nm (*SigmaAldrich*) weighing from 0.1 to 5.0 wt% was added to HD powder before feeding it into JM. The nanopowder was introduced by mixing the substance with a spoon. Cold isostatically pressed green compacts were sintered at 1353 K for 4 h under a vacuum of 10^{-5} mBar. The sintered magnets were slowly cooled down to room temperature with a total cooling time of approximately 3 h.

Magnetic properties at room and elevated temperatures were measured applying a Vibrating Sample Magnetometer (VSM) installed into the *Cryogenic Limited HTVSM 700* system with a maximum field of 14 T and a maximum temperature of 700 K. Demagnetization factors for rectangular samples to correct the measurements were calculated using analytic expression provided by Aharoni [21]. Sometimes descending and ascending hysteresis loops are not totally symmetrical due to instrument drift. In case of minor discrepancies in coercivity and remanence values, the hysteresis loop shifts were calculated and adjusted. Force calculations were based on the experimental information of magnetic moment, sample volume, demagnetization factor, and external and internal fields. Vacuum permeability was used to convert the measured data to the external field.

X-ray diffraction patterns were obtained using the *Rigaku SmartLab* diffractometer with Cu Kα radiation on crushed (powdered) samples placed on a silicon plate. The densities of the samples were measured by the *Micromeritics AccuPyc 1340* helium gas pycnometer, providing a skeleton density value. The phase concentration and the average grain size were analysed adopting the *ImageJ* software applied to Scanning Electron Microscope (SEM) micrographs. Energy Dispersive X-ray Spectroscopy (EDS) mapping was performed with the *Hitachi TM3000* electron microscope. Total oxygen content was determined by the *Eltra ONH2000* oxygen analyser for bulk samples of about 150 mg each as an average content of at least five measurements.

3. Results and discussion

3.1. Phase composition and density

X-ray studies were performed to identify the phase composition of the magnets and to clarify the influence of carbide on their microstructure. XRD measurements were performed for the sintered magnets with 0, 0.1, 0.5, 1 and 2 wt% of nano-TiC added as shown in Fig. 1. The well-defined peaks were indexed as $Nd_2Fe_{14}B$ hard phase for all samples, refined with the Rietveld method. The black full lines indicate the measured data. It was not possible to identify the TiC phase for the samples with low dopant content up to 1 wt%. The analysis of XRD patterns showed single low intensity peaks corresponding to the TiC phase that were observed at approximately 2θ =36° and 61° for the samples with higher dopant content (1 and 2 wt%) [22]. It is important to note that phase quantification through XRD measurements is limited when the total content of the phase is less than 5 wt%.

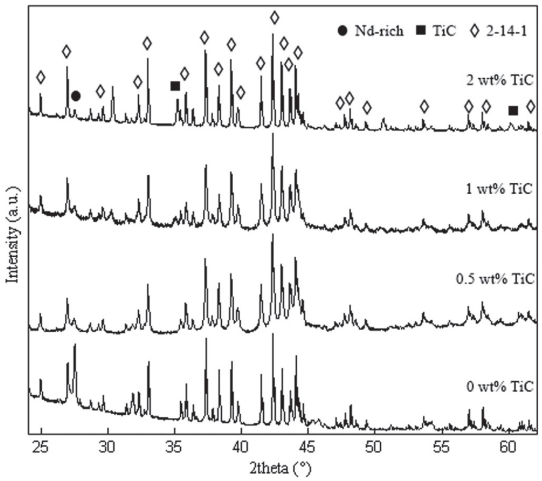

Fig. 1. X-ray patterns of 0, 0.5, 1 and 2 wt% nano-TiC Nd-Fe-B sintered magnets.

The single peaks not defined by $Nd_2Fe_{14}B$ and TiC phases were observed at 2θ =27°, 30° and 52°. The comparison of peak intensities at 2θ =27° suggests that the secondary phase peaks are decreasing with increasing TiC concentration. This leads to a conclusion that the secondary phase corresponds to the Nd-rich phase or neodymium oxide since the amount of the Nd-rich phase decreases with increasing TiC content from about 11% for the undoped sample to 7% for the magnet with 1 wt% nano-TiC inclusion. Visually, it can be observed on microstructure figures in Fig. 2 Section 3.2. Most probably the other single peaks correspond to the minor TiB_2 phase with the maximum peak at 2θ =52°. As shown in Table 1, the total oxygen content appears to increase slightly for the samples with higher dopant concentration. This increase can be attributed to the oxygen pickup by finer intergranular RE regions and formation of oxides.

Lattice parameters of the hard magnetic phase were determined from the Rietveld refinement as demonstrated in Table 1. They are close to the values reported with a = b =8.789 Å and c =12.189 Å of the tetragonal $Nd_2Fe_{14}B$ unit cell [23]. There is practically no change in lattice parameters with the increase in additive concentration, which suggests that the hard magnetic phase is not doped with TiC and carbide particles behave as inclusions between the grains in RE-rich phase regions. It seems that TiC does not decompose during processing and acts as a grain refinement agent in the Nd-rich phase.

With increasing TiC content, the theoretically expected maximum density decreases by 2.4% at the highest TiC content of 5 wt%. The relative skeleton density for the doped samples is in accordance with the expected maximum density shown in Table 1. Generally, with increasing TiC content, the density is slightly decreasing. All samples, except for the one with the highest TiC content of 5%, comply with the industrial standards in regard to the density of the magnet and can thus be used for further characterization.

3.2. Microstructure

SEM-EDS was performed to determine the distribution of additives in the microstructure of the magnets. SEM images of the initial sample and 1 wt% nano-TiC containing sample are displayed in Fig. 2a and b respectively, and EDS mapping of magnet with 1 wt% nano-TiC in Fig. 2d. The lighter phases correspond to the mixture of RE-rich phases and the darker phase to the $Nd_2Fe_{14}B$. TiC-free samples have a coarser structure with an average grain size of about 8 μm (Fig. 2a), whereas 1 wt% nano-TiC addition produces a finer more homogeneous struc-

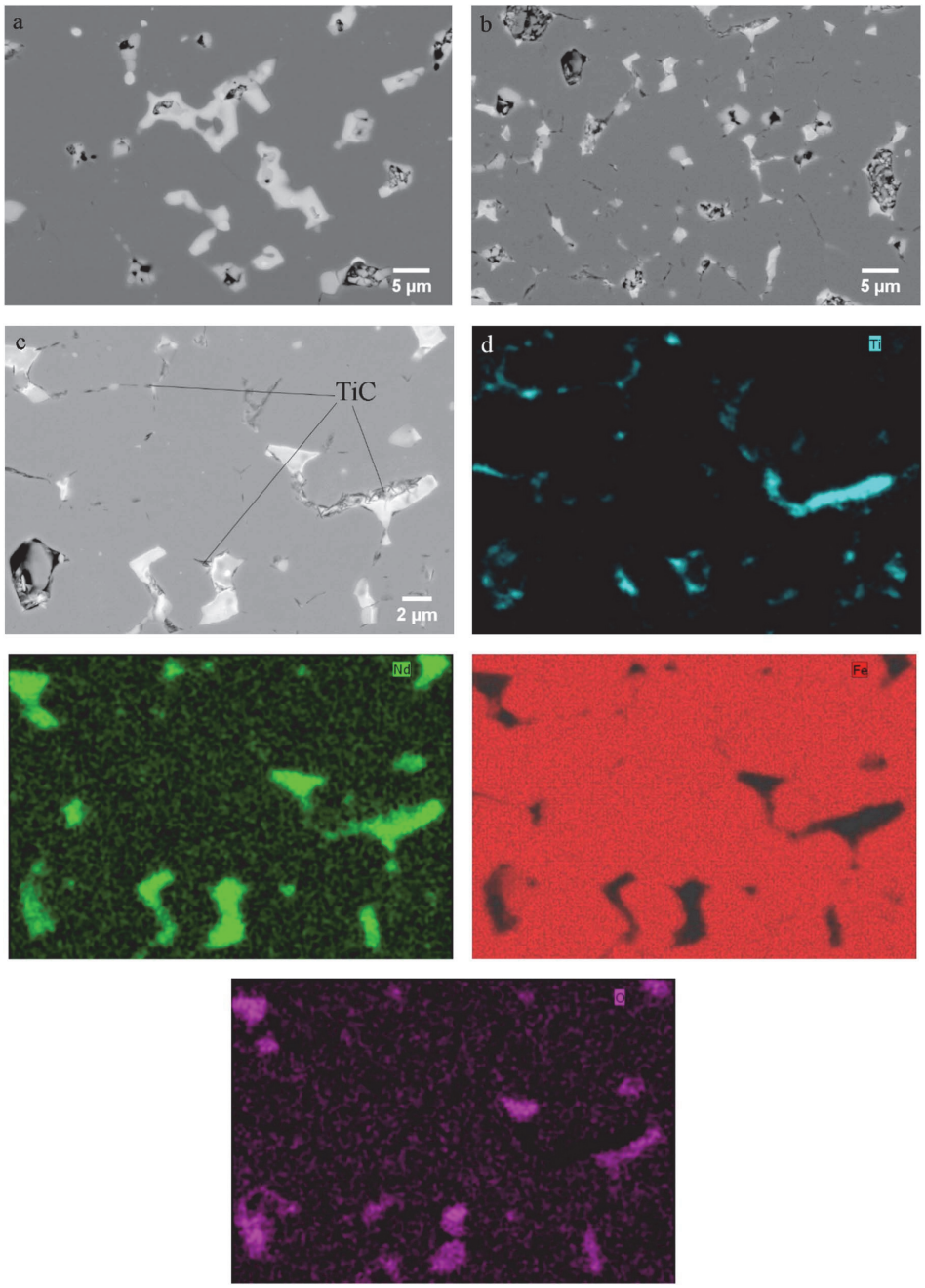

Fig. 2. Microstructure: a) SEM image of the initial sintered magnet without TiC addition, b) sample with 1 wt% of TiC, c) sample with 1 wt% of TiC, TiC particles are visible, d) EDS mapping of the whole area of the Fig. 2c for Ti, Nd, Fe and O.

ture with an average grain size of about 6.5 μm and a lower percentage of nonmagnetic phase (Fig. 2b). Fig. 2c and EDS mapping of the Ti element (Fig. 2d) indicate that this element is concentrated mostly in the RE-rich phase and in between of the grains and is almost not present in the hard phase. This result is in agreement with X-ray and Rietveld along with oxygen content (Fig. 2d) results presented in the previous paragraph. The TiC particles look like thin long clusters (lamellas) lined along the grains (Fig. 2c). The grain refinement can be explained by the effect of nano-TiC particles distributed between the grains acting as inhibitors of the grain growth. The proposed mechan-

Table 1
Lattice parameters a, b and c of the Nd-Fe-B phase doped with TiC determined from Rietveld refinement of X-ray diffraction patterns. The relative density and oxygen content of the sintered magnets is also listed.

Designation	a, b[Å]	c[Å]	Relative Density	Oxygen Content [wt%]
0TiC	8.792	12.176	0.99	0.22
0.1TiC	8.796	12.189	0.99	0.28
0.2TiC	–	–	0.94	0.29
0.5TiC	8.796	12.189	0.96	0.29
1TiC	8.797	12.179	0.96	0.30
2TiC	8.798	12.183	1.00	–
5TiC	–	–	0.92	–

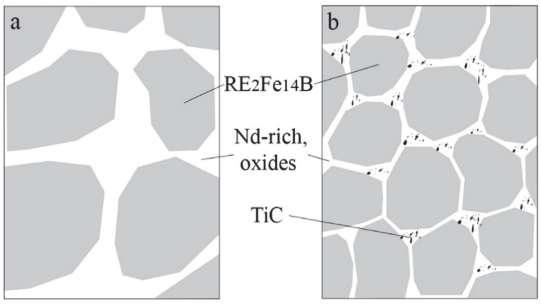

Fig. 3. Mechanism of microstructure development with the magnet composition modified by TiC addition.

ism of microstructure development is illustrated in Fig. 3. In Fig. 2c two RE-rich phases can be clearly identified. The mapping of oxygen (Fig. 2d) indicate that less bright RE regions correspond to RE oxides, while bright areas surrounding the oxides (Fig. 2c) attributes to the metallic Nd as no oxygen has been detected. TiC particles occupy the regions rich of metallic Nd (Fig. 2c).

The elemental concentrations were determined by EDS quantitative analysis in the core of the $Nd_2Fe_{14}B$ grains and intergranular regions. It was found that the concentration of Ti varies significantly through the RE-rich region. Ti content was not higher than 0.4 wt% (± 0.05%) for the hard phase and varied between 1 (± 0.1%) and 13 wt% (± 0.5%) for the RE-rich phase. EDS quantification proved the carbide was not dissolved in the hard magnetic phase. Similar results that in comparison with the hard phase, where the Ti content was not more than 0.1 at%, grain boundaries and triple junctions contained 2.8...45 at% Ti have been reported in previous research [24]. EDS analysis revealed also a significant variability of oxygen content in different phases. Generally, for the hard phase the oxygen level was below the detection limit of EDS analysis. In RE-rich regions, the oxygen content reached 6...10 wt% with the measurement uncertainty of about 2%. These measurements support the data addressed above in regard to the higher oxidation of the RE-rich phase and oxides mixture as minor phases.

Fig. 3a provides a schematic illustration of the initial magnet. Fig. 3b shows the influence of TiC addition.

3.3. Magnetic properties

Magnetic properties of remanence (B_r), coercivity (H_{ci}) and maximum energy product (BH_{max}) measured at room temperature can be seen in Fig. 4. In comparison to the samples without carbide, introducing a small amount of TiC causes a sudden decrease of remanence at TiC concentration 0.1 wt% and at the same time a remarkable increase in coercivity. The effect was confirmed with several experiments with the same additive concentration. This phenomenon is often caused by ineffective alignment of the powder during the production phase; however, this was not the case in this experiment. With the small concentration of 0.1 wt% TiC the difference in properties is quite significant, which may be related to the influential effect of nano particles. Generally, TiC has a positive influence on coercivity, which increases with TiC higher concentrations (Fig. 4) and tends to decrease with TiC concentration exceeding 1 wt%. The remanence value remains nearly unchanged and it decreases with higher dopant concentrations at 2 and 5 wt% of carbide addition due to the nonmagnetic TiC phase. The maximum energy product is the highest for the magnet with 1 wt% TiC as can be seen in Fig. 4.

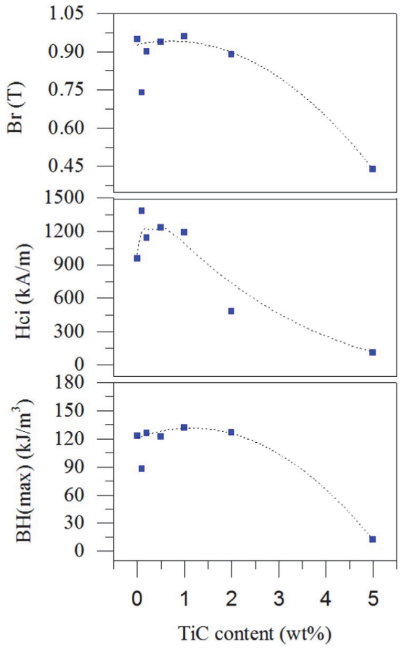

Fig. 4. Magnetic properties of TiC doped Nd-Fe-B magnets at room temperature as a function of TiC content.

3.4. Thermal stability

Magnetic properties for sintered Nd-Fe-B magnets with TiC at elevated temperatures were measured. The second quadrant of the magnetization curves for the 1 wt% doped sample at temperatures from 293 to 498 K is shown in Fig. 5. The temperature stability of magnetic materials is often described by the temperature coefficients

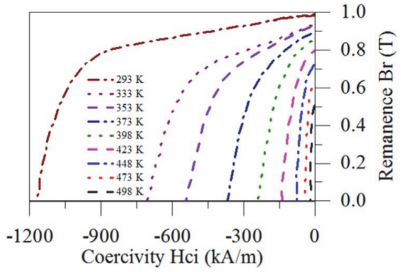

Fig. 5. Second quadrant magnetization curves of 1 wt% TiC containing magnet at different temperatures.

Table 2
Temperature coefficients, the maximum working point and the Curie temperature.

Designation	α[%/K] 373 K	β [%/K] 373 K	Tm [K]	Tc [K]
0TiC	−0.148	−1.466	333 (± 5)	583 (± 10)
0.1TiC	−0.112	−1.338	353(± 5)	613(± 10)
0.2TiC	−0.139	−2.184	373(± 5)	623(± 10)
0.5TiC	−0.116	−1.912	373(± 5)	633(± 10)
1TiC	−0.098	−2.699	373(± 5)	623(± 10)
2TiC	−0.160	−1.852	353(± 5)	603(± 10)
5TiC	−0.306	−1.902	333(± 5)	593(± 10)

for specific temperatures. The temperature coefficients for remanence α are defined by the difference in remanence divided by a temperature change multiplied by remanence at reference temperature:

$$\alpha=\frac{(B_r(T_r)-B_r(T))}{(B_r(T))\bullet(Tr-T)}, \quad (1)$$

where $B_r(T_r)$ refers to remanence at room temperature T_r and $B_r(T)$ to remanence at reference temperature T. The temperature coefficient of coercivity β is given by the difference in coercive strength divided by a temperature change times the coercivity at reference temperature:

$$\beta=\frac{(H_{cj}(T_r)-H_{cj}(T))}{(H_{cj}(T))\bullet(Tr-T)}, \quad (2)$$

where $H_{cj}(T_r)$ refers to coercivity at room temperature T_r and $H_{cj}(T)$ to coercivity at reference temperature T [24]. The maximum operating temperature T_m was estimated as a temperature at which not more than 5% loss of remanence occurred [26,27]. The Curie temperature T_C was considered as a temperature at which remanence reached 0 T, because the Curie point is reached when the magnetic material changes its behaviour to paramagnetic [3,25].

The temperature coefficients for remanence (α) and coercivity (β) together with the Curie temperature (T_C) and maximum operating (T_m) temperatures are displayed in Table 2. Compared to the initial characteristics, the highest working temperature and the Curie temperature of 373 K and 633 K respectively are found for the magnet with 0.5 wt% nano-TiC. The magnet with 1 wt% TiC showed 10 K lower Curie temperature. The mechanism influencing the thermal stability improvement of magnets with TiC additions are not clearly defined and understood. Several reasons have been proposed. Zhang *et.al.* propose the maximum operating point being influenced only by the increase of coercivity inhibiting the reversal processes [16]. In accordance to Chin *et.al.,* alloying with Ti results in reduction of reversible losses at temperatures up to 498 K due to the intrinsic improvement of anisotropy field [28]. This allows magnets to work at higher temperatures for longer period of time. Goto et.al. propose the coercivity and consequently thermal stability improvement due to strain induced in $Nd_2Fe_{14}B$ lattice for TiC alloyed materials [29]. In addition, the ferromagnetic behaviour of RE-rich phases especially grain boundaries have been reported [30,31]. Moreover, adding small amounts of V, Mo or W to Nd-Fe-B magnets results in formation of intergranular boride phases like V_2FeB_2, Mo_2feB_2 or WFeB acting as domain walls pinning sites and are responsible for increased coercivity and thermal characteristics. It is believed that similar TiFeB phase may occur [32,33]. In the present work as TiC is situated in RE-rich areas, it is assumed to have the influence in there or at the grain boundaries. Curie temperature of the magnets is increased already with 0.1 wt% of nanoTiC inclusion, and remains constant even with TiC inclusions up to 2 wt%. As such phenomenon was not seen with micrometer sized TiC alloying, we believe the mechanism of increased thermal stability is related to solubility of TiC in RE-rich phase and in the grain boundaries. The mechanism could lay in increased internal strains in microstructure or altered grain boundaries. Revealing the exact mechanisms need further investigations in the future. VSM measurements made at 700 K proved the samples with TiC behave as ferromagnetics and show a weak magnetic loop while undoped sample became nonmagnetic. Fig. 6 shows the change of coercivity (b and d) and remanence (a and c) at high temperatures in terms of stability. The whole temperature range between 293 K and 673 K can be observed in graphs c and d and losses at lower temperatures (293...523 K) in graphs a and b. At low temperatures the difference in remanence is not significant, but at elevated temperatures the magnets with nano-carbide are more stable. In respect to coercivity, the outcome is quite similar at higher temperatures, whereas at lower temperatures the coercive force

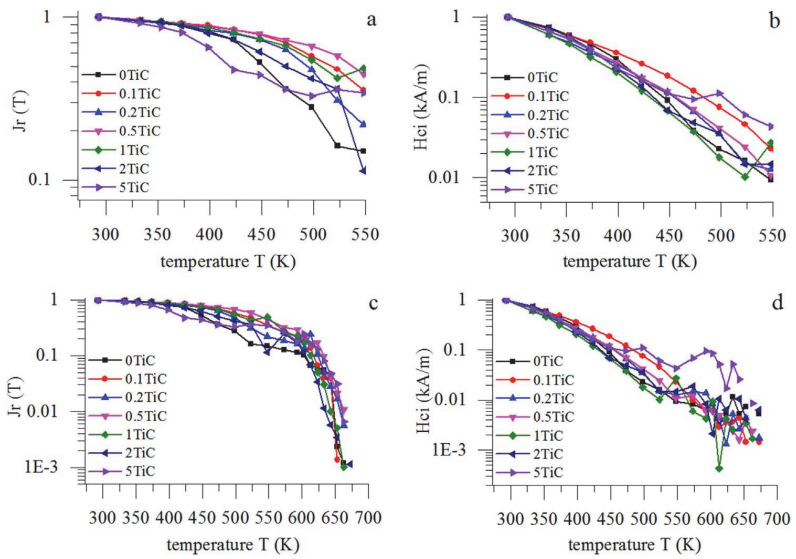

Fig. 6. Temperature dependence of remanence (a and c) and coercivity (b and d) for magnets with different TiC addition levels. Fig. 6a and b show lower temperatures region (293...523 K) while Fig. 6c and d show the whole range of temperatures (293...673 K).

decreases slightly faster. At temperatures higher than 598 K, coercivity becomes irregular and it is difficult to predict the total loss of the coercive force of materials. This can be confirmed by the temperature coefficients shown in Table 2.

The current trend in Nd-Fe-B magnet fabrication is to increase the thermal stability of RE magnets by Dy addition. However, the availability of Dy is quite critical and at higher Dy concentrations remanence decreases significantly. Diffusion technique is adopted to enrich just the boundaries of $Nd_2Fe_{14}B$ grains with Dy; however, the size of these magnets is limited to several millimetres only [34]. TiC addition can become an alternative to Dy doping in order to improve the thermal properties of magnets. A benefit of introducing TiC nanoparticles into RE magnets composition lies in a possibility to mix the nanoparticles after casting the strip cast flakes of the magnetic alloy.

4. Conclusions

This paper examined the effect of 0.1...5 wt% TiC nanoparticles addition into Nd-Fe-B sintered magnets on their magnetic properties, thermal behaviour and microstructure. According to the findings obtained in the research, the following conclusions can be drawn:

1. In the main, TiC particles are concentrated intergranularly in the RE-rich phase and show almost no evidence of dissolving in the main phase. Already at as small concentrations as 0.1 wt% TiC nanopowder additions lead to a finer microstructure and decreased volume fraction of the nonmagnetic phase.
2. The addition of nano-TiC to RE magnets by mixing the carbide together with hydrogen decrepitated strip cast powder produced an improvement of their magnetic properties, in particular coercivity. The concentration of up to 1 wt% of nano-TiC appears to increase coercivity without a significant decrease in remanence.
3. The hysteresis loop for magnets doped with 1 wt% TiC generated properties as follows: coercivity 1188 kA/m, remanence 0.96 T and maximum energy product 132 kJ/m^3.
4. TiC addition can significantly improve the thermal stability and the Curie temperature of the magnet. At 1 wt% of nano-TiC the Curie temperature T_C can be raised to 623 K.

Acknowledgements

This research has been partially supported by a project “Permanent magnets for sustainable energy application (MagMat)” financed by the European Regional (Social) Fund under project 3.2.1101.12-0003 in Estonia. This work is part of the REEgain Innovation Consortium funded by the Innovation Fund Denmark (www.REEgain.dk).

A special gratitude should be given to Molycorp Silmet R & D Director Ms Jane Paju for providing experimental materials, assisting in characterization and supporting the research team throughout the project.

References

[1] M. Sagawa, S. Fujimura, N. Togawa, H. Yamamoto, Y. Matsuura, New material for permanent magnets on a base of Nd and Fe, J. Appl. Phys. 55 (1984) 2083–2087.
[2] S. Pandian, V. Chandrasekaran, G. Markandeyulu, K.J.L. Iyer, K.V.S. Rama Rao, Effect of Al, Cu, Ga, and Nb additions on the magnetic properties and microstructural features of sintered NdFeB, J. Appl. Phys. 92 (2002) 6082–6086.
[3] J.M.D. Coey, Rare-Earth Iron Permanent Magnets, Claredon Press, Oxford, Oxford, 2006.
[4] J.P. Nozieres, R. Perrier de la Bathie, Hot worked Nd-Fe-B permanent magnets: effect of additional element such as Dy, Si, Ce, Ti, Co and others, IEEE Trans. Magn. 25 (1989) 4117–4119.
[5] L.Q. Yu, J. Zhang, S.Q. Hu, Z.D. Han, M. Yan, Production for high thermal stability NdFeB magnets, J. Magn. Magn. Mater. 320 (2008) 1427–1430.
[6] P. Tenaud, F. Vial, M. Sagawa, Improved corrosion and temperature behaviour of modified Nd-Fe-B magnets, IEEE Trans. Magn. 26 (1990) 1930–1932.
[7] H. Bala, G. Pawlowska, S. Szymura, V.V. Sergeev, Yu.M. Rabinovich, Corrosion characteristics of NdFeB sintered magnets containing various alloying elements, J. Magn. Magn. Mater. 87 (1990) 255–259.
[8] W.Q. Liu, H. Sun, X.F. Yi, X.C. Liu, D.T. Zhang, M. Yue, J.X. Zhang, Coercivity enhancement in Nd-Fe-B sintered permanent magnet by Dy nanoparticles doping, J. Alloy. Compd. 501 (2010) 67–69.
[9] A.S. Kim, F.E. Camp, Effect of minor grain boundary additives on the magnetic properties of NdFeB magnets, IEEE Trans. Magn. 31 (1995) 3620–3622.
[10] G. Bai, R.W. Gao, Y. Sun, G.B. Han, B. Wang, Study of high-coercivity sintered NdFeB magnets, J. Magn. Magn. Mater. 308 (2007) 20–23.
[11] Y. Matsuura, S. Hirosawa, H. Yamamoto, S. Fujimura, M. Sagawa, Magnetic properties of the $Nd_2(Fe_{1-x}Co_x)_{14}B$ system, Appl. Phys. Lett. 46 (1985) 306–310.
[12] F.E. Camp, A.S. Kim, Effect of microstructure on the corrosion behaviour on NdFeB and NdFeCoAlB magnets, J. Appl. Phys. 70 (1991) 6348–6350.
[13] M. Sagawa, S. Fujimura, H. Yamamoto, Y. Matsuura, K. Higara, Permanent magnets materials based on the rare-earth-iron-boron tetragonal compounds, IEEE Trans. Magn. 20 (1984) 1584–1589.
[14] D.J. Branagan, R.W. McCallum, Precipitation phenomenon in stoichiometric $Nd_2Fe_{14}B$ alloys modified with titanium and titanium with carbon, J. Alloy. Compd. 230 (1995) 67–75.
[15] C.H. Chiu, H.W. Chang, C.W. Chang, W.C. Chang, The effect of Ti and C on the phase evolution and magnetic properties of $Pr_9Fe_{bal}Ti_xB_{11-y}C_y$ (x=0–4, y=0–11) nanocomposites, J. Appl. Phys. 99 (2006).
[16] R. Zhang, Y. Liu, J. Li, S. Gao, M. Tu, Effect of Ti & C substitution on the magnetic properties and microstructures of rapidly-quenched NdFeB alloy, Mater. Charact. 59 (2008) 642–646.
[17] P. Haijun, Z. Maocai, B. Xiaoqian, Effect of doping of Ti and C on crystallization and magnetic properties of NdPrFeB thick melt-spun ribbons, Rare Met. Mat. Eng. 41 (2012) 212–214.
[18] W. Cong, G. ZhiMeng, S. YanLi, B. XiaoQian, C. ZhiAn, Effect of titanium substitution on magnetic properties and microstructure of nanocrystalline monophase Nd-Fe-B Magnets, J. Nanomater. 2012 (2012).
[19] M.J. Kramer, C.P. Li, K.W. Dennis, R.W. McCallum, C.H. Sellers, D.J. Branagan, L.H. Lewis, J.Y. Wang, Effect of TiC additions to the microstructure and magnetic properties of $Nd_{9.5}Fe_{84.5}B6Nd_{9.5}Fe8_{4.5}B_6$ melt-spun ribbons, J. Appl. Phys. 83 (1998) 6631–6633.
[20] M. Arenas, G.W. Warren, C.P. Li, K.W. Dennis, R.W. McCallum, Corrosion and hydrogen absorption in melt Spun NdFeB-TiC bonded magnets, IEEE Trans. Magn. 33 (1997) 3901–3903.
[21] A. Aharoni, Demagnetizing factors for rectangular ferromagnetic prisms, J. Appl. Phys. 83 (1998) 3432–3434.
[22] R.O. Elliot, C.P. Kempter, Thermal expansion of some transition metals carbides, J. Phys. Chem. 62 (1958) 630–631.
[23] L.X. Liao, Z. Altounian, D.H. Ryan, Cobalt site preferences in iron rare-earth-based compounds, Phys. Rev. B. 47 (1993) 230–241.
[24] O. Filip, R. Hermann, L. Schultz, Growth kinetics and TiC precipitation phenomena in Nd-Fe-B-Ti-C melts in dependence on cooling parameters and composition, Mater. Sci. Eng. A 375–377 (2004) 1044–1047.
[25] R. Hilzinger, W. Rodewald, Magnetic Materials: Fundamentals, Products, Properties, Applications, Publicis Publishing, Erlangen, 2013.
[26] S.R. Trout, Material selection of permanent magnets, considering thermal properties correctly, Proceedings of Electrical Insulation Conference and Electrical Manufacturing & Coil Winding Conference, 2001, pp. 365-370.
[27] Y. Kato, Thermal stability of sintered and bonded rare-earth magnets, J. Appl. Phys. 85 (1999) 4868–4870.
[28] T.S. Chin, C.H. Lin, Y.H. Huang, J.M. Jau, Enhanced thermal stability of sintered (Nd, Dy)(Fe, Co)B magnets by the addition of Ta or Ti, IEEE Trans. Magn. 29 (6) (1993) 2788–2790.
[29] R. Goto, K. Takagi, A. Hosokawa, K. Ozaki, Proceedings of the 24th International Workshop on Rare-Earth and Future Permanent Magnets and Their Applications (REPM 16), Darmstadt, Germany, 2016.
[30] Y. Murakami, T. Taginaki, T.T. Sasaki, Y. Takeno, H.S. Park, T. Matsuda, T. Ohkubo, K. Hono, D. Shindo, Magnetism of ultrathin intergranular boundary regions in Nd–Fe–B permanent magnets, Acta Mater. 71 (2014) 370–379.
[31] H. Sepehri-Amin, T. Ohkubo, T. Shima, K. Kono, Grain boundary and interface chemistry of an Nd–Fe–B-based sintered magnet, Acta Mater. 60 (2011) 819–830.
[32] T.Y. Chu, T.S. Chin, C.H. Lin, J.M. Yao, Evidence of domain-wall pinning in W-doped (NdDy)(FeCo)B sintered magnets, J. Appl. Phys. 76 (1994) 6834–6836.
[33] J. Bernardi, J. Fidler, F. Födermayr, The effect of V or W additives to microstructure and coercivity of Nd-Fe-B based magnets, IEEE Trans. Magn. 28 (5) (1992) 2127–2129.
[34] K. Löewe, C. Brombacher, M. Katter, O. Gutfleisch, Temperature-dependent Dy diffusion processes in Nd–Fe–B permanent magnets, Acta Mater. 83 (2015) 248–255.

DISSERTATIONS DEFENDED AT TALLINN UNIVERSITY OF TECHNOLOGY ON *MECHANICAL ENGINEERING*

1. **Jakob Kübarsepp**. Steel-Bonded Hardmetals. 1992.

2. **Jakub Kõo**. Determination of Residual Stresses in Coatings &Coated Parts. 1994.

3. **Mart Tamre**. Tribocharacteristics of Journal Bearings Unlocated Axis. 1995.

4. **Paul Kallas**. Abrasive Erosion of Powder Materials. 1996.

5. **Jüri Pirso**. Titanium and Chromium Carbide Based Cermets. 1996.

6. **Heinrich Reshetnyak**. Hard Metals Serviceability in Sheet Metal Forming Operations. 1996.

7. **Arvi Kruusing**. Magnetic Microdevices and Their Fabrication methods. 1997.

8. **Roberto Carmona Davila**. Some Contributions to the Quality Control in Motor Car Industry. 1999.

9. **Harri Annuka**. Characterization and Application of TiC-Based Iron Alloys Bonded Cermets. 1999.

10. **Irina Hussainova**. Investigation of Particle-Wall Collision and Erosion Prediction. 1999.

11. **Edi Kulderknup**. Reliability and Uncertainty of Quality Measurement. 2000.

12. **Vitali Podgurski**. Laser Ablation and Thermal Evaporation of Thin Films and Structures. 2001.

13. **Igor Penkov**. Strength Investigation of Threaded Joints Under Static and Dynamic Loading. 2001.

14. **Martin Eerme**. Structural Modelling of Engineering Products and Realisation of Computer-Based Environment for Product Development. 2001.

15. **Toivo Tähemaa**. Assurance of Synergy and Competitive Dependability at Non-Safety-Critical Mechatronics Systems design. 2002.

16. **Jüri Resev**. Virtual Differential as Torque Distribution Control Unit in Automotive Propulsion Systems. 2002.

17. **Toomas Pihl**. Powder Coatings for Abrasive Wear. 2002.

18. **Sergei Letunovitš**. Tribology of Fine-Grained Cermets. 2003.

19. **Tatyana Karaulova**. Development of the Modelling Tool for the Analysis of the Production Process and its Entities for the SME. 2004.

20. **Grigori Nekrassov**. Development of an Intelligent Integrated Environment for Computer. 2004.

21. **Sergei Zimakov**. Novel Wear Resistant WC-Based Thermal Sprayed Coatings. 2004.

22. **Irina Preis**. Fatigue Performance and Mechanical Reliability of Cemented Carbides. 2004.

23. **Medhat Hussainov**. Effect of Solid Particles on Turbulence of Gas in Two-Phase Flows. 2005.

24. **Frid Kaljas**. Synergy-Based Approach to Design of the Interdisciplinary Systems. 2005.

25. **Dmitri Neshumayev**. Experimental and Numerical Investigation of Combined Heat Transfer Enhancement Technique in Gas-Heated Channels. 2005.

26. **Renno Veinthal**. Characterization and Modelling of Erosion Wear of Powder Composite Materials and Coatings. 2005.

27. **Sergei Tisler**. Deposition of Solid Particles from Aerosol Flow in Laminar Flat-Plate Boundary Layer. 2006.

28. **Tauno Otto**. Models for Monitoring of Technological Processes and Production Systems. 2006.

29. **Maksim Antonov**. Assessment of Cermets Performance in Aggressive Media. 2006.

30. **Tatjana Barashkova**. Research of the Effect of Correlation at the Measurement of Alternating Voltage. 2006.

31. **Jaan Kers**. Recycling of Composite Plastics. 2006.

32. **Raivo Sell**. Model Based Mechatronic Systems Modeling Methodology in Conceptual Design Stage. 2007.

33. **Hans Rämmal**. Experimental Methods for Sound Propagation Studies in Automotive Duct Systems. 2007.

34. **Meelis Pohlak**. Rapid Prototyping of Sheet Metal Components with Incremental Sheet Forming Technology. 2007.

35. **Priidu Peetsalu**. Microstructural Aspects of Thermal Sprayed WC-Co Coatings and Ni-Cr Coated Steels. 2007.

36. **Lauri Kollo**. Sinter/HIP Technology of TiC-Based Cermets. 2007.

37. **Andrei Dedov**. Assessment of Metal Condition and Remaining Life of In-service Power Plant Components Operating at High Temperature. 2007.

38. **Fjodor Sergejev**. Investigation of the Fatigue Mechanics Aspects of PM Hardmetals and Cermets. 2007.

39. **Eduard Ševtšenko**. Intelligent Decision Support System for the Network of Collaborative SME-s. 2007.

40. **Rünno Lumiste**. Networks and Innovation in Machinery and Electronics Industry and Enterprises (Estonian Case Studies). 2008.

41. **Kristo Karjust**. Integrated Product Development and Production Technology of Large Composite Plastic Products. 2008.

42. **Mart Saarna**. Fatigue Characteristics of PM Steels. 2008.

43. **Eduard Kimmari**. Exothermically Synthesized B_4C-Al Composites for Dry Sliding. 2008.

44. **Indrek Abiline**. Calibration Methods of Coating Thickness Gauges. 2008.

45. **Tiit Hindreus**. Synergy-Based Approach to Quality Assurance. 2009.

46. **Karl Raba**. Uncertainty Focused Product Improvement Models. 2009.

47. **Riho Tarbe**. Abrasive Impact Wear: Tester, Wear and Grindability Studies. 2009.

48. **Kristjan Juhani**. Reactive Sintered Chromium and Titanium Carbide-Based Cermets. 2009.

49. **Nadežda Dementjeva**. Energy Planning Model Analysis and Their Adaptability for Estonian Energy Sector. 2009.

50. **Igor Krupenski**. Numerical Simulation of Two-Phase Turbulent Flows in Ash Circulating Fluidized Bed. 2010.

51. **Aleksandr Hlebnikov**. The Analysis of Efficiency and Optimization of District Heating Networks in Estonia. 2010.

52. **Andres Petritšenko**. Vibration of Ladder Frames. 2010.

53. **Renee Joost**. Novel Methods for Hardmetal Production and Recycling. 2010.

54. **Andre Gregor**. Hard PVD Coatings for Tooling. 2010.

55. **Tõnu Roosaar**. Wear Performance of WC- and TiC-Based Ceramic-Metallic Composites. 2010.

56. **Alina Sivitski**. Sliding Wear of PVD Hard Coatings: Fatigue and Measurement Aspects. 2010.

57. **Sergei Kramanenko**. Fractal Approach for Multiple Project Management in Manufacturing Enterprises. 2010.

58. **Eduard Latõsov**. Model for the Analysis of Combined Heat and Power Production. 2011.

59. **Jürgen Riim**. Calibration Methods of Coating Thickness Standards. 2011.

60. **Andrei Surzhenkov**. Duplex Treatment of Steel Surface. 2011.

61. **Steffen Dahms**. Diffusion Welding of Different Materials. 2011.

62. **Birthe Matsi**. Research of Innovation Capasity Monitoring Methodology for Engineering Industry. 2011.

63. **Peeter Ross**. Data Sharing and Shared Workflow in Medical Imaging. 2011.

64. **Siim Link**. Reactivity of Woody and Herbaceous Biomass Chars. 2011.

65. **Kristjan Plamus**. The Impact of Oil Shale Calorific Value on CFB Boiler Thermal Efficiency and Environment. 2012.

66. **Aleksei Tšinjan**. Performance of Tool Materials in Blanking. 2012.

67. **Martinš Sarkans**. Synergy Deployment at Early Evaluation of Modularity of the Multi-Agent Production Systems. 2012.

68. **Sven Seiler**. Laboratory as a Service – A Holistic Framework for Remote and Virtual Labs. 2012.

69. **Tarmo Velsker**. Design Optimization of Steel and Glass Structures. 2012.

70. **Madis Tiik**. Access Rights and Organizational Management in Implementation of Estonian Electronic Health Record System. 2012.

71. **Marina Kostina**. Reliability Management of Manufacturing Processes in Machinery Enterprises. 2012.

72. **Robert Hudjakov**. Long-Range Navigation for Unmanned Off-Road Ground Vehicle. 2012.

73. **Arkadi Zikin**. Advanced Multiphase Tribo-Functional PTA Hardfacings. 2013.

74. **Alar Konist**. Environmental Aspects of Oil Shale Power Production. 2013.

75. **Inge Roos**. Methodology for Calculating CO_2 Emissions from Estonian Shale Oil Industry. 2013.

76. **Dmitri Shvarts**. Global 3D Map Merging Methods for Robot Navigation. 2013.

77. **Kaia Lõun**. Company's Strategy Based Formation of e-Workplace Performance in the Engineering Industry. 2013.

78. **Maido Hiiemaa**. Motion Planner for Skid-Steer Unmanned Ground Vehicle. 2013.

79. **Dmitri Goljandin**. Disintegrator Milling System Development and Milling Technologies of Different Materials. 2013.

80. **Dmitri Aleksandrov**. Light-Weight Multicopter Structural Design for Energy Saving. 2013.

81. **Henrik Herranen**. Design Optimization of Smart Composite Structures with Embedded Devices. 2014.

82. **Heiki Tiikoja**. Experimental Acoustic Characterization of Automotive Inlet and Exhaust System. 2014.

83. **Jelena Priss**. High Temperature Corrosion and Abrasive Wear of Boiler Steels. 2014.

84. **Aare Aruniit**. Thermoreactive Polymer Composite with High Particulate Filler Content. 2014.

85. **Dmitri Gornostajev**. Development of the Calculation Method for Barge Hull. 2014.

86. **Liina Lind**. Wear of PVD Coatings on Fineblanking Punches. 2014.

87. **Nikolai Voltšihhin**. Design and Technology of Oxides-Containing Ceramic-Based Composites. 2014.

88. **Aleksander Šablinski**. RANS Numerical Modelling of Turbulent Polydispersed Flows in CFB Freeboard. 2015.

89. **Tanel Aruväli**. Wireless Real-time Monitoring of Machining Processes. 2015.

90. **Andrei Bogatov**. Morphological Changes on Diamond and DLC Films During Sliding Wear. 2015.

91. **Raimo Kabral**. Aero-Acoustic Studies and Innovative Noise Control with Application to Modern Automotive Gas Exchange System. 2015.

92. **Jevgeni Sahno**. Dynamic Management Framework for Continuous Improvement of Production Processes. 2015.

93. **Ott Pabut**. Optimal Design of Slotless Permanent Magnet Generators. 2015.

94. **Merili Kukuškin**. Value Centric Business Development for Estonian Manufacturing Small and Medium Sized Enterprises. 2015.

95. **Kaimo Sonk**. Development of Additive Manufacturing Based on Functional Requirements. 2015.

96. **Marina Aghayan**. Functionalization of Alumina Nanofibers with Metal Oxides. 2016.

97. **Marek Jõeleht**. Titanium Carbide Cermet as Ballistic Protection Material. 2016.

98. **Heikki Sarjas**. Novel Synthesized and Milled Carbide-based Composite Powders for HVOF Spray. 2016.

99. **Klodian Dhoska**. Measurement Methods with 3D Coordinate Measuring Machine and Improved Characterization Setup for Detector Performance. 2016.

100. **Aleksei Snatkin**. Development and Optimisation of Production Monitoring System. 2016.

101. **Igor Poljantšikov**. Partners Selection Tool for Virtual Enterprise in SMEs Network. 2016.

102. **Sergei Žigailov**. Experimental and Analytical Modelling of Pelvic Motion. 2016.

103. **Rommi Källo**. Synergy-Based Chaos Control in the Multi-Agent Hierarchical Systems. 2016.

104. **Der-Liang Yung**. ZrC-based and ZrC-doped Composites for High-Temperature and Wear Applications. 2016.

105. **Viive Pille**. Development of a Model for the Prevention of Work-Related Musculoskeletal Disorders in the Upper Extremities. 2016.

106. **Agus Pramono**. Investigation of Severe Plastic Deformation Processes for Aluminum Based Composites. 2016.